SIGNAL PROCESSING TECHNIQUES FOR TARGET DETECTION AND ESTIMATION FOR RADAR SYSTEMS

Ph.D. Thesis

by

UDAY KUMAR SINGH

DISCIPLINE OF ELECTRICAL ENGINEERING
INDIAN INSTITUTE OF TECHNOLOGY INDORE

AUGUST, 2020

SIGNAL PROCESSING TECHNIQUES FOR TARGET DETECTION AND ESTIMATION FOR RADAR SYSTEMS

A THESIS

Submitted in partial fulfillment of the

requirements for the award of the degree

of

DOCTOR OF PHILOSOPHY

by

UDAY KUMAR SINGH

DISCIPLINE OF ELECTRICAL ENGINEERING

INDIAN INSTITUTE OF TECHNOLOGY INDORE

AUGUST, 2020

INDIAN INSTITUTE OF TECHNOLOGY INDORE

CANDIDATE'S DECLARATION

I hereby certify that the work which is being presented in the thesis entitled "**SIGNAL PROCESSING TECHNIQUES FOR TARGET DETECTION AND ESTIMATION FOR RADAR SYSTEMS**" in the partial fulfillment of the requirements for the award of the degree of DOCTOR OF PHILOSOPHY and submitted in the DISCIPLINE OF ELECTRICAL ENGINEERING, Indian Institute of Technology Indore, is an authentic record of my own work carried out during the time period from Oct 2015 to Jun 2020 under the joint supervision of Dr. Vimal Bhatia, Professor, Indian Institute of Technology Indore, India and Dr. Amit Kumar Mishra, Professor, University of Cape Town, South Africa.

The matter presented in this thesis has not been submitted by me for the award of any other degree of this or any other institute.

21/07/2020
Signature of the student with date
(UDAY KUMAR SINGH)

This is to certify that the above statement made by the candidate is correct to the best of my knowledge.

21/07/2020	21/07/2020
Signature of Thesis Supervisor with date	Signature of Thesis Supervisor with date
(Dr. VIMAL BHATIA)	**(Dr. AMIT KUMAR MISHRA)**

Uday Kumar Singh has successfully given his Ph.D. Oral Examination held on.......... 11/02/2021

Signature of Chairperson (OEB)	Signature of External Examiner	Signature of Thesis Supervisor #1
Date: 11/02/2021	Date: 11/02/2021	Date: 11/02/2021

Signature of Thesis Supervisor #2
Date: 11/02/2021

Signature of PSPC Member #1	Signature of PSPC Member #2	Signature of Convener, DPGC
Date: 11/02/2021	Date: 11/02/2021	Date: 11/02/2021

Signature of Head of Discipline
Date: 11/02/2021

ACKNOWLEDGEMENTS

Firstly, I would like to express my sincere gratitude to my supervisors Dr. Vimal Bhatia and Dr. Amit Kumar Mishra, for the support they provided me throughout my Ph.D. study. I am also thankful to them for keeping patience, motivating me, and imparting me with immense knowledge. Moreover, their guidance helped me in all the time of research and writing of this thesis. In-fact, I could not have imagined having better supervisors and mentors for my Ph.D. study.

Besides my supervisors, I am genuinely thankful to my senior Dr. Rangeet Mitra, for his excellent teaching and helping me in evolving from a naive to a professional. Further, I want to thank my PSPC committee members: Dr. Somnath Dey, and Dr. Mukesh Kumar, for their insightful comments, encouragement, and for all the hard questions which forced me to widen my research from various perspectives. I would also like to thank all the faculty and staff members of the electrical engineering discipline of IIT Indore for their timely support and cooperation.

Next, I would like to thank my fellow lab-mates for encouraging, for happy working environment, and for all the fun we have had in the last four and a half years of my Ph.D. Particularly, I would like to thank Dr. Praveen Kumar Singya (Big bro), Anuj Agarwal (Bro), Purva Sharma (Choti), Deepak, Pragya Swami, and Arijit, for supporting me during hard times and accompanying me for odd time tea and snacks.

I would also like to thank the Visvesvaraya Ph.D. scheme of the Ministry of Electronics and Information Technology, Government of India, and IIT Indore for providing financial assistance. I would also like to take this opportunity to thank the Visvesvaraya Ph.D. scheme for funding my research papers publication charges. Without this, I wouldn't have been able to complete my Ph.D. thesis on the stipulated time.

Last but not least, I would like to thank my family: my parents and my brothers for supporting me spiritually throughout writing this thesis and my whole life in general.

UDAY KUMAR SINGH

Dedicated to my parents and siblings

ABSTRACT

With the continuous increase in cases of enemy attacks, road accidents, goods trafficking, and burglary attempts, surveillance is necessary for the safety of the country, human wealth, and property. Since the inception of RADAR (during the second World War), which is an acronym for radio detection and ranging, radar has been extensively used for surveillance and monitoring. In-fact with continuous technological advancement and because of the advent of various digital signal processing schemes, researchers are continuously working to enhance the performance of radar systems. The two essential aspects of radar systems are detection and estimation. The detector gives an estimate of the number of targets present in the surveillance environment. Subsequently, the estimator yields the estimates of the location and speed of the detected targets. Practically, the reflected signal processed for the detection of targets and estimation of their range and velocity, are heavily perturbed by thermal noise and clutter. Consequently, perturbation because of thermal noise and clutter hinders the perfect detection of targets and accurate estimation of their location and velocity.

The goal of this thesis is to propose new techniques for target detection and estimation of the target's range and velocity by suppressing the effects of thermal noise and clutter. For this purpose, in this thesis, the following works are done.

Firstly, the orthogonal frequency division multiplexing (OFDM) based radar system is explored for the detection of a small boat in sea clutter. For this, we propose a technique to generate radar return for OFDM waveform using collected radar return data for stepped frequency waveform. We then derive the system model for the estimated radar return data specific to the OFDM waveform. Further, a detection test is proposed for the derived signal model and surveillance environment. The close match between the derived analytical expressions and simulation results validates the performance of the proposed detector.

For estimation of the target's range and velocity, an adaptive estimator based on a sparse kernel least mean square algorithm is proposed. Being an adaptive algorithm, the estimates are obtained by low computational complexity, and the accuracy of estimates is guaranteed by the convex nature of optimizing cost function in reproducing kernel Hilbert space. Subsequently, an adaptive kernel width optimization technique is proposed to further lower the computational complexity of the proposed estimator. An expression for the Cramer-Rao lower bound (CRLB) is derived and validated for the proposed estimator over linear frequency modulated, and OFDM radar systems.

In the next work, we propose kernel maximum correntropy based estimators for range and velocity estimation in non-Gaussian clutter. Additionally, an adaptive update equation is derived for optimization of the kernel-width, which further lowers the dictionary-size, and variance of the proposed estimator. For the performance evaluation of the proposed estimators, an expression is derived for the CRLB using a modified Fisher information matrix (FIM).

Next, a kernel minimum error entropy (KMEE) based estimator is proposed for the estimation of multiple targets' direction of departure (DOD), the direction of arrival (DOA), and the Doppler shift with multiple input multiple output radar in non-Gaussian clutter. The computational complexity of the proposed KMEE based estimator is reduced by incorporation of novelty criterion based sparsification technique. Analytical expressions are derived for the variance of estimation-error in DOD, DOA, and Doppler shift. Further, for assessing the accuracy of the proposed estimator, the CRLB is calculated using the Modified FIM.

Lastly, two efficient low complexity estimators, namely, the extended Kalman filter (EKF) and the unscented Kalman filter (UKF), are proposed. The EKF is advantageous due to its implementation simplicity and fast computation; however, a derivative-based implementation limits its use. The UKF outperforms the EKF and offers better stability due to a derivative-free implementation. Simulation results reveal improved accuracy achieved by the proposed EKF and UKF based estimators. Moreover, the EKF and UKF based estimators show a closer match with the CRLBs compared with the existing approaches along-with low computational complexity.

Contents

List of Figures

List of Tables

List of Algorithms

List of Abbreviations

AWGN additive white Gaussian noise.

CCDF complementary cumulative distribution function.

CNR clutter to noise ratio.

CPI coherent pulse interval.

CRLB Cramer-Rao Lower Bound.

DFT discrete Fourier transform.

DOA direction of arrival.

DOD direction of departure.

EKF extended Kalman filter.

EMSE excess mean square error.

FIR finite impulse response.

FT Fourier transform.

GLRT generalized likelihood ratio test.

IDFT inverse discrete Fourier transform.

IR impulse response.

ITL information-theoretic learning.

KAF kernel adaptive filter.

KLMS kernel least mean square.

KMC kernel maximum correntropy.

KMEE kernel minimum error entropy.

LFM linear frequency modulated.

LMS least mean square.

LS least squares.

MCC maximum correntropy criterion.

MEE minimum error entropy.

MIMO multiple input multiple output.

ML maximum likelihood.

MSE mean square error.

NC novelty criterion.

NMF normalized matched filter.

NMSE normalized mean square error.

OFDM orthogonal frequency division multiplexed.

PAPR peak to average power ratio.

PDF probability density function.

PRI pulse repetition interval.

PSK phase shift key.

RCS radar cross section.

RKHS reproducing kernel Hibert space.

ROC receiver operating characterstics.

SCR signal to clutter ratio.

SF stepped frequency.

SIRP spherically invariant random process.

SNR signal to noise ratio.

UKF unscented Kalman filter.

List of Symbols, Notations and Operations

$\mathbb{R}$	set of real numbers
$\mathbb{C}$	set of complex numbers
$\mathbb{H}$	represents a high dimensional Hilbert space
$\kappa(\cdot)$	Gaussian kernel function
$\Phi(\cdot)$	implicit mapping function
$\|\cdot\|_2$	l_2 norm in Euclidean space
$\langle\cdot,\cdot\rangle_{\mathbb{H}}$	inner product in Hilbert space
$\lvert\cdot\rvert$	represents the matrix determinant operator
$(\cdot)^T$	transpose of a vector or a matrix
$(\cdot)^H$	conjugate transpose of a vector or a matrix
$\Lambda(\cdot)$	detector test statistics
λ	detection threshold
$\mathcal{R}(\cdot)$	rank of a matrix
L	number of sub-carriers / number of time samples
M	number of radar pulses in one coherent pulse interval
N	dimension of a vector
P	number of targets / number of scatteres
T_o	pulse width
T_{PRI}	pulse repetition interval
N_{tx}	number of transmitter antenna
N_{rx}	number of receiver antenna
$\mathcal{P}(\cdot)$	probability density function of a random variable
$\mathcal{J}(\cdot)$	cost function
$vec(\cdot)$	arranging the elements of a matrix in a vector
P_{D}	probability of detection
P_{FA}	probability of false alarm
α	texture enhancement factor of **c**
ν	shape parameter of α
μ_c	size parameter of α
τ_o	true delay
f_d	true Doppler shift
f_c	carrier frequency
σ	Gaussian kernel function width
σ_c	correntropy function Gaussian kernel width
σ_k	adaptive Gaussian kernel function width
σ_d	width of the kernel function used for probability density function approximation

$d(k)$	true value of τ_o or f_d at k^{th} iteration
$e(k)$	scalar estimation error at k^{th} iteration
$g(\cdot)$	true unknown mapping function
$\boldsymbol{\omega}(k)$	unknown weight vector in $\mathbb{H}$ at k^{th} iteration
Ω_w^2	variance of the elements of **w**
$\mathbf{h}$	true radar channel impulse response
$\boldsymbol{\mathcal{P}}$	projection matrix
$\hat{\mathbf{h}}$	estimated radar channel impulse response
$\mathbf{tr}$	trace of a matrix
$\mathbf{c}$	non-Gaussian K distributed clutter
$\mathbf{e}_k$	vector estimation error at k^{th} iteration
$\mathbf{r}(k)$	radar return for single antenna radar system at k^{th} iteration
$\mathbf{r}_k$	radar return for multiple input multiple output radar system at k^{th} iteration
$\mathbf{w}$	additive white Gaussian distributed random vector
$\mathbf{z}$	complex correlated Gaussian distributed random vector (speckle component of **c**)
$\boldsymbol{\Omega}_k$	unknown weight matrix in$\mathbb{H}$ at k^{th} iteration
$\boldsymbol{\Sigma}_{\mathbf{w}}$	covariance matrix of **w**
$\boldsymbol{\Sigma}_{\mathbf{z}}$	normalized covariance matrix of **z**
$\boldsymbol{\Sigma}$	covariance matrix of the joint perturbation of **c** and **w**
$\boldsymbol{\eta}_k$	modeling error
$\mathbf{v}_k$	measurement noise
$\mathbf{Q}_k$	covariance matrix of $\boldsymbol{\eta}_k$
$\mathbf{R}_k$	covariance matrix of $\mathbf{v}_k$
$\mathbf{P}_{k\|k}$	covaraince matrix of state vector
$\mathbf{F}_k$	state matrix
$\mathbf{H}_k$	measurement matrix

Chapter 1

Introduction

In this Chapter, firstly, the motivation is given. Subsequently, various topics that are used to develop the detection and estimation algorithms in forthcoming Chapters are discussed. The Chapter ends with a thesis outline and a summary of the contribution of the thesis.

1.1 Motivation

In the various military, civilian and autonomous vehicle applications, to curb the rapid increase in enemies attempts of infiltrating a country's border and vehicles collision, efficient surveillance and monitoring system is needed. Since the inception of RADAR (which is the acronym for Radio Detection and Ranging), during World War II, radar systems are enormously used for monitoring and tracking in various military, civilian, and autonomous vehicle applications [1, 4]. Eventually, with the advent of digital signal processing and the rapid increase in digital technology, the earlier radar systems have been evolved in terms of yielding better performance in a variety of real environments. The two main performance evaluation criterion for the radar system is detection and estimation. Studies have shown and proved that in many cases, the detection performance of the radar system could be enhanced by exploiting diversity provided by processing sub-carriers of a multi-carrier waveform individually [5–7]. Therefore, there is a possibility of developing a technique to employ multi-carrier waveform like OFDM waveform in radar systems mounted for the surveillance of the heavily perturbed marine environment. Further, the conventional estimation techniques are based on batch processing [2, 8, 9], i.e.; the radar observations are stored and then processed simultaneously. This makes the conventional estimators time-consuming and unsuitable for radar applications demanding fast processing of data. Hence, there is a scope of developing adaptive estimation techniques suitable for tracking and monitoring applications as they provide an online estimate of required parameters. Furthermore, in practice, the radar return is affected by the clutter, this makes the conventional estimators unsuitable for practical employment as the conventional estimation techniques are developed assuming the absence of clutter [2, 8, 9]. Hence, there is a scope of developing adaptive estimation techniques capable of dealing with the deleterious effects of non-Gaussian clutter. In a nutshell, to enhance the detection and estimation performance of the various single antenna and multiple input multiple output (MIMO) radar systems, in this thesis, efficient detection and different adaptive estimation techniques along with Kalman filter based estimation techniques are developed.

1.2 Radar Systems

As illustrated in Fig. 1.1, in a basic radar system, the baseband pulsed waveform of specific bandwidth and modulation (chosen specific to the application) is generated by the pulse generator. For the surveillance of the radar environment, before transmission, the baseband waveform is up-converted to a broadband pulsed waveform centered at a very high-frequency via up converter. In a mono-static radar system, the same antenna system is used for transmission of waveform and reception of reflection from the target. The duplexer separates the transmitted waveform and received reflection, and diverts them to the antenna and receiver section, respectively. After reception of reflection from the target, commonly called radar return, before further processing, the radar return is down-converted to baseband frequency. Subsequently, the radar return is discretized and converted into discrete samples, and the resultant radar observations are arranged in a 2D radar matrix with row and column corresponds to slow time usually termed as pulse repetition interval (PRI), and fast time range gate, respectively [1, 4]. After that, the radar observations are processed for the surveillance and monitoring of the environment. The detector gives an estimate of the number of targets present in the surveillance environment. Subsequently, the estimator yields the estimates of the corresponding range and velocity of the detected targets.

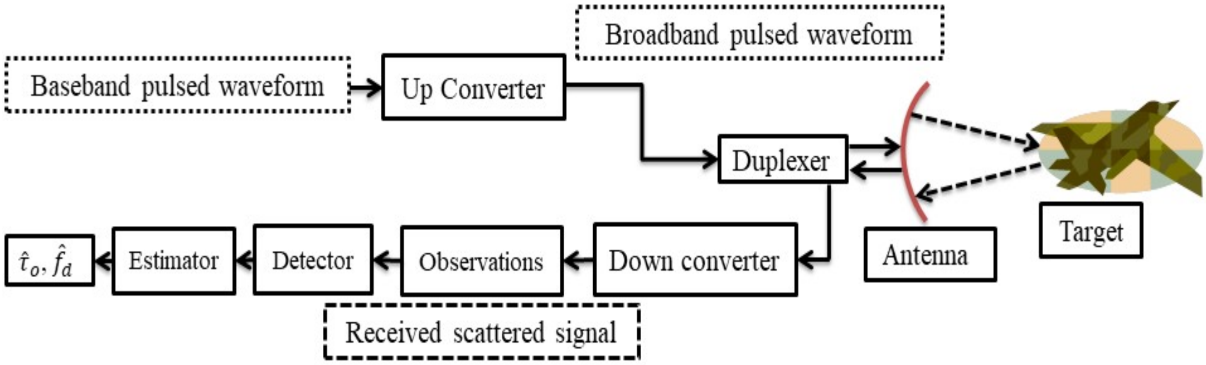

Figure 1.1: Block diagram of basic radar system [1]

In this thesis, the developed detection and estimation algorithms are tested over the two basic types of radar systems, single antenna radar systems and multi-antenna radar systems. Particularly, in Chapter 2, Chapter 3 , Chapter 4, and Chapter 6 the algorithms are developed for single antenna mono-static radar systems and in Chapter 5, the algorithms are developed for multiple antenna radar system. Therefore, in the forthcoming subsections, a single antenna radar system and MIMO radar system are briefly discussed.

1.2.1 Single Antenna Radar Systems

In this work, three basic types of single-antenna radar systems, LFM, SF, and OFDM radar systems, are used to validate the performance of proposed detection and estimation algorithms. As the name implies, the three types of radar systems use different modulation techniques for the baseband pulse according to the application and bandwidth requirement. For instance, LFM radar and SF radar are being used for a very long time for various military and civilian applications. In comparison to LFM and SF radar, OFDM radar is newer and introduced with the intent of combining the functionality of communication systems and radar systems [7, 10, 11].

Schematic of LFM waveform for single PRI ($= T_{\text{PRI}}$) transmitted by LFM radar is shown

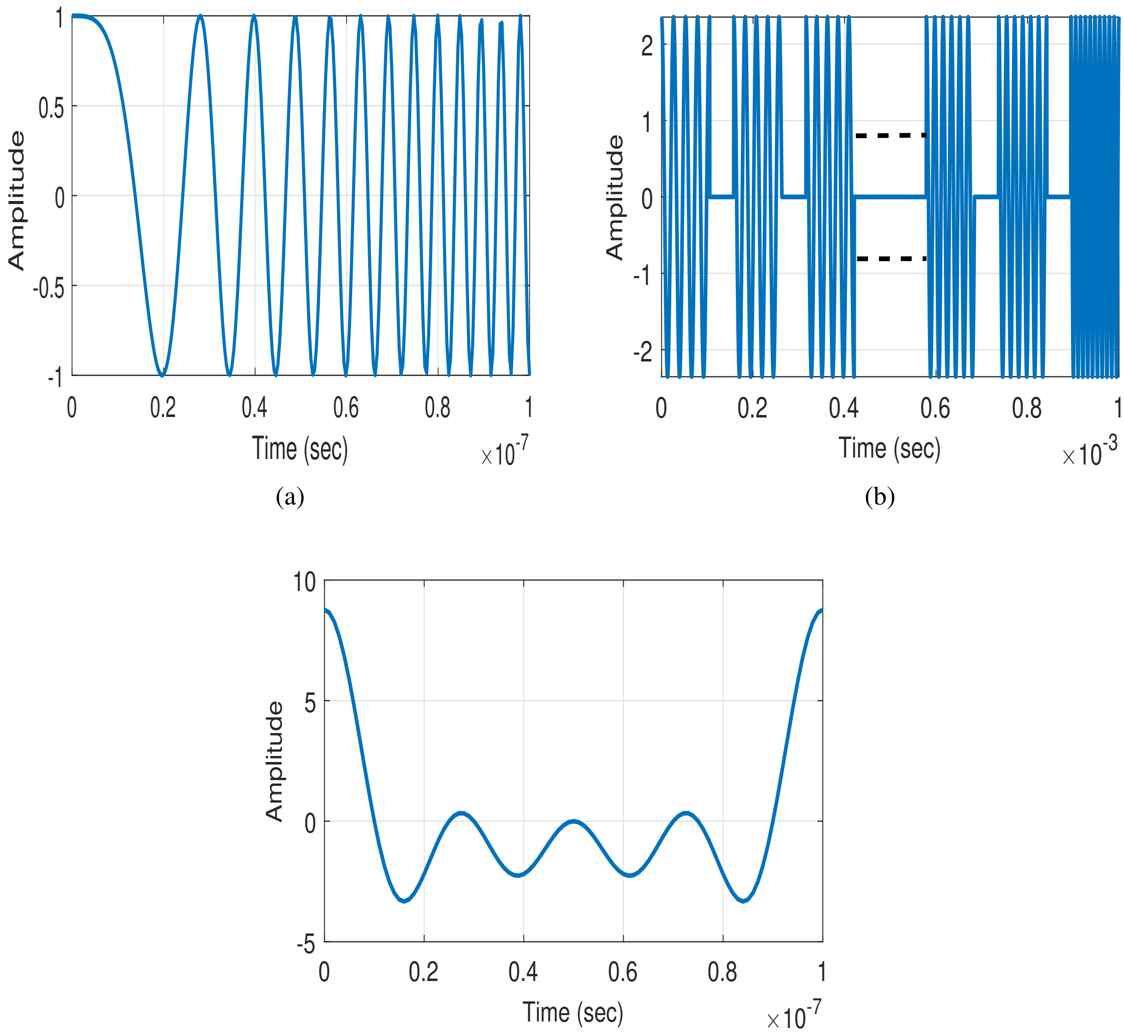

(a) (b) (c)

Figure 1.2: Schematic of radar waveform transmitted in (a) LFM radar, (b) SF radar, and (c) OFDM radar.

in Fig. 1.2a. The waveform is simulated according to the specifications given in Table. 1.1. Contrary to single tone pulsed radar waveform, the frequency of the LFM waveform increases linearly. This linear modulation of frequency reduces the unwanted side-lobes in the pulse compression output. Further, the schematic of the SF waveform for the group of 25 PRIs is shown in Fig. 1.2b. As shown in Fig. 1.2b, unlike LFM radar, instead of transmitting the waveform with linear increment in one PRI, the SF radar transmits the chunk of single tone pulses in the group of PRIs. The pulses are centered at different frequencies, and these frequencies are obtained by consecutively increasing the frequency of the starting pulse. The specifications of the SF waveform are given in Table. 1.1. The

OFDM waveform transmitted by OFDM radar is illustrated in Fig. 1.2c, the waveform is simulated by the specifications given in Table. 1.1. The transmitted OFDM waveform is the summation of the finite number of sub-carriers, which oscillates with frequencies; integer multiple of the reciprocal of the pulse width. The linear relation between the frequency and pulse width of the sub-carriers guarantees the orthogonality between sub-carriers. This in turn makes the OFDM radar bandwidth-efficient in comparison to other conventional radar systems. Moreover, in detection, the processing of each OFDM sub-carrier separately at the receiver provides gain in performance over conventional waveforms [5, 6].

Table 1.1: Example specifications for LFM waveform, SF waveform, and OFDM waveform shown in Fig. 1.2

LFM waveform	Values	SF waveform	Values	OFDM waveform	Values
Number of frequencies	8	Number of channels	25	Number of sub-carriers	4
Frequency interval	625 KHz	Frequency step size	5 MHz	Subcarrier spacing	1.25 MHz
Center frequency	9 GHz	Center frequency	9 GHz	Center frequency	9 GHz
Bandwidth	5 MHz	Bandwidth	125 MHz	Bandwidth	5 MHz
Pulse duration	0.1 μs	Pulse duration	0.2 μs	Pulse duration	1 μs
PRI	0.1 ms	PRI	0.1 ms	PRI	0.1 ms

1.2.2 Multiple Input Multiple Output Radar System

In a communication system, multiple antennas with diversity in transmitting signal has proved to provide performance gains over a single-antenna radar system. With the intent to improve the performance of a radar system, the concept of MIMO radar has been introduced, and similar to communication systems use of multiple antennas to transmit orthogonal radar waveform and receiving the reflections from multiple antennas is proven to be beneficial for radar systems. For instance, contrary to a standard phased-array radar, which too have multiple antennas and transmits scaled versions of a single waveform, a MIMO radar system can transmit via its antennas multiple probing signals that may be chosen quite freely. Particularly, in MIMO radar, if the transmitter has N_{tx} antennas and receiver has N_{rx} antennas, then $N_{tx}N_{rx}$ different signals are processed at the receiver for detection of targets and estimation of their parameters. Processing N_{tx} different reflections for each receive antenna provides an extra look at the targets and enhances the performance of the radar system. To validate the improvement in the performance of MIMO radar over a single-antenna radar system, receiver operating characterstics (ROC) of the detector based on generalized likelihood ratio test (GLRT) [12] for the different number of antenna configuration is illustrated in Fig. 1.3. As shown in Fig. 1.3, for same probability of false alarm (P_{FA}) and for $N_{tx} = 2$ and $N_{rx} = 1$, MIMO radar system provides significant gain in probability of detection (P_{D}) over antenna configuration with $N_{tx} = 1$ and $N_{rx} = 1$ which corresponds to single antenna radar system. Further, performance of the MIMO radar system increases with increase in N_{tx} and N_{rx}, and this provides a strong argument to replace the single antenna radar system with the MIMO radar system. Further, in spite of adequate research in the MIMO radar system, there is still a scope of development, particularly in enhancing the performance of MIMO radar system in the presence of non-Gaussian clutter. Therefore, with the objective of improving performance of the MIMO radar system, in Chapter 5, estimator capable of estimating the location (in terms of the direction of arrival (DOA) and direction of departure (DOD)), and velocity of multiple targets in the presence of non-Gaussian clutter is developed.

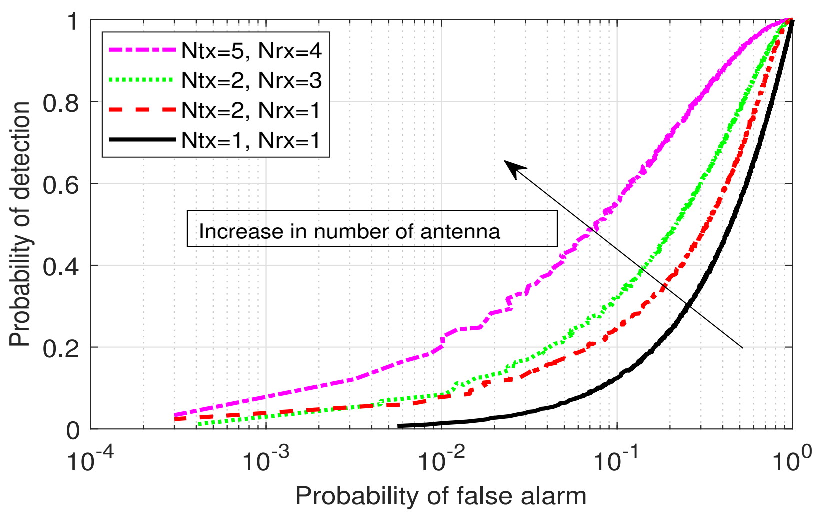

Figure 1.3: ROC of GLRT detector for different number of transmit and receive antenna.

1.3 Introduction to Kernel Adaptive Filter based Estimation Techniques for Radar Systems

In a radar system, the accurate estimation of the target's range and velocity is not only essential for determining the position and state of the target but also essential for continuous tracking of the target. For years estimators based on batch processing of radar observations like a Fourier transform (FT), least squares (LS), and multiple signal classification techniques commonly known as MUSIC are used for the estimation [2, 8, 9, 13]. In batch processing techniques, the observations are first accumulated and processed in a group to extract the significant information, which makes the conventional non-adaptive estimators time/computationally expensive to compute the estimates of target parameters. As a result, the batch processing techniques are not suitable for radar applications demanding fast processing of radar observations, particularly in applications like military surveillance and target tracking. Moreover, with an assumption of Gaussian distribution for thermal noise, the solution yield by FT and LS is based on the maximum likelihood (ML). In radar returns (shown in 3.9, 3.20, and 4.7), as the required parameters resemble with targets' range and velocity is hidden as frequency of an exponential [1, 4], the solution provided by ML doesn't have a closed-form solution [14]. Consequently, the solution relied on approximation and this results in sub-optimality of the estimates. Because of the limitations mentioned above of conventional estimation techniques, there is a scope of novel and efficient estimators capable of accurately estimating the target's unknown parameters hidden as frequency in radar returns perturbed by thermal noise and clutter.

For single antenna radar system, the generalized radar return for m^{th} pulse in a coherent pulse interval (CPI) of M pulses and l^{th} frequency/time sample can be mathematically expressed as

$$r(m,l) = \exp(j2\pi m\theta_1)\exp(j2\pi l\theta_2) + c(m,l) + w(m,l), \tag{1.1}$$

where θ_1 and θ_2 are the unknown parameters corresponding to target's range and velocity, respectively, $c(m,l)$ is the clutter sample and $w(m,l)$ is the thermal noise.

In (1.1), it should be noted that, since we are concerned with the estimation of the target's range and velocity, the term corresponding to the target's complex amplitude has been omitted (considering the target is the ideal reflector).

As illustrated in (1.1), the parameters of interest (θ_1 and θ_2) are related to the radar return ($r(m,l)$) via complex exponential. Further, in (1.1), for given θ_1 or vice versa, if the inverse relationship $\left(g(r(m,l)) = \{\theta_1, \theta_2\}\right)$ between the unknown parameter set ($\{\theta_1, \theta_2\}$) and $r(m,l)$ is known, the set of unknown parameters $\{\theta_1, \theta_2\}$ can be efficiently estimated. However, estimation of $g(\cdot)$ is non-trivial and not straightforward. Nevertheless, $g(\cdot)$ can be estimated by adaptive kernel based function approximation algorithms commonly known as kernel adaptive filter (KAF)s.

In wireless communication, the KAFs are applied to perform various function approximation problems, for instance, to recreate/estimate the transmitted symbols at the receiver from received symbols affected by channel non-linearity and thermal noise [15–18]. In this thesis, for the first time the problem of estimating θ_1 and θ_2 utilizing (1.1) is dealt with the perspective of solving function approximation problem. Particularly, in Chapter 3, Chapter 4, and Chapter 5, various KAFs based estimators which include estimators based on kernel least mean square (KLMS), kernel maximum correntropy (KMC), and kernel minimum error entropy (KMEE), respectively are developed and tested over different radar systems perturbed by thermal noise and clutter. Therefore, in this section, a brief introduction to KAFs based estimation techniques is given.

For estimation, at the k^{th} instant, estimators based on KAF firstly transform the radar return ($\mathbf{r}(k)$) for all m and l and for given θ_1 and θ_2 to reproducing kernel Hibert space (RKHS) ($\mathbb{H}$) via an implicit mapping function $\Phi(\cdot)$. After transforming $\mathbf{r}(k)$ to $\mathbb{H}$, at k^{th} instant for an arbitrary weight vector $\boldsymbol{\omega}(k-1)$ in $\mathbb{H}$ the estimate of $g(\cdot)$ which in turn give the estimate of desired parameter ($d(k)$) can be written as

$$\hat{d}(k) = \hat{g}(\mathbf{r}(k)) = \langle \boldsymbol{\omega}(k-1), \Phi(\mathbf{r}(k)) \rangle_{\mathbb{H}} \tag{1.2}$$

In 1.2, from basic adaptive filtering theory, it is explicit that for some optimum $\boldsymbol{\omega}(o)$, the obtained estimate ($\hat{d}(k)$) can approximately resemble to the true value ($d(k)$) s.t. $\hat{d}(k) = \langle \boldsymbol{\omega}(o), \Phi(\mathbf{r}(k)) \rangle_{\mathbb{H}} \simeq d(k)$. The $\boldsymbol{\omega}(k-1)$ reach the $\boldsymbol{\omega}(o)$ by iteratively updating $\boldsymbol{\omega}(k-1)$ as follows

$$\boldsymbol{\omega}(k) = \boldsymbol{\omega}(k-1) - \mu \nabla_{\boldsymbol{\omega}(k-1)} \mathcal{J}_k(\boldsymbol{\omega}) \tag{1.3}$$

where $\mathcal{J}_k(\boldsymbol{\omega})$ is the suitable cost function, and $e(k) = d(k) - \langle \boldsymbol{\omega}(k-1), \Phi(\mathbf{r}(k)) \rangle_{\mathbb{H}}$ is the error in estimation.

As shown in (1.3), in order to update $\boldsymbol{\omega}(k)$ iteratively (with increment in k), $\mathcal{J}_k(\boldsymbol{\omega})$ is successively optimized in terms of $\boldsymbol{\omega}(k-1)$ till the minimum of $e(k)$, which in-fact corresponds to the closeness of $\boldsymbol{\omega}(k-1)$ to $\boldsymbol{\omega}(o)$ is reached. For optimum working of the estimator based on KAF, the $\mathcal{J}_k(\boldsymbol{\omega})$ will be chosen according to the statistics of the observation. For instance, if the observation is perturbed by Gaussian distributed thermal noise, mean square error (MSE), i.e. $\mathcal{J}_k(\boldsymbol{\omega}) = \mathbb{E}[|e(k)|^2]$ is the suitable criterion for updating $\boldsymbol{\omega}(k)$. However, in case the observation is perturbed by non-Gaussian clutter, the MSE will not yield suitable results, and therefore, some suitable optimization criterion like maximum correntropy criterion (MCC) and minimum error entropy (MEE) is needed. Different optimization criterion corresponds to a different type of estimators based on KAFs. In this thesis, particularly in Chapter 3, Chapter 4, and Chapter 5, since, the estimation is performed in the presence of thermal noise and clutter, the employed optimizing criterion, cost function, and type of KAF based estimators in accordance with the type of statistics of perturbation are described in Table 1.2.

Table 1.2: Types of criterion, cost function, and KAF based estimators according to a different type of perturbation

Criterion	Cost function ($\mathcal{J}_k(\boldsymbol{\omega})$)	Perturbation	KAF
MSE	$\mathbb{E}[|e(k)|^2]$	Thermal noise	KLMS
MCC	$\mathbb{E}\big[\exp\big(-\frac{e^2(k)}{2\sigma_c^2}\big)\big]$	Thermal noise and clutter	KMC
MEE	$\mathbb{E}[\phi(\mathcal{P}_{e(k)}(e(k)))]$	Thermal noise and clutter	KMEE

where σ_c is the correntropy Gaussian kernel width, $\mathcal{P}_{e(k)}(e(k))$ is the density function of $e(k)$, and ϕ is the entropy function.

For illustration, the performance of estimators based on KLMS, KMC, and KMEE

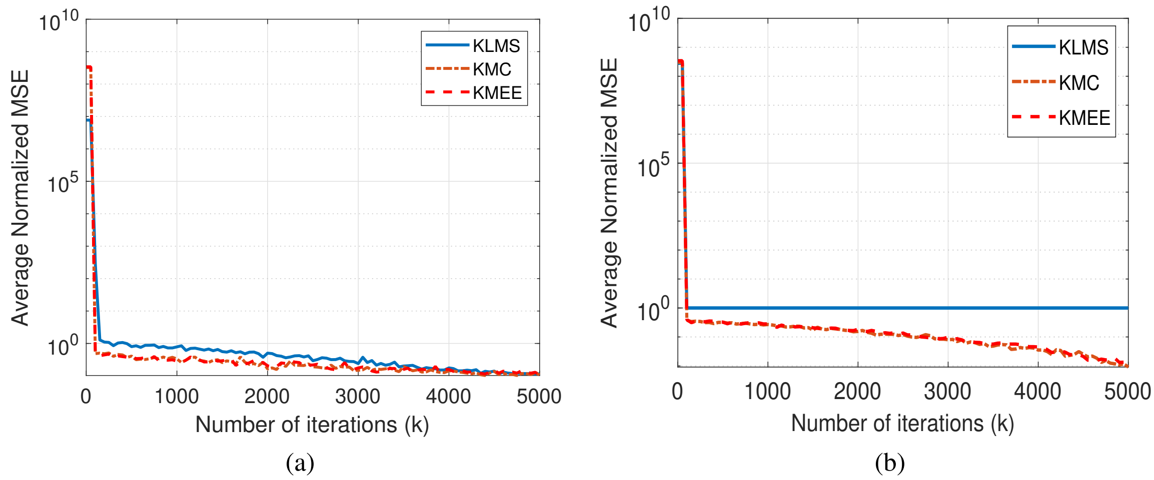

Figure 1.4: Average NMSE in the estimation of Doppler shift in MIMO radar system using estimators based on KLMS, KMC, and KMEE in the presence of (a) Gaussian noise, and (b) Gaussian noise and non-Gaussian clutter.

for estimation of Doppler shift in MIMO radar in the presence of Gaussian distributed thermal noise, and Gaussian distributed thermal noise plus non-Gaussian distributed clutter is shown in Fig. 1.4a, and Fig. 1.4b, respectively. Particularly, as shown in Fig. 1.4a, in the presence of Gaussian noise, minimum and approximately equal normalized MSE (NMSE) is achieved by the estimators based on KLMS, KMC, and KMEE. This is because estimators based on KLMS, KMEE, and KMEE is capable of dealing with Gaussian noise. On the contrary, since the estimator based on KLMS, is not capable of dealing with the effects of non-Gaussian clutter, higher MSE is achieved by the estimator based on KLMS, as shown in Fig. 1.4b. However, estimators based on KMC and KMEE, due to the optimization of MCC and MEE, handles the effect of non-Gaussian clutter and consequently, yield minimum MSE in the estimation.

In Chapter 3 and Chapter 4 (where scalar parameter estimation is considered), if θ_k is the parameter true value to be estimated and $\hat{\theta}_k$ is the estimate of θ_k, then the NMSE for K iterations is defined as $\frac{1}{K}\sum_{k=1}^{K}\frac{(\theta_k-\hat{\theta}_k)^2}{\theta_k^2}$. Similarly, in Chapter 5 (where vector parameter estimation is considered), if $\boldsymbol{\theta}_k$ is the parameter true value to be estimated and $\hat{\boldsymbol{\theta}}_k$ is the estimate of $\boldsymbol{\theta}_k$, then the average NMSE for K iterations is defined as $\frac{1}{K}\sum_{k=1}^{K}\frac{\|\boldsymbol{\theta}_k-\hat{\boldsymbol{\theta}}_k\|^2}{\|\boldsymbol{\theta}_k\|^2}$.

1.4 Introduction to Kalman Filter based Estimation Techniques for Radar Systems

Referring to radar return model $r(m,l)$, illustrated by (1.1) of Subsection 1.3, the unknown information corresponds to range and velocity of the target, denoted by θ_1, and θ_2, respectively, are assumed constant for processing interval of CPI of M pulses. This follows assumption of constant target velocity $vT << \frac{c}{2B}$, i.e. for $T = MT_{\text{PRI}}$, target remains in the same range gate. However, for some radar applications like target tracking, where continuous monitoring of the moving and accelerating target is necessary, the above assumption about the target is ruled out [1, 4, 19]. Therefore, for such radar applications, at an arbitrary time interval of k, if the target is assumed to move with a velocity s.t. causing the target's Doppler shift to increment by Doppler resolution $\left(\frac{1}{T_{\text{PRI}}M}\right)$ which in turn results in increment of delay by delay resolution $\left(\frac{1}{2B}\right)$, the mathematical model defining the state of the target, is formulated as

$$\boldsymbol{\theta}_{k+1} = f(\boldsymbol{\theta}_k) + \boldsymbol{\eta}_k = \boldsymbol{\theta}_k + \Delta\boldsymbol{\theta} + \boldsymbol{\eta}_k, \text{ for } k = [1, 2, \ldots, K] \tag{1.4}$$

where $\boldsymbol{\theta} = [\theta_1 \ \theta_2]^T$, $\Delta\boldsymbol{\theta} = [\frac{1}{2B} \ \frac{1}{T_{PRI}M}]^T$, and $\boldsymbol{\eta}_k$ represents error in modeling the dynamic state of the target.

Using (1.1) and (1.4) with an assumption of perturbation due to thermal noise, the measurement model defining the radar return corresponding to the state model (1.4) is given by

$$\mathbf{y}_{k+1} = h(\mathbf{x}_{k+1}) + \mathbf{v}_{k+1} \tag{1.5}$$

where $h(\mathbf{x}_{k+1}) = \begin{bmatrix} \mathbf{Re}\left(\exp(j2\pi m\boldsymbol{\theta}_{k+1}(1))\exp(j2\pi l\boldsymbol{\theta}_{k+1}(2))\right) \\ \mathbf{Im}\left(\exp(j2\pi m\boldsymbol{\theta}_{k+1}(1))\exp(j2\pi l\boldsymbol{\theta}_{k+1}(2))\right) \end{bmatrix}$, and $\mathbf{v}_k$ represents measurement noise.

The problem of estimating delay and Doppler shift utilizing $r(m,l)$ is formulated as state-space estimation problem consist of state and measurement model as (1.4), and

(1.5), respectively. The celebrated Kalman filter has been effectively used for handling the state space estimation problem [19–22]. Further, in Chapter 6, non-linear versions of the Kalman filter called the extended Kalman filter (EKF), and an unscented Kalman filter (UKF) is developed and found to outperform the conventional estimator based on FT and adaptive estimator based on KLMS developed in Chapter 3. Therefore, in this section, a brief introduction about the basic working of the Kalman filter is given.

The Kalman filter works in two phases a) Prediction and b) Update, over time the filter recursively repeats the prediction and update step until the filter converges to a minimum MSE level. The two phases of the Kalman filter are described as follows:

Prediction: Starting with the initial prediction of state vector, $\hat{\boldsymbol{\theta}}_o$, and initial state error covariance matrix $\mathbf{P}_o = \mathbb{E}[\hat{\boldsymbol{\theta}}_o \hat{\boldsymbol{\theta}}_o^T]$, the state vector and state error covariance matrix at k^{th} time instant are predicted by

$$\begin{aligned}\hat{\boldsymbol{\theta}}_{k|k-1} &= \mathbf{F}_{k-1}\hat{\boldsymbol{\theta}}_{k-1} + \boldsymbol{\eta}_{k-1} \\ \mathbf{P}_{k|k-1} &= \mathbf{F}_{k-1}\mathbf{P}_{k-1}\mathbf{F}_{k-1}^T + \mathbf{Q}_{k-1}\end{aligned} \tag{1.6}$$

where $\mathbf{F}_{k-1}$ is the state matrix, and $\mathbf{Q}_{k-1} = \mathbb{E}[\boldsymbol{\eta}_{k-1}\boldsymbol{\eta}_{k-1}^T]$ is the process covariance matrix

Update: Subsequently, following prediction, using the Kalman gain matrix, $\mathbf{K}_k = \mathbf{P}_k\mathbf{H}_k^T(\mathbf{H}_k\mathbf{P}_k\mathbf{H}_k^T + \mathbf{R}_k)^{-1}$ (where $\mathbf{H}_k$ is the measurement matrix, and $\mathbf{R}_k = \mathbb{E}[\mathbf{v}_k\mathbf{v}_k^T]$ is the measurement noise covariance matrix), the predicted state vector and state error covariance matrix is updated by

$$\begin{aligned}\hat{\boldsymbol{\theta}}_k &= \hat{\boldsymbol{\theta}}_{k|k-1} + \mathbf{K}_k(\mathbf{y}_k - \mathbf{H}_k\hat{\boldsymbol{\theta}}_{k|k-1}) \\ \mathbf{P}_k &= (\mathbf{I} - \mathbf{K}_k\mathbf{H}_k)\mathbf{P}_{k|k-1}\end{aligned} \tag{1.7}$$

In Chapter 6, two estimators based on the non-linear extension of Kalman filter and popularly known as EKF and UKF are developed and tested for LFM radar system. The obtained MSE convergence plot in the estimation of delay for the LFM radar system using estimators based on EKF, UKF, and KLMS Modified-novelty criterion (NC) is shown

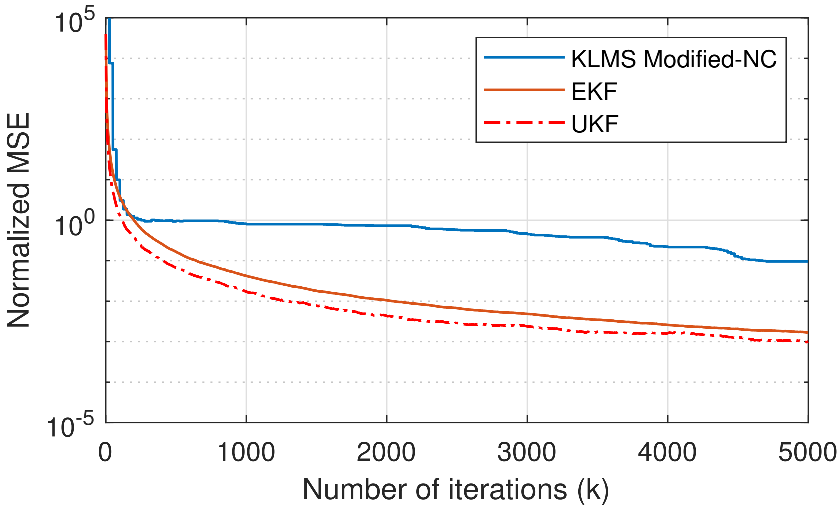

Figure 1.5: Normalized MSE convergence plot in the estimation of delay using estimators based on EKF, UKF, and KLMS Modified-NC.

in Fig. 1.5. As shown in Fig. 1.5, estimators based on EKF and UKF outperforms the estimator based on KLMS Modified-NC (developed in Chapter 3) and achieves minimum MSE of order 10^{-2} in the estimation of delay. Further, as illustrated in Fig. 1.5, UKF provides slightly lower MSE than EKF. The detailed working of the developed estimators based on EKF and UKF is given in Chapter 6.

1.5 Non-Gaussian K-Distributed Clutter

In this thesis, particularly in Chapter 2, Chapter 4, and Chapter 5, to consider the effect of the non-Gaussian radar return, the clutter $\mathbf{c}$ is modeled by a spherically invariant random process (SIRP). SIRP is mathematically described by a local Gaussian distribution with variance modulated by an independent scalar random process [23] and [24]. Hence, the clutter $\mathbf{c}$ can be mathematically modeled as

$$\mathbf{c} \in \mathbb{C}^{N\times 1} = \sqrt{\alpha}\mathbf{z} \tag{1.8}$$

where $\alpha \in \mathbb{R}$ is a Gamma random variable with shape and size parameter, as ν (controls the non-Gaussianity of the clutter) and μ_c (the average power of the clutter), respectively, independent of $\mathbf{z}$, and $\mathbf{z}$ is a complex correlated multi-dimensional Gaussian vector with a normalized covariance matrix $\mathbf{\Sigma_z}$ and zero mean vector, i.e, $\mathbf{z} \in \mathcal{N}_{\mathbb{C}}(\mathbf{0}, \mathbf{\Sigma_z})$. As α is Gamma distributed, $\mathbf{c}$ follows K distribution, which is the generic distribution for modeling clutter.

The probability density function (PDF) of α is given by [25]

$$\mathcal{P}_{\alpha}(\alpha) = \frac{1}{\Gamma(\nu)}\left(\frac{\nu}{\mu}\right)^{\nu} \tau^{(\nu-1)} \exp\left(- \left(\frac{\nu}{\mu}\right)\alpha\right), \quad \alpha \geq 0. \tag{1.9}$$

For a given value of texture enhancement α, and for N-dimensional vector $\mathbf{z}$, PDF of $\mathbf{c}$ is given as

$$\mathcal{P}_{\mathbf{c}|\alpha}(\mathbf{c} \mid \alpha) = \frac{1}{\pi^N |\mathbf{\Sigma}_{\mathbf{c}|\alpha}|} \exp(-\mathbf{c}^H \mathbf{\Sigma}_{\mathbf{c}|\alpha}^{-1} \mathbf{c}), \tag{1.10}$$

where $\mathbf{\Sigma}_{\mathbf{c}|\alpha}$ is given by

$$\mathbf{\Sigma}_{\mathbf{c}|\alpha} = \mathbb{E}\{\mathbf{c}\mathbf{c}^H \mid \alpha\} = \mathbb{E}\{\sqrt{\alpha}\mathbf{z}\sqrt{\alpha}\mathbf{z}^H\} = \alpha\mathbf{\Sigma_z}. \tag{1.11}$$

Substituting (6.13) in (1.10) yields the final expression for the PDF of $\mathbf{c}$ given α as,

$$\mathcal{P}_{\mathbf{c}|\alpha}(\mathbf{c} \mid \alpha) = \frac{1}{\pi^N \alpha^N |\mathbf{\Sigma_z}|} \exp\left(- \frac{\mathbf{c}^H \mathbf{\Sigma_z}^{-1} \mathbf{c}}{\alpha}\right). \tag{1.12}$$

Finally, expression for the PDF of K-distributed clutter ($\mathbf{c}$) is obtained by averaging (1.12) with respect to α and is expressed as

$$\mathcal{P}(\mathbf{c}) = \int_0^{\infty} \mathcal{P}_{\mathbf{c}|\alpha}(\mathbf{c} \mid \alpha)\mathcal{P}_{\alpha}(\alpha) d\alpha. \tag{1.13}$$

1.6 Thesis Outline and Contributions

The organization and contributions of the thesis are described as follows:

Chapter 1. Introduction: In this Chapter, firstly, the motivation behind the work is given, which is followed by a brief discussion of various topics used in the development of detection and estimation algorithms. The thesis outline and a summary of thesis contributions are given in the last.

Chapter 2. Target Detection in Sea Clutter using OFDM Radar: In this Chapter, a method is developed for the detection of a small boat in the sea environment using the OFDM waveform. Firstly, a technique is proposed to generate radar return for OFDM waveform using collected real-time radar return data for stepped frequency waveform. Subsequently, the mathematical model for the estimated radar return data corresponding to the OFDM waveform is derived. Further, a detection test based on modified GLRT is proposed for the derived signal model and surveillance environment. Simulation results reveal the improvement in target detection employing OFDM waveform over SF waveform and conventional normalized matched filter (NMF). The performance is further improved as the number of OFDM sub-carriers increases.

Chapter 3. Range and Velocity Estimation in Gaussian Noise: In this Chapter, adaptive estimators based on the KLMS algorithm are proposed. Further, to facilitate sparse learning without affecting estimator's performance, Platt's NC is used to limit the increasing size of the training samples, result in estimator based on KLMS-NC. Additionally, a technique for tuning the kernel width from observations is proposed and is found to be suitable in terms of MSE and computational complexity. Furthermore, an analytical expression is derived for the Cramer-Rao Lower Bound (CRLB) of the proposed estimators. Lastly, from the simulations, it is observed that the variance of the estimates corresponding to the proposed estimators is lower than the existing non-adaptive estimation techniques, and is closer to the achievable CRLB.

Chapter 4. Range and Velocity Estimation in non-Gaussian Clutter: In this Chapter, for estimation of target's range and velocity in the presence of non-Gaussian clutter, two new KMC based estimation algorithms are proposed. Estimation is performed utilizing MCC in RKHS, which provides accurate estimate in the presence of non-Gaussian clutter. Further, to facilitate sparse learning, and for lowering computational complexity without affecting estimator-performance, NC is used to limit the increasing size of training samples and the resulting estimator is named KMC-NC. Additionally, a technique is explored for tuning the hyper-parameter σ from radar returns, and an adaptive update equation is derived for its convergence to an appropriate value. Subsequently, for the considered radar systems analytical expressions are derived for the CRLBs of the proposed RKHS based estimators. Lastly, simulations performed over realistic LFM and SF radar systems reveal that the proposed KMC based estimators provide significant gain over existing KLMS based estimators along with lower computational complexity.

Chapter 5. Estimator for MIMO Radar: In this Chapter, an estimator for DOD, DOA, and Doppler shift for multiple targets using MIMO radar in the presence of non-Gaussian clutter is proposed. The effect of non-Gaussian clutter is handled by introducing the adaptive estimator based on KMEE. Additionally, the computational complexity is reduced by the incorporation of the sparsification technique based on NC, and the resulting estimator is termed KMEE-NC. Performance of the proposed algorithm is compared with the derived MCRLB for DOD, DOA, and Doppler shift. Further, the accuracy of the proposed estimator is validated through computer simulations over realistic MIMO radar systems. The obtained simulation results reveal the viability of the proposed KMEE-NC based estimator over another counterpart kernel-based adaptive estimators and conventional estimators.

Chapter 6. Range and Velocity Estimation using EKF and UKF based estimators: In this Chapter, two new estimation techniques, based on EKF and UKF, for both delay and Doppler shift estimation are proposed. The EKF is advantageous due to its implementation simplicity and fast computation; however, a derivative-based implementation limits its use. The UKF outperforms the EKF and offers better stability due to a derivative-free implementation. Better performance of the proposed estimators is guaranteed by the proximity of the variance of the proposed estimator to CRLB in contrast to conventional estimators based on FT and KLMS.

Chapter 7. Conclusion, Limitations and Future Work: In this Chapter, the conclusions drawn from the contributions and results of all Chapters are summarized. Further, the scope for extension of the present work is also discussed.

Chapter 2

Target Detection in Sea Clutter using OFDM Radar

As shown in Fig.1.1 of Chapter 1 1, the primary step in the processing of radar return after discretization is detection. Detection indicates the presence of targets in the surveillance environment[1, 4]. Thus, in this Chapter, for detection of target in sea clutter, one of the newer types of multi-carrier waveform is explored for surveillance in marine environment. Studies have shown potential merits of multi-carrier waveform like OFDM over traditionally used waveforms [5–7, 10, 11, 26, 27]. Some of these advantages include waveform diversity which leads to better detection performance[28–30]. However, to the best of authors' knowledge, the merits of OFDM waveform have not yet been verified and validated using real radar return from sea clutter. The system model considered in the literature either considers a noise-free environment or the environment where clutter and thermal noise follows a Gaussian distribution. This makes the existing algorithms unsuitable for practical radar environment, which is affected by the interference that follows a non-Gaussian distribution. Moreover, as [8, 13, 31] lack in measuring the performance of target detector, their robustness and suitability against dynamic interference environment is not guaranteed.

With the intent of analyzing the performance of OFDM waveform for marine application, firstly, a technique to estimate the radar return for the OFDM waveform utilizing the available radar return data set for SF waveform is proposed. The data set for SF waveform is taken from CSIR 2006 OTB 2006 Measurement Trial [32]. The estimation of radar return is done in two steps. In the first step, impulse response (IR) of the radar system for a single CPI is estimated by LS [33]. Then, the estimated IR is used for the estimation of OFDM radar return. Further, a detailed analytical expression for the system model corresponding to the estimated data at a particular range gate is proposed. Furthermore, the GLRT based sub-optimum detector is proposed, and its performance is compared with the existing NMF (optimum for conventional radar) [34]. Finally, to verify improvement in the performance of detection test, the analytical expression of the P_{FA}, and P_{D} for the proposed detection test are derived.

The rest of the Chapter is organized as follows: Method to transform radar return data for SF waveform into radar return for OFDM waveform is described first. Then, the proposed OFDM radar system model for the considered surveillance environment is described. Next Section discussed the proposed modified target detection algorithm for a single range gate and fixed CPI. Further, analytical expression for P_{D} and P_{FA} for the proposed detection algorithm under Gaussian assumption are derived. Subsequently, simulation results for the estimated IR of the radar channel and the proposed detector's performance obtained from estimated OFDM radar return data are given. Performance of the proposed detector obtained by the analytical expressions for ROC and P_{FA} is discussed next. Finally, the last Section concludes the work.

2.1 Estimation of Radar Return

To obtain the radar returns for the OFDM waveform, the complete radar system (including radar channel, down converter, a pulse compressor, and sampler), which was used to record the original radar returns for SF waveform ($y_{\text{SFW}}(n)$), is modeled as finite impulse response (FIR) filter. Two main steps of data transformation are: estimation of radar system IR and estimation of the response of the radar system for OFDM waveform (considered as echoes for OFDM waveform).

2.1.1 Estimation of Radar Impulse Response

Without loss of generality, let the radar system IR be approximated as an complex FIR filter IR with K-unknown complex coefficients $\mathbf{h} \in \mathbb{C}^{K\times1} = [h(0), h(1), \cdots, h(K-1)]^T$. Following this assumption, the response of an unknown radar system in terms of the transmitted signal (x_{SFW}) in the time domain is given by

$$y_{\text{SFW}}(n) = \sum_{k=0}^{K-1} h(k)x_{\text{SFW}}(n-k) + e(n), \; n = 0, 1, \cdots, N-1, \tag{2.1}$$

where $e(n)$ is the error in approximating the radar system as FIR filter [34, 35], $n = (0, 1, \cdots, N-1)$ represents the index for the dimension of the fast time within one CPI, $y_{\text{SFW}}(n)$ represents the radar return for SFwaveform.

For known values of $y_{\text{SFW}}(n)$ and $x_{\text{SFW}}(n)$, values of filter coefficients $\mathbf{h}$ can be estimated by minimizing the LS cost function [34], given as

$$\mathcal{J}(\mathbf{h}) = \sum_{n=0}^{N-1} \mid e(n) \mid^2 = \|\mathbf{e}\|^2 \,, \tag{2.2}$$

where, $\mathbf{e} \in \mathbb{C}^{N\times1} = [e(0), e(1), \cdots, e(N-1)]^T$.

Term $\mathbf{e}$ in (2.2), can then be written as

$$\mathbf{e} = \mathbf{y}_{\text{SFW}} - \mathbf{X}_{\text{SFW}}\mathbf{h}, \tag{2.3}$$

where $\mathbf{y}_{\text{SFW}} \in \mathbb{C}^{N\times1} = [y_{\text{SFW}}(0), y_{\text{SFW}}(1), \cdots, y_{\text{SFW}}(N-1)]^T$,

$$\mathbf{X}_{\text{SFW}} \in \mathbb{C}^{N\times K} = \begin{bmatrix} x_{\text{SFW}}(0) & x_{\text{SFW}}(-1) & \dots & x_{\text{SFW}}(-(K-1)) \\ x_{\text{SFW}}(1) & x_{\text{SFW}}(0) & \dots & x_{\text{SFW}}(1-(K-1)) \\ \vdots & \vdots & \vdots & \vdots \\ x_{\text{SFW}}(N-1) & x_{\text{SFW}}(N-2) & \dots & x_{\text{SFW}}(N-(K-1)) \end{bmatrix}$$

and $\mathbf{h} = [h(0), h(1), \cdots, h(K-1)]^T$.

From (2.3) and (2.2), yield

$$\begin{aligned}\mathcal{J}(\mathbf{h}) &= \|\mathbf{y}_{\text{SFW}} - \mathbf{X}_{\text{SFW}}\mathbf{h}\|^2 = (\mathbf{y}_{\text{SFW}} - \mathbf{X}_{\text{SFW}}\mathbf{h})^H(\mathbf{y}_{\text{SFW}} - \mathbf{X}_{\text{SFW}}\mathbf{h}) \\ &= \mathbf{y}_{\text{SFW}}^H\mathbf{y}_{\text{SFW}} - \mathbf{y}_{\text{SFW}}^H\mathbf{X}_{\text{SFW}}\mathbf{h} - (\mathbf{X}_{\text{SFW}}\mathbf{h})^H\mathbf{y}_{\text{SFW}} + (\mathbf{X}_{\text{SFW}}\mathbf{h})^H(\mathbf{X}_{\text{SFW}}\mathbf{h}).\end{aligned} \tag{2.4}$$

To obtain the value of **h** which minimizes (2.4), the differentiation of (2.4) with respect to **h** is equated to zero as

$$\mathbf{X}_{\text{SFW}}{}^H\mathbf{X}_{\text{SFW}}\mathbf{h} - \mathbf{X}_{\text{SFW}}^H\mathbf{y}_{\text{SFW}} = 0. \tag{2.5}$$

From (2.5), the estimate of **h** is given by

$$\hat{\mathbf{h}} = (\mathbf{X}_{\text{SFW}}^H\mathbf{X}_{\text{SFW}})^{-1}\mathbf{X}_{\text{SFW}}^H\mathbf{y}_{\text{SFW}}. \tag{2.6}$$

2.1.2 Estimation of Radar Response for OFDM Pulsed Waveform

After estimating the filter coefficients of the radar system, response of the radar system (modeled by the FIR system) for the OFDM waveform is evaluated. For IR estimation and radar return data estimation, the response of the radar system is calculated for single CPI, and given by the convolution of $\hat{h}(k)$ and $x_{\text{OFDM}}(k)$. The following relationship in time domain describes the response of the radar system for OFDM waveform

$$y_{\text{OFDM}}(n) = \sum_{k=0}^{K-1} \hat{h}(k)x_{\text{OFDM}}(n-k), n = 0, 1, \cdots, N-1.$$

Arranging $y_{\text{OFDM}}(n)$ in vector yields the estimated radar return for OFDM waveform as

$$\mathbf{y}_{\text{OFDM}} = \mathbf{X}_{\text{OFDM}}\hat{\mathbf{h}}. \tag{2.7}$$

To validate the correctness of the measured OFDM radar return data, Doppler processing over measured OFDM radar return and available SF radar return data set are shown in Fig. 2.1a and Fig. 2.1b, respectively. As shown in Fig. 2.1a and Fig. 2.1b, the Doppler spectrum of measured OFDM radar return follows the Doppler spectrum of original SF radar return.

2.1.3 System Model

In this section, a system model for the estimated data is proposed, and the analytical expression corresponding to the estimated scattered radar return for the OFDM waveform is described.

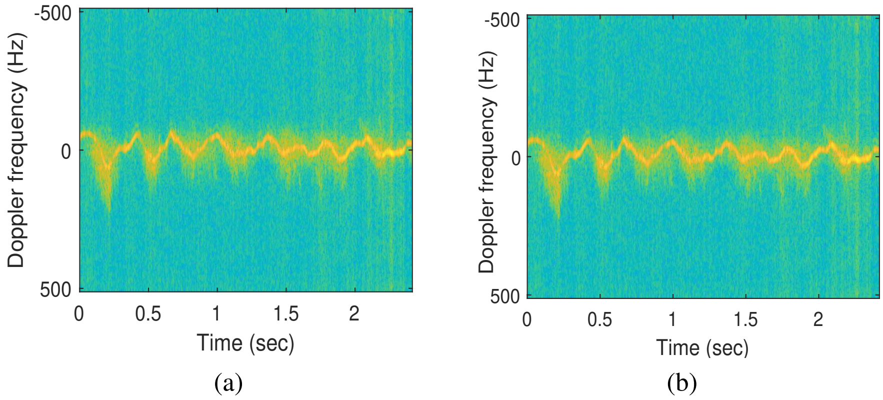

Figure 2.1: (a) Doppler spectrum of measured OFDM radar return, (b) Doppler spectrum of original SF radar return data set.

Let us consider an OFDM waveform $s(t)$ of L-sub-carriers modulated by complex a_l phase codes from the set $\mathbf{a} = [a_0, a_1, ..., a_{L-1}]$. If the sub-carriers in frequency domain are spaced by Δf, then the expression for $s(t)$ is given by

$$s(t) = \sum_{l=0}^{L-1} a_l \exp(j2\pi l \Delta f t) \ \text{ for } \ 0 \leq t \leq T_o. \tag{2.8}$$

where T_o is the OFDM waveform duration without cyclic prefix. The sub-carriers are orthogonal for $T_o = \frac{1}{\Delta f}$. In this work, the echoes of the prior pulse reach the receiver before the next pulse is transmitted, thereby avoiding inter-symbol interference [36].

Let f_c be the center frequency of transmission; then the transmitted signal is given by

$$\tilde{S}(t) = s(t)\exp(j2\pi f_c t) = \sum_{l=0}^{L-1} a_l \exp(j2\pi f_l t). \tag{2.9}$$

where $f_l = f_c + l\Delta f$ is the sub-carrier frequency.

Radar return corresponding to $\tilde{S}(t)$ is the sum of delayed and time scaled version of $\tilde{S}(t)$. Let us consider that the radar surveillance environment consists of P scatterers out of which one is the target and others represent clutter. Scatterers are at distances $(R_p)_{p=1}^{P}$, moving with a velocity vector $(\mathbf{v}_p)_{p=1}^{P}$ and causing the delay $(\tau_p)_{p=1}^{P}$. The complex scattering coefficient (x_{lp}) of p^{th} scatterer for l^{th} sub-carrier is unknown but deterministic.

After making these basic assumptions, the received radar return for the l^{th} sub-carrier and for the p^{th} scatterer is given by

$$\tilde{r}_{lp}(t) = x_{lp}\tilde{s}_l(\gamma_p(t - \tau_p)) + \tilde{w}_l(t), \tag{2.10}$$

where $\tilde{s}_l = a_l \exp(j2\pi f_l t)$. The $\gamma_p = 1 + \beta_p$, where $\beta_p = \frac{2\langle \vec{\mathbf{v}}_p, \mathbf{u}\rangle}{c}$ is the relative Doppler shift of the p^{th} scatterer and c is the velocity of light, and $\tilde{w}_l$ represents the thermal noise along the l^{th} subchannel. Hence, the received signal return from P scatterer along L subchannels is given by

$$\tilde{r}(t) = \sum_{p=1}^{P}\sum_{l=0}^{L-1} r_{lp}(t). \tag{2.11}$$

Substituting (2.10) in (2.11), yields

$$\tilde{r}(t) = \left\{\sum_{p=1}^{P}\sum_{l=0}^{L-1} a_l x_{lp} \exp(j2\pi l\Delta f(t - \tau_p)) \exp(j2\pi f_l \beta_p(t - \tau_p))\right\} \exp(j2\pi f_c t) + \tilde{w}(t), \tag{2.12}$$

where $\tilde{w}(t)$ is the combined effect of thermal noise across all L subchannels and P scatterers i.e $\tilde{w}(t) = \sum_{p=1}^{P}\sum_{l=0}^{L-1} \tilde{w}_l(t)$.

Thus, the corresponding complex envelope after removing the carrier $(\exp(j2\pi f_c t))$ is given by

$$r(t) = \sum_{p=1}^{P}\sum_{l=0}^{L-1} a_l x_{lp} \exp(j2\pi l\Delta f(t - \tau_p)) \exp(j2\pi f_l \beta_p(t - \tau_p)) + w(t). \tag{2.13}$$

Since the estimated data set is the radar return from the single target, (2.13) can be simplified by separating the terms for the phase shifts corresponding to the target.

Remaining $P-1$ terms in the outer summation corresponds to the sea clutter. Thus, (2.13) can be written as

$$r(t) = \sum_{l=0}^{L-1} a_l x_{lt} \exp(j2\pi l\Delta f(t-\tau_t)) \exp(j2\pi f_l \beta_t (t-\tau_t)) + c(t) + w(t), \tag{2.14}$$

where x_{lt}, τ_t, and β_t are the scattering coefficient, delay and relative Doppler shift respectively, corresponding to the target, and $c(t)$ represent the clutter.

Before further processing, (2.14) is sampled with the sampling interval of $mT_{\text{PRI}} + \tau_t$, $m = 0, 1, ..., M-1$, where m is the index for slow time dimension. Hence, the discrete complex envelope of the received signal at the output of the l^{th} subchannel is

$$r_l(m) = a_l x_{l_t} \exp(j2\pi m f_{lD_t} T_{\text{PRI}}) + c_l(m) + w_l(m) \; l = 0, 1, ..., L-1, \; m = 0, 1, ..., M-1, \tag{2.15}$$

where the constant $\exp(j2\pi ml\Delta f T_{\text{PRI}})$ is considered along with the scattering coefficient (x_{lt}), and $f_{lD_t} = (f_c + l\Delta f)\frac{2\langle \vec{v}_{Pt}, \boldsymbol{u}\rangle}{c}$ is the Doppler shift along l^{th} subchannel.

Arranging returns of all L subchannels into one $L \times 1$ dimension vector, yields

$$\mathbf{r}(m) = \mathbf{A}\mathbf{X}_t \boldsymbol{\phi}(m) + \mathbf{c}(m) + \mathbf{w}(m), \; m = 0, 1, ..., M-1, \tag{2.16}$$

where

- $\mathbf{r}(m) = [r_0(m), r_1(m), ..., r_{L-1}(m)]^T$ is the $L \times 1$ dimension vector of sub-carrier return,
- $\mathbf{A} = \mathbf{diag}[a_0, a_1, ..., a_{L-1}]$ is the $L \times L$ diagonal matrix of optimized (peak to average power ratio (PAPR)) transmitted phase codes,
- $\mathbf{X}_t = \mathbf{diag}[x_{0_t}, x_{1_t}, ..., x_{(L-1)_t}]$ is the $L \times L$ diagonal matrix of scattering coefficients across L subchannels,
- $\boldsymbol{\phi}(m) = [\exp(j2\pi m f_{0D_t} T_{\text{PRI}}), \exp(j2\pi m f_{1D_t} T_{\text{PRI}}), ..., \exp(j2\pi m f_{(L-1)D_t} T_{\text{PRI}})]^T$ is the $L \times 1$ dimension vector of phase shifts corresponding to different Doppler frequencies $f_{D_t} = [f_{0D_t}, f_{1D_t}, ..., f_{(L-1)D_t}]$ across L subchannels,

- $\mathbf{c}(m) = [c_0(m), c_1(m), ..., c_{L-1}(m)]^T$ is the $L \times 1$ dimension vector of sea clutter return across L subchannels,

- $\mathbf{w}(m) = [w_0(m), w_1(m), ..., w_{L-1}(m)]^T$ is the $L \times 1$ dimension vector of the samples of thermal noise across L subchannels.

Subsequently, concatenating all the temporal radar return data column-wise into a matrix of dimension $L \times M$, the mathematical description for the OFDM radar return matrix whose columns corresponds to the estimated OFDM radar return data is given by

$$\mathbf{R} = \mathbf{A}\mathbf{X}_t\mathbf{\Phi} + \mathbf{C} + \mathbf{W}. \tag{2.17}$$

where

- $\mathbf{R} = [\mathbf{r}(0), \mathbf{r}(1), ..., \mathbf{r}(M-1)]$ is the $L \times M$ matrix of all temporal returns,

- $\mathbf{\Phi} = [\boldsymbol{\phi}(0), \boldsymbol{\phi}(1), ..., \boldsymbol{\phi}(M-1)]$ is the $L \times M$ matrix of phase shifts corresponding to temporal components m,

- $\mathbf{C} = [\mathbf{c}(0), \mathbf{c}(1), ..., \mathbf{c}(M-1)]$ is the $L \times M$ matrix representing sea clutter returns follows the distribution define in Section 1.5 of Chapter 1,

- $\mathbf{W} = [\mathbf{w}(0), \mathbf{w}(1), ..., \mathbf{w}(M-1)]$ is the $L \times M$ matrix representing additive white Gaussian noise (AWGN) samples s.t. $\mathbf{w}(m) \in \mathcal{N}_{\mathbb{C}}(\mathbf{0}, \Omega_w^2\mathbf{I})$.

2.2 Target Detection Test

In this section, a target detection test for the considered OFDM radar model perturbed by sea clutter as described in (2.17) is proposed. The sea clutter follows the distribution described in Subsection 1.5 of Chapter 1. For target detection, the proposed detection algorithm is described next. Following this, to verify correctness of the detection test, an analytical expression for P_{D} and P_{FA} of the detection test statistics is derived. The obtained theoretical expression for P_{D} and P_{FA} validates ROC of the proposed detection algorithm.

2.2.1 Modified Target Detection Test

In this section, for target detection, a sub-optimal GLRT based detector is developed and discussed. The detector described in [37], proposed detection of the perfectly known signal by considering the unknown texture enhancement factor α, and the known covariance matrix $\mathbf{\Sigma_z}$ of speckle component ($\mathbf{z}$). From (2.16), due to unknown scattering coefficient $\mathbf{X}_t$, the signal is not perfectly known at the receiver. Additionally, the covariance matrix $\mathbf{\Sigma_z}$ is also unknown. As the proposed system model (2.17) has unknown but deterministic $\mathbf{X}_t$, and it is applied over both the estimated radar return data and simulated data, the detection test is modified by replacing the unknown $\mathbf{X}_t$ and $\mathbf{\Sigma_z}$ in GLRT by their ML estimates.

There are two hypothesis to perform the detection test, $\mathcal{H}_0$ for target absent, and $\mathcal{H}_1$ for target present. Hence, after applying assumption of sea clutter dominance over the thermal noise, (2.17) yields

$$\begin{aligned} \mathcal{H}_1 :& \mathbf{r}_v = \mathbf{p}_v + \mathbf{c}_v, \\ \mathcal{H}_0 :& \mathbf{r}_v = \mathbf{c}_v, \end{aligned} \tag{2.18}$$

where $\mathbf{r}_v = \mathrm{vec}(\mathbf{R})$, $\mathbf{p}_v = \mathrm{vec}(\mathbf{A}\mathbf{X}_t\mathbf{\Phi})$, and $\mathbf{c}_v = \mathrm{vec}(\mathbf{C})$.

Test statistics $\Lambda(\mathbf{r})$ is the ratio of likelihood of $\mathbf{r}_v$ for two different hypothesis $\mathcal{H}_0$ and $\mathcal{H}_1$.

$$\Lambda(\mathbf{r}_v) = \frac{\mathcal{P}(\mathbf{r}_v; \hat{\mathbf{X}}_t; \hat{\mathbf{\Sigma}}_1, \mathcal{H}_1)}{\mathcal{P}(\mathbf{r}_v; \hat{\mathbf{\Sigma}}_0, \mathcal{H}_0)} \underset{\mathcal{H}_0}{\overset{\mathcal{H}_1}{\gtrless}} \lambda, \tag{2.19}$$

where $\mathcal{P}(\mathbf{r}_v; \hat{\mathbf{X}}_t; \hat{\mathbf{\Sigma}}_1, \mathcal{H}_1)$ [1] is the PDF of $\mathbf{r}_v$ under hypothesis $\mathcal{H}_1$. Since under hypothesis $\mathcal{H}_1$, $\mathbf{X}_t$ and $\mathbf{\Sigma}_1$ are unknown, $\mathcal{P}(\mathbf{r}_v; \hat{\mathbf{X}}_t; \hat{\mathbf{\Sigma}}_1, \mathcal{H}_1)$ is parametrized by the estimates of $\mathbf{X}_t$ and $\mathbf{\Sigma}_1$. Similarly, $\mathcal{P}(\mathbf{r}_v; \hat{\mathbf{\Sigma}}_0, \mathcal{H}_0)$ is the PDF of $\mathbf{r}_v$ under hypothesis $\mathcal{H}_0$. Similar to case with hypothesis $\mathcal{H}_1$, since under hypothesis $\mathcal{H}_0$, $\mathbf{\Sigma}_0$ is unknown, the PDF ($\mathcal{P}(\mathbf{r}_v; \hat{\mathbf{\Sigma}}_0, \mathcal{H}_0)$) is parametrized by the estimates of $\mathbf{\Sigma}_0$. Further, $\hat{\mathbf{X}}_t$ is the ML estimate of scattering coefficient matrix $\mathbf{X}_t$. The $\hat{\mathbf{\Sigma}}_1$, and $\hat{\mathbf{\Sigma}}_0$ are the ML estimates of covariance matrices $\mathbf{\Sigma}_1$,

[1] the semicolon (;) is used to represent parametrization, and comma "," represents under a hypothesis.

and $\mathbf{\Sigma}_0$, respectively.

As no close form expression for $\mathcal{P}(\mathbf{r}_v;\hat{\mathbf{X}}_t;\hat{\mathbf{\Sigma}}_1,\mathcal{H}_1)$ and $\mathcal{P}(\mathbf{r}_v;\hat{\mathbf{\Sigma}}_0,\mathcal{H}_0)$ is available, (2.19) can be further simplified as

$$\Lambda(\mathbf{r}_v) = \frac{\int_0^\infty \mathcal{P}(\mathbf{r}_v \mid \alpha;\hat{\mathbf{X}}_t;\hat{\boldsymbol{\alpha}}_{1|\alpha},\mathcal{H}_1)\mathcal{P}_\alpha(\alpha)d\alpha}{\int_0^\infty \mathcal{P}(\mathbf{r}_v \mid \alpha;\hat{\mathbf{\Sigma}}_{0|\alpha},\mathcal{H}_0)\mathcal{P}_\alpha(\alpha)d\alpha} \underset{\mathcal{H}_0}{\overset{\mathcal{H}_1}{\gtrless}} \lambda. \tag{2.20}$$

where $\mathcal{P}(\mathbf{r}_v \mid \alpha;\hat{\mathbf{X}}_t;\hat{\mathbf{\Sigma}}_{1|\alpha},\mathcal{H}_1)$ and $\mathcal{P}(\mathbf{r}_v \mid \alpha;\hat{\mathbf{\Sigma}}_{0|\alpha},\mathcal{H}_0)$ are the conditional PDF of $\mathbf{r}_v$ under hypothesis $\mathcal{H}_1$ and $\mathcal{H}_0$, respectively, conditioned on α.

For formulating the GLRT, firstly, the texture (α) under both hypothesis supposing that all other parameters are known are estimated, then the remaining unknown parameters are replaced by their ML estimates.

From [37], for a known covariance matrix $\mathbf{\Sigma}_\mathbf{z}$, the $\hat{\mathbf{\Sigma}}_{0|\alpha} = \hat{\alpha}_0\mathbf{\Sigma}_\mathbf{z}$, and $\hat{\mathbf{\Sigma}}_{1|\alpha} = \hat{\alpha}_1\mathbf{\Sigma}_\mathbf{z}$. Since, $\mathbf{z}$ is Gaussian distributed correlated random process [25, 37, 38], the $\hat{\alpha}_0$ and $\hat{\alpha}_1$ are considered to be the ML estimates of the unknown clutter powers. The same are estimated by considering the following two likelihood functions

$$\mathcal{P}(\mathbf{r}_v|\alpha_0;\mathcal{H}_0) = \frac{1}{\pi^M\alpha_0^M|\mathbf{\Sigma}_\mathbf{z}|}\exp(\frac{-\mathbf{r}_v^H\mathbf{\Sigma}_\mathbf{z}^{-1}\mathbf{r}_v}{\alpha_0}),$$
$$\mathcal{P}(\mathbf{r}_v|\alpha_1;\mathcal{H}_1) = \frac{1}{\pi^M\alpha_1^M|\mathbf{\Sigma}_\mathbf{z}|}\exp(\frac{-(\mathbf{r}_v-\mathbf{p}_v)^H\mathbf{\Sigma}_\mathbf{z}^{-1}(\mathbf{r}_v-\mathbf{p}_v)}{\alpha_1}). \tag{2.21}$$

Hence, ML estimate of α_0 and α_1 is given by

$$\hat{\alpha}_0 = \frac{1}{M}\mathbf{r}_v^H\mathbf{\Sigma}_\mathbf{z}^{-1}\mathbf{r}_v.$$
$$\hat{\alpha}_1 = \frac{1}{M}(\mathbf{r}_v-\mathbf{p}_v)^H\mathbf{\Sigma}_\mathbf{z}^{-1}(\mathbf{r}_v-\mathbf{p}_v). \tag{2.22}$$

Using (2.20), (2.21), and (2.22), the test statistics $\Lambda(\mathbf{r}_v)$ is given by

$$\Lambda(\mathbf{r}_v) \in \mathbb{R} = \left(\frac{\hat{\alpha}_0}{\hat{\alpha}_1}\right)^M \underset{\mathcal{H}_0}{\overset{\mathcal{H}_1}{\gtrless}} \lambda = \left(\frac{\hat{\alpha}_0}{\hat{\alpha}_1}\right) \underset{\mathcal{H}_0}{\overset{\mathcal{H}_1}{\gtrless}} \lambda', \tag{2.23}$$

where $\lambda' = (\lambda)^{\frac{1}{M}}$.

Substituting (2.22) in (2.23), yields the final expression for test statistics as

$$\Lambda(\mathbf{r}_v) = \frac{\mathbf{r}_v^H \hat{\boldsymbol{\Sigma}}_{\mathbf{z}}^{-1} \mathbf{r}_v}{(\mathbf{r}_v - \mathrm{vec}(\mathbf{A}\hat{\mathbf{X}}_t\boldsymbol{\Phi}))^H \hat{\boldsymbol{\Sigma}}_{\mathbf{z}}^{-1} (\mathbf{r}_v - \mathrm{vec}(\mathbf{A}\hat{\mathbf{X}}_t\boldsymbol{\Phi}))} \underset{\mathcal{H}_0}{\overset{\mathcal{H}_1}{\gtrless}} \lambda^{'}. \tag{2.24}$$

where $\hat{\boldsymbol{\Sigma}}_{\mathbf{z}} = \frac{1}{I}\sum_{i=1}^{I}\left(\frac{M}{\mathbf{r}_v^{i\,H}\mathbf{r}_v^{i}}\right)\mathbf{r}_v^{i}\mathbf{r}_v^{i\,H}$ is the ML estimate of speckle covariance matrix $\boldsymbol{\Sigma}_{\mathbf{z}}$ obtained from the I observations of $\mathbf{r}_v$ from different range gates under hypothesis $\mathcal{H}_0$, and $\hat{\mathbf{X}}_t = \mathbf{diag}(\mathbf{diag}(\mathbf{A}^{-1}\mathbf{R}\boldsymbol{\Phi}^H(\boldsymbol{\Phi}\boldsymbol{\Phi}^H)^{-1}))$ is the ML estimate of $\mathbf{X}_t$.

2.2.2 Theoretical Analysis of Proposed Detector

From (2.24), it can be analyzed that for a given clutter power $\mu\mathbf{tr}(\boldsymbol{\Sigma}_{\mathbf{z}})$, better estimate of $\mathbf{X}_t$ yields higher value of test statistics $\Lambda(\mathbf{r}_v)$ which in turn improves the proposed detector's performance. In (2.24), for fixed signal to clutter ratio (SCR) $= \frac{\mathbf{p}_v^H\mathbf{p}_v}{2\mu\mathbf{tr}(\boldsymbol{\Sigma}_{\mathbf{z}})}$, increasing L yields better estimate of $\mathbf{X}_t$ ($\hat{\mathbf{X}}_t$). Consequently, as $\hat{\mathbf{X}}_t$ approaches $\mathbf{X}_t$, the denominator in (2.24) reduces further, thereby increasing the value of $\Lambda(\mathbf{r}_v)$. Subsequently, $\Lambda(\mathbf{r}_v)$ crosses $\lambda^{'}$ more number of times, and hence results in better target detection. Therefore, for same P_{FA} and λ, in addition to providing frequency diversity, the OFDM waveform provides additional information about the target from multiple scattering centers, which resonate differently at different sub-carrier frequency [5].

Further, a closed-form expression for P_{D} and P_{FA} for K-distributed clutter is difficult to achieve, hence the sea clutter is assumed to be uncorrelated Gaussian distributed. This assumption is feasible for a very high value of shape parameter ν, as given in [25], generally for $\nu \gtrsim 20$, the PDF $\mathcal{P}_{\alpha}(\alpha)$ can be denoted as a Dirac function concentrated around the deterministic value $\alpha = \mu_c$. Consequently, as $\mathcal{P}_{\mathbf{c}_v}(\mathbf{c}_v) = \int_0^{\infty}\mathcal{P}_{\mathbf{c}_v|\alpha}(\mathbf{c}_v|\alpha)\mathcal{P}_{\alpha}(\alpha)d\alpha$, the clutter PDF $\mathcal{P}_{\mathbf{c}_v}(\mathbf{c}_v)$ reduces to multivariate Gaussian. For mathematical tractability and simplicity of theoretical analysis, the test statistics in (2.23) is represented as

$$\Lambda'(\mathbf{r}_v) = \Lambda(\mathbf{r}_v)^{\frac{1}{M}} - 1 = \left(\frac{\hat{\alpha}_0}{\hat{\alpha}_1}\right) - 1. \tag{2.25}$$

For Gaussian distributed sea clutter, the ML estimates ($\hat{\alpha}_0$ and $\hat{\alpha}_1$) are given by

$$\hat{\alpha}_0 = \frac{1}{M}\mathbf{tr}(\mathbf{R}^H\mathbf{R}). \tag{2.26}$$

$$\hat{\alpha}_1 = \frac{1}{M}\mathbf{tr}((\mathbf{R} - \mathbf{A}\mathbf{X}_t\mathbf{\Phi})^H(\mathbf{R} - \mathbf{A}\mathbf{X}_t\mathbf{\Phi})). \tag{2.27}$$

From (2.25), (2.26) and (2.27) yield,

$$\Lambda'(\mathbf{R}) = \frac{\mathbf{tr}(\mathbf{R}^H\mathcal{P}\mathbf{R})}{\mathbf{tr}(\mathbf{R}^H\mathcal{P}_\perp\mathbf{R})}, \tag{2.28}$$

where $\mathcal{P} = \mathbf{\Phi}^H(\mathbf{\Phi}\mathbf{\Phi}^H)^{-1}\mathbf{\Phi}$ is the projection matrix, and $\mathcal{P}_\perp$ is the orthogonal projection matrix related to $\mathcal{P}$ as $\mathcal{P}_\perp = \mathbf{I} - \mathcal{P}$ (the dimension of $\mathbf{I}$ is $M \times M$).

The analytical expressions for P_{D} and P_{FA} for the test statistics (2.28) are given by the following relations

$$P_{\text{D}} = \int_{\lambda_g}^{\infty} \mathcal{P}_{\mathcal{H}_1}(\Lambda'(\mathbf{R}))d\Lambda'(\mathbf{R}) \tag{2.29}$$

$$P_{\text{FA}} = \int_{\lambda_g}^{\infty} \mathcal{P}_{\mathcal{H}_0}(\Lambda'(\mathbf{R}))d\Lambda'(\mathbf{R}), \tag{2.30}$$

where λ_g is the detection threshold, $\mathcal{P}_{\mathcal{H}_1}(\Lambda'(\mathbf{R}))$ is the PDF of $\Lambda'(\mathbf{R})$ under hypothesis $\mathcal{H}_1$, and $\mathcal{P}_{\mathcal{H}_0}(\Lambda'(\mathbf{R}))$ is the PDF of $\Lambda'(\mathbf{R})$ under hypothesis $\mathcal{H}_0$.

Under Gaussian assumption for sea clutter, both the numerator and the denominator of (2.28) under hypothesis $\mathcal{H}_0$ are central Chi-Squared distributed random variables

$$\mathbf{tr}(\mathbf{R}^H\mathcal{P}\mathbf{R}) \sim \chi^2_{v_1} \quad \text{under} \quad \mathcal{H}_0 \tag{2.31}$$

$$\mathbf{tr}(\mathbf{R}^H\mathcal{P}_\perp\mathbf{R}) \sim \chi^2_{v_2} \quad \text{under} \quad \mathcal{H}_0, \tag{2.32}$$

where $v_1 = 2L\mathcal{R}(\mathcal{P})$ and $v_2 = 2L\mathcal{R}(\mathcal{P}_\perp)$ are the degrees of freedom for numerator and denominator respectively. Since, the ratio of central Chi-Squared distributed random variable follows central F_{v_1,v_2} distribution, hence under $\mathcal{H}_0$, $\Lambda'(\mathbf{R})$ is distributed as

$$\Lambda'(\mathbf{R}) \sim F_{v_1,v_2}. \tag{2.33}$$

Using (2.30), the expression for P_{FA} can be defined in terms of the right tail probability $(Q_{F_{v_1,v_2}}(\lambda_g))$ of F_{v_1,v_2} as

$$P_{\text{FA}} = Q_{F_{v_1,v_2}}(\lambda_g), \tag{2.34}$$

where

$$Q_{F_{v_1,v_2}}(\lambda_g) = \int_{\lambda_g}^{\infty} \frac{(\frac{v_1}{v_2})^{\frac{v_1}{2}} \Lambda'(\mathbf{R})^{\frac{v_1}{2}-1}}{B(\frac{v_1}{2}, \frac{v_2}{2})(1 + \frac{v_1}{v_2}\Lambda'(\mathbf{R}))^{\frac{v_1+v_2}{2}}} d\Lambda'(\mathbf{R}) \tag{2.35}$$

and B represents Beta function. Hence, the theoretical value of P_{FA} is obtained by solving (2.35) numerically with the method given in [39].

Contrary to the case under hypothesis $\mathcal{H}_0$, numerator of (2.28) under hypothesis $\mathcal{H}_1$ is non-central Chi-Squared distributed random variable $(\chi'^2_{v_1}(\delta))$ with a non-centrality parameter $\delta = \mathbf{tr}\{(\mathbf{AX}_t\mathbf{\Phi})(\mathbf{AX}_t\mathbf{\Phi})^H\}$, and the denominator is central Chi-Squared distributed random variable $(\chi^2_{v_2})$. Hence, their distribution are as follows:

$$\mathbf{tr}(\mathbf{R}^H\mathcal{P}\mathbf{R}) \sim \chi'^2_{v_1}(\delta) \quad \text{under} \quad \mathcal{H}_1. \tag{2.36}$$

$$\mathbf{tr}(\mathbf{R}^H\mathcal{P}_\perp\mathbf{R}) \sim \chi^2_{v_2} \quad \text{under} \quad \mathcal{H}_1. \tag{2.37}$$

Since the ratio of non-central and central Chi-squared distributed random variables is non-central $F'_{v_1,v_2}(\delta)$ distributed, under hypothesis $\mathcal{H}_1$, $\Lambda'(\mathbf{R})$ is distributed as

$$\Lambda'(\mathbf{R}) \sim F'_{v_1,v_2}(\delta). \tag{2.38}$$

Thus P_{D} as shown in (2.29) can be written as the right tail probability

$(Q_{F'_{v_1,v_2}(\delta)}(\lambda_g))$ of $F'_{v_1,v_2}(\delta)$

$$P_{\text{D}} = Q_{F'_{v_1,v_2}(\delta)}(\lambda_g), \tag{2.39}$$

where

$$Q_{F'_{\nu_1,\nu_2}(\delta)}(\lambda_g) = \int_{\lambda_g}^{\infty} \exp(\frac{-\delta}{2}) \sum_{k=0}^{k=\infty} \frac{(\delta/2)^k}{k!} \frac{(\frac{\nu_1}{\nu_2})^{\frac{1}{2}\nu_1+k}}{B(\frac{\nu_1+2k}{2}, \frac{\nu_2}{2})} \Lambda'(\mathbf{R})^{\frac{\nu_1}{2}+k-1}(1+\frac{\nu_1}{\nu_2}\Lambda'(\mathbf{R}))^{\frac{-1}{2}(\nu_1+\nu_2)-k}$$

$$d\Lambda'(\mathbf{R}). \tag{2.40}$$

Similar to P_{FA} as shown in (2.35), theoretical values of P_{D} for different values of detection threshold λ_g and L is obtained by solving (2.40) numerically.

Hence, from (2.35) and (2.40), the analytical expression for ROC of (2.28), parametrized by λ_g and L is given by

$$P_{\text{D}} = Q_{F'_{\nu_1,\nu_2}(\delta)}(Q^{-1}_{F_{\nu_1,\nu_2}}(P_{\text{FA}})). \tag{2.41}$$

2.3 Simulation Results and Discussion

In this section, simulation results to validate the proposed method of estimating OFDM radar return data and performance analysis of the proposed detector for estimated and simulated data are described in detail.

Table 2.1: Specifications for SF waveform (x_{SFW}) and OFDM waveform (x_{OFDM}).

SF waveform (x_{SFW})	Values	OFDM waveform (x_{OFDM})	Values
Number of frequency channels	25	Number of sub-carriers (L)	2^l; $l = 2, 3, 4, 5$
Frequency step size	5 MHz	Sub-carrier spacing (Δf)	31.25 to 3.9063 MHz
Center frequency (f_c)	9 GHz	Center frequency (f_c)	9 GHz
Bandwidth (B)	125 MHz	Bandwidth (B)	125 MHz
Pulse duration (T_{SF})	0.1 μs	Pulse duration ($T_o = \frac{1}{\Delta f}$)	0.032 to 0.256 μs
Pulse repetition interval (T_{PRI})	0.04 ms	Pulse repetition interval (T_{PRI})	0.04 ms
Target velocity range	$(-8.34, 8.34)$ m/s	Target velocity range	$(-8.34, 8.34)$ m/s

2.3.1 Estimation of Radar Return Data

Simulations for estimation of OFDM radar return is performed in two steps. In the first step, IR $\mathbf{h}$ of the radar system is estimated by LS using the generated input signal $x_{\text{SFW}}(n)$ and the output signal $y_{\text{SFW}}(n)$ depicted in Fig. 2.2a and Fig. 2.2b, respectively. For simulations, $y_{\text{SFW}}(n)$ is taken from a single CPI of the original radar return data set from the CSIR 2006 OTB 2006 Measurement Trial [40], and $x_{\text{SFW}}(n)$ is generated according

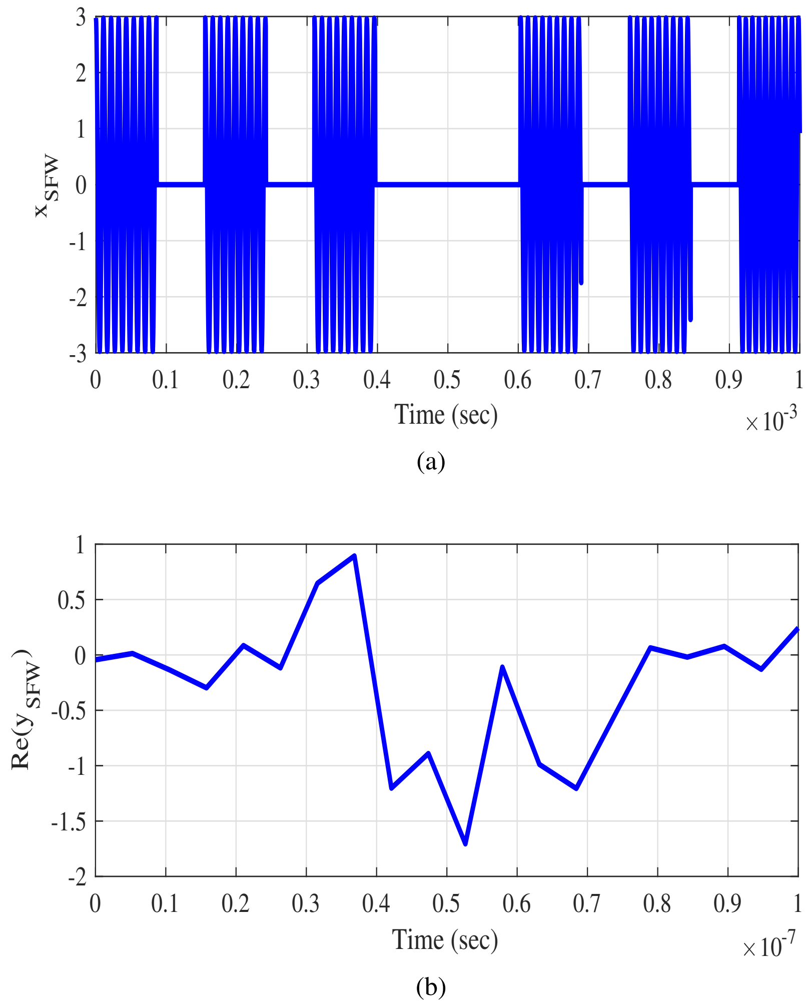

Figure 2.2: (a) Burst of 25 pulses for one CPI representing the group of stepped frequency pulses (x_{SFW}), (b) Real part of recorded radar return (y_{SFW}) for SF waveform for single PRI.

to the specifications of the transmitted SF waveform, provided with the data sets and described in Table-2.1. Estimated radar system IR for a single CPI is shown in Fig. 2.3a. The OFDM radar return data $y_{\text{OFDM}}(n)$ is estimated by observing response of the radar system for generated OFDM waveform $x_{\text{OFDM}}(n)$ as shown in Fig. 2.3b for four sub-carriers. Specifications for $x_{\text{OFDM}}(n)$ is given in Table-2.1. Particularly, for OFDM waveform for $L = 4$ and maximum $L = 32$, estimated OFDM radar return data ($y_{\text{OFDM}}(n)$) is shown in Fig. 2.4a and Fig. 2.4b, respectively.

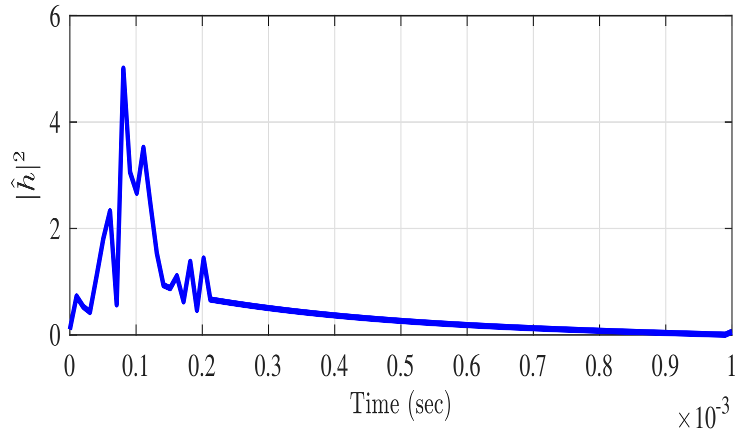

(a)

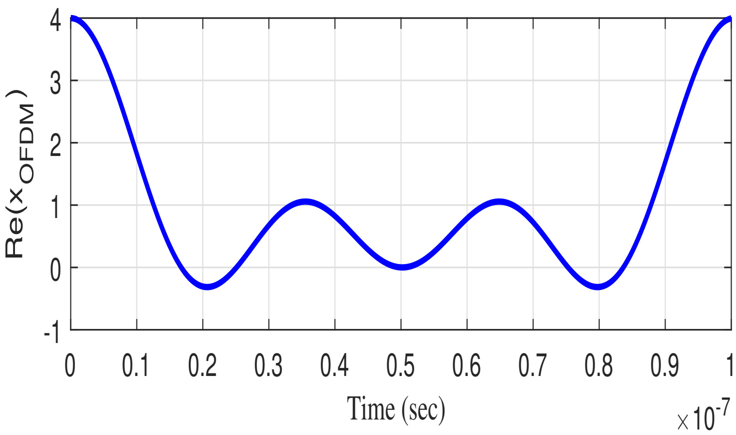

(b)

Figure 2.3: (a) Amplitude square of estimated radar system IR coefficients $|\hat{h}|^2$, (b) Real part of incorporated OFDM waveform (x_{OFDM}) for one single PRI.

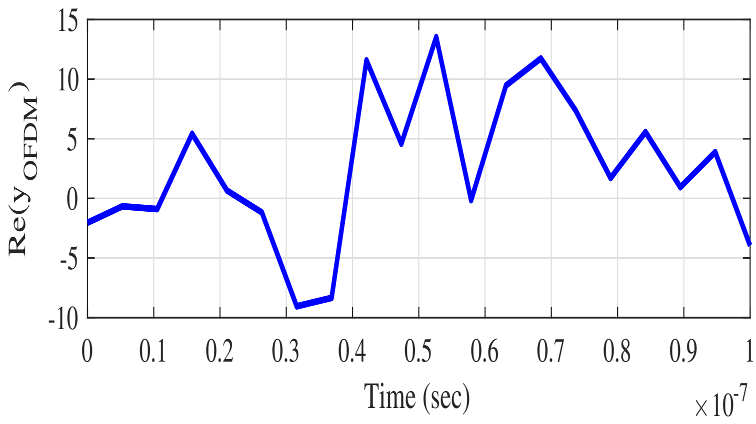

(a)

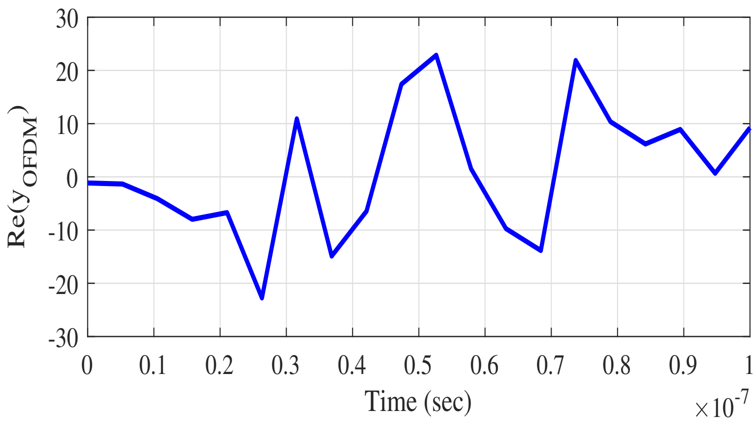

(b)

Figure 2.4: (a) Real part of an estimated radar return (y_{OFDM}) for $L = 4$, (b) Real part of an estimated radar return (y_{OFDM}) for $L = 32$.

2.3.2 Detector Performance for Estimated OFDM Radar Return

Performance of the proposed methodology of incorporating OFDM waveform in radar systems is examined by analyzing the performance of the detection test given by (2.24). The expected range of required detection threshold λ for which the detection test is evaluated is calculated by utilizing the data from the observation corresponding to hypothesis $\mathcal{H}_0$. The comparative plot for P_{FA} for different values of λ corresponding to SF waveform and different OFDM sub-carriers is shown in Fig. 2.5a. The decrease in P_{FA} as L increases is observed in Fig. 2.5a, this reflects an improvement in the performance of target detection test by exploiting the frequency diversity of an OFDM waveform. Moreover, as shown in Fig. 2.5b, in the case of OFDM radar, receiving echoes for each OFDM sub-carrier separately provide an additional "look" at the target, resulting in improved target detection capability over SF radar and conventional NMF. Furthermore, from Fig. 2.5b, at $P_{\text{FA}} = 10^{-2}$, the P_{D} achieved by SF radar and NMF is 0.2, and for the OFDM radar P_{D} ranges from 0.2 to 0.75, hence better P_{D} is obtained in the case of OFDM radar, which can further be enhanced by varying the number of sub-carriers. Effect of high resolution and frequency diversity attained by an OFDM waveform is reflected by a decrease in P_{FA} and improvement in P_{D}, as shown in Fig. 2.5a-2.5b (Please note that, since the real data is limited in number the resulting plots are not smooth).

2.3.3 Detector Performance for Simulated OFDM Radar Return

The performance improvement observed by utilizing estimated OFDM radar return is validated by running the detection test over simulated data as well as by using (2.17). For K-distributed clutter, there is no closed form expression that relates P_{FA}, λ, and P_{D}, hence, the detection test is done for an ensemble for 10^5 Monte Carlo simulations. In (2.17), $\mathbf{\Phi}$ is generated for fixed target Doppler frequency set $f_{D_t} = [f_{0D_t}, f_{1D_t}, ..., f_{(L-1)D_t}]$. The elements of f_{D_t} takes value from the known Doppler frequency range (Doppler spread) i.e. from $\{-\frac{1}{2T_{\text{PRI}}}, \cdots, \frac{1}{2T_{\text{PRI}}}\}$. The diagonal elements of the matrix $\mathbf{A}$ are chosen from the optimized set of phase codes with low PAPR. The values for diagonal elements

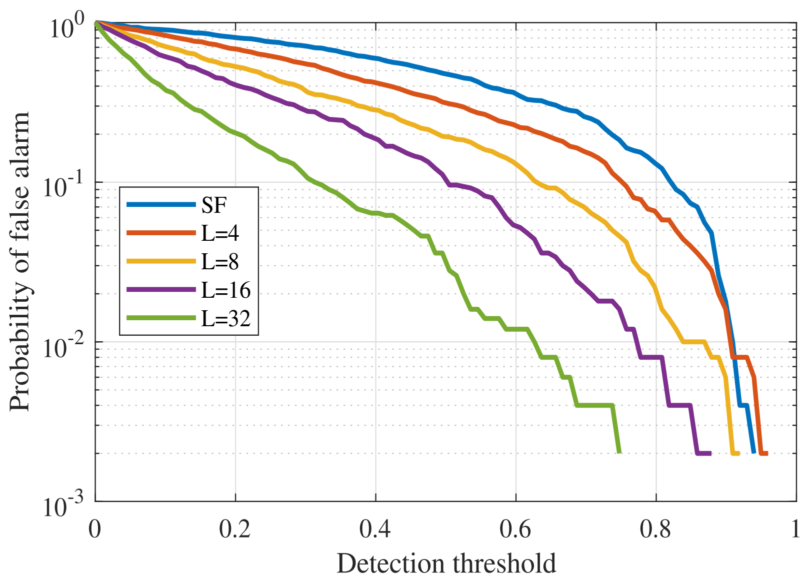

(a)

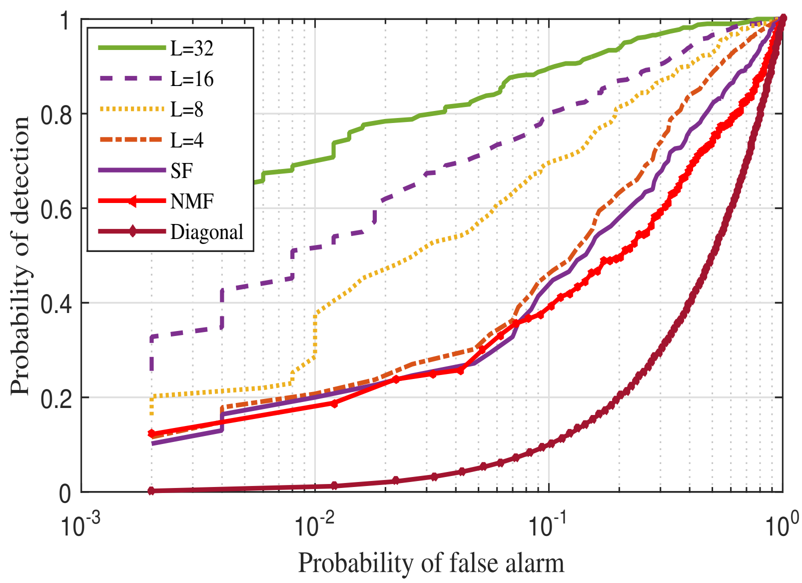

(b)

Figure 2.5: (a) Probability of false alarm for SF waveform and OFDM waveform comprises different number of sub-carriers, (b) ROC of proposed detector test statistics and conventional NMF detector.

of $\mathbf{X}_t$ is realized from the normal distribution having zero mean and unit variance i.e. $\mathbf{diag}(\mathbf{X}_t) \in \mathcal{N}_{\mathbb{C}}(\mathbf{0}, \mathbf{I})$. To replicate the sea clutter by which the estimated OFDM radar return data is affected, the K-distributed clutter part of (2.17) is simulated by utilizing the relation shown in Subsection 1.5 of Chapter 1.

The elements of $\mathbf{z}$ are realized as $\mathbf{z} \in \mathcal{N}_{\mathbb{C}}(\mathbf{0}, \mathbf{\Sigma_z})$, where $\mathbf{\Sigma_z}$ has elements $(\mathbf{\Sigma_z})_{ij} = \rho^{|i-j|}\, \forall\, i, j \in \{1, ..., M\}$, where ρ is the one-lag correlation coefficient. The simulation for obtaining detector performance is run for $M = 11$, the SCR is set at -10 dB, and $\rho = 0.9$. The obtained simulation results for P_{FA} and ROC are shown in Fig. 2.6a and Fig. 2.6b, respectively. As observed from Fig. 2.6a-2.6b, detector ROC and P_{FA} obtained by utilizing the simulated data follow similar trend as the detector ROC and P_{FA} have followed for estimated OFDM radar return data, shown in Fig. 2.5a-2.5b. Particularly, as shown in Fig. 2.6b, proposed detector test statistics surpasses the performance of conventional NMF detector. In Fig. 2.6b, the diagonal line corresponding to $P_{\text{FA}} = P_{\text{D}}$ is shown with line in brown. This analysis validates proposed method for estimating OFDM radar return from the real radar return, since, both the simulated and measured radar return follows a similar ROC trend.

2.3.4 Detector Performance under Gaussian Approximation for Sea Clutter

In this section, performance of the proposed detection test under the assumption of uncorrelated Gaussian distributed sea clutter is demonstrated. For this, the detection test derived for a very high value of ν, described by (2.28) is used. For simulations, signal part of the observations $\mathbf{R}$ is generated as described in Subsection 2.1.3 for K-distributed clutter. However, the sea clutter, $\mathbf{C}$, is realized as $\mathbf{C} \in \mathcal{N}_{\mathbb{C}}(\mathbf{0}, \Omega^2\mathbf{I})$, where Ω^2 is variance of the Gaussian distributed sea clutter. The SCR, defined as $\frac{\mathbf{tr}\{(\mathbf{A}\mathbf{X}_t\mathbf{\Phi})(\mathbf{A}\mathbf{X}_t\mathbf{\Phi})^H\}}{ML\Omega^2}$, is set at -10 dB and $M = 11$. As observed from Fig. 2.7a and Fig. 2.7b, with increase in L, both the P_{FA} and ROC has similar performance improvement as followed by the ROC and P_{FA} for estimated and simulated OFDM radar return data. Moreover, in Fig. 2.7b, the diagonal line corresponding to $P_{\text{FA}} = P_{\text{D}}$ is shown with line in brown. This analysis

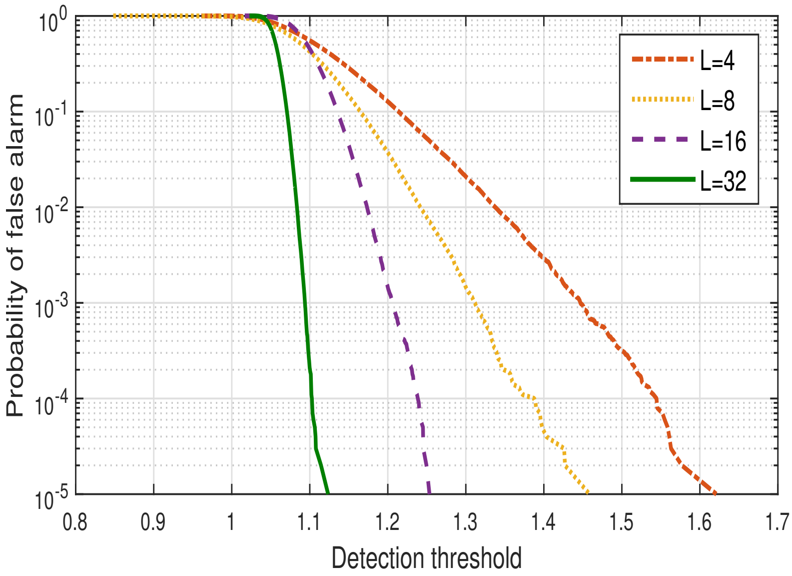

(a)

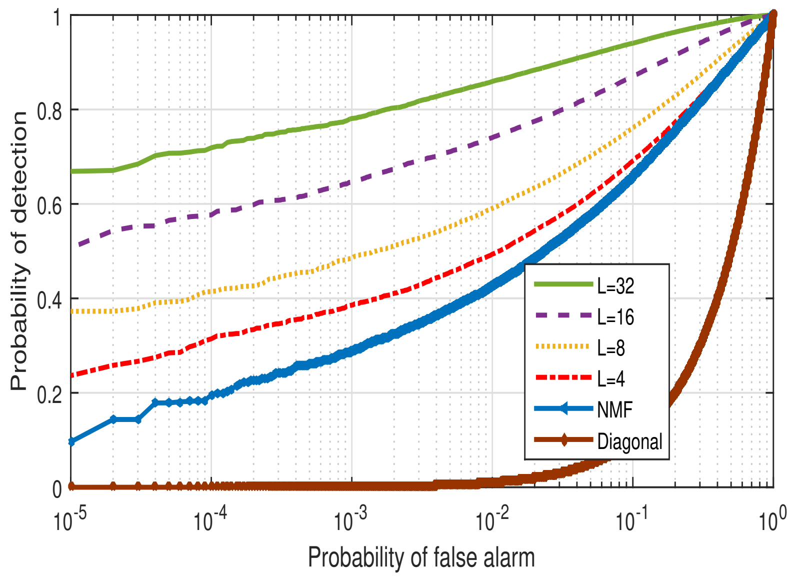

(b)

Figure 2.6: (a) Probability of false alarm utilizing simulated OFDM radar return data, (b) ROC of proposed detector test statistics utilizing simulated OFDM radar return data and NMF detector.

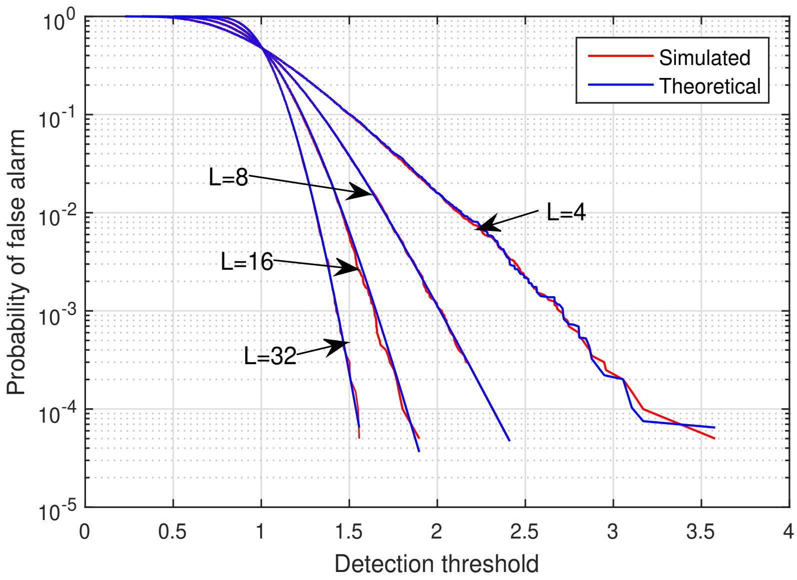

(a)

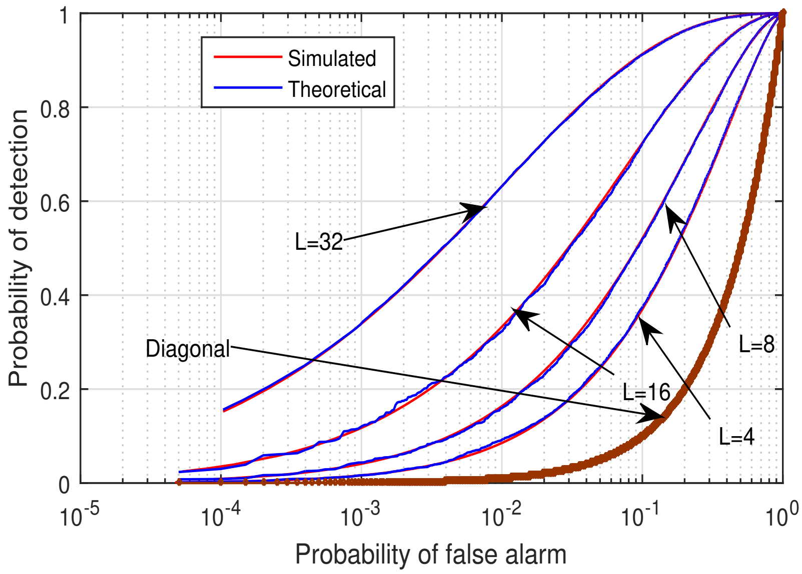

(b)

Figure 2.7: (a) Probability of false alarm utilizing simulated OFDM radar return data and derived analytical expression under the assumption of Gaussian distributed sea clutter, (b) ROC utilizing simulated OFDM radar return data and derived analytical expression under the assumption of Gaussian distributed sea clutter.

validates correctness and suitability of the proposed system model and detection test for surveillance in the marine sea environment.

2.4 Summary

In this Chapter, detection of small boat in the sea environment using OFDM waveform as a transmitted surveillance waveform is performed. A method to estimate the OFDM radar return data using CSIR recorded radar return data for SF waveform is proposed. System model corresponding to the mathematical representation of radar echoes for OFDM waveform is proposed. The derived system model demonstrates the frequency diversity obtained after employing the OFDM waveform in a radar system. Further, detection of the target utilizing estimated data is done by modified GLRT. Simulation results for P_{FA} and P_{D}, clearly show improvement in target detection over conventional NMF. The performance is further improved as the number of OFDM sub-carriers increases. The obtained improvement in detector performance with a number of OFDM sub-carriers is validated through analytical expressions of P_D and P_{FA}, and by detector's performance obtained by utilizing simulated data. The demonstrated improvement in detection performance implies superiority and suitability of OFDM waveform over the conventional radar waveforms.

In subsequent Chapters, KAFs and Kalman filter based estimation techniques are explored to estimate the range and velocity of a detected target.

Chapter 3

Range and Velocity Estimation in Gaussian noise

In Chapter 2, technique of detecting the target using OFDM radar is described. The detection gives an estimate of a number of targets present in the surveillance environment. As mentioned in Section 1.2 of Chapter 1, after detection the subsequent step is the estimation of range and velocity of the detected targets. Target's range is proportional to the delay by which the returning radar return is received; similarly, the target's velocity is also proportional to the frequency shift in the carrier frequency of the transmitted signal. Consequently, a target's range and velocity are estimated by estimating the delay and Doppler shift introduce by the range and velocity of the target, respectively [1, 4]. Therefore in this and subsequent Chapters, to accurately estimate a target's delay and Doppler shift, various kernel-based adaptive estimators have been developed and tested over different radar systems, including conventional LFM and SF radar systems, and recently introduced OFDM radar system.

In this Chapter, to improve delay and Doppler shift estimation in presence of thermal noise, adaptive estimators based on KLMS in RKHS is proposed. Since, popular estimator based FT [2, 8] optimizes non-convex ML cost function, it is prone to inaccurate estimates of delay and Doppler shift, especially in low signal to noise ratio (SNR) region. In comparison to existing estimator based on FT, the proposed estimation approach has a global minima, due to the optimization of convex cost-function in RKHS [15, 16, 41]. Moreover, unlike existing estimation approaches for the aforementioned parameters, wherein the estimator's performance is typically enhanced by increasing the number of observations (thereby increasing computational complexity), the proposed KLMS based estimation technique selectively adapts the estimator in RKHS using the Platt's NC [17, 18, 42, 43]. This yields a sparse estimator named as KLMS-NC for unknown parameters in RKHS, and convergence to the optimal parameter value is achieved by using a dictionary of a finite number of observations. Upon sparsification by NC, the proposed estimator is found to be computationally simple for practical deployment. Another challenge with KLMS is in choosing an appropriate width of the popular Gaussian kernel. Silverman's rule yields the width of a kernel by exploiting the statistical properties of the incoming observation [44]. However, the kernel width obtained by Silverman's rule is not always optimal [45], and is prone to estimation errors. Hence, in this Chapter, the kernel width using the incoming radar observations are learned and adapt, the resulting estimator is named as KLMS-Modified NC. The estimator based on KLMS-Modified NC, yields better convergence and smaller dictionary sizes, thereby providing a versatile and robust estimator for the estimation of delay and Doppler shift.

The Chapter is organized as follows: A brief introduction to the LFM and OFDM radar system along with a detailed review of an OFDM radar return data matrix is given first. Then, the proposed methodology of using KLMS based algorithms (KLMS, KLMS-NC, and KLMS-Modified NC) for parameter estimation is described. After that, for the estimator based on KLMS-Modified NC, the expression for the bound on kernel width learning parameter is derived. Further, explicit derivation of the CRLB for delay and Doppler shift estimation is described. The description of the simulations of the proposed estimators over practical radar-scenarios is given next. Finally, conclusions are drawn.

3.1 System Model

The proposed estimation algorithms, are applied to two basic monostatic radar systems namely; LFM radar and OFDM radar. For many years LFM waveform is being used as a surveillance waveform in radar systems. In [46], the author introduced a multicarrier waveform for radar systems called OFDM waveform and demonstrated the similarity of its ambiguity plot to an ideal ambiguity plot (low side-lobe levels and narrow main-lobe width). Initially, the idea of incorporating OFDM waveform in radar system was pursued with the objective of combining communication and radar sensing together, specific to vehicular systems [8, 47–49]. Eventually, researchers started exploring the utility of OFDM waveform for other surveillance applications as well [31, 36, 50–53].

The radar environment and preliminary processing of echoes for LFM radar and OFDM radar are same, with the only difference being in the type of modulation adopted for continuous time baseband pulse $s(t)$. Since two commonly used radar waveforms LFM and OFDM are considered, the corresponding system model are described separately for LFM and OFDM radar system.

In a given CPI, let radar system transmits M radar pulses [31, 54]. The transmitted waveform is the pulse of a finite width which repeats after a certain PRI. Processing of the waveform is considered on PRI basis, thus for CPI of M transmitted pulses, any arbitrary m^{th} transmitted pass-band pulse at central frequency f_c is

$$s_m(t) = \{s(t - mT_{\text{PRI}})\} \exp(j2\pi f_c t), \tag{3.1}$$

where $s(t)$ is the baseband transmitted pulse and T_{PRI} is the PRI.

The echo from the target is the delayed version of $s_m(t)$. If echo is from a single target located at an unknown range R and approaching towards the radar with an unknown velocity v, then the time-delay by which an arbitrary m^{th} pulse in CPI gets delayed is

$$\tau_m = \tau_o - \frac{2}{c}\{vmT_{\text{PRI}}\}, \tag{3.2}$$

where c is the velocity of light, and τ_o, is the unknown delay introduced in the pulse because of the initial position of a target, given by $\tau_o = \frac{2R}{c}$.

The received baseband radar return for any arbitrary m^{th} pulse is

$$r_m(t) = \zeta\{s_m(t - \tau_m)\} + w(t), \tag{3.3}$$

where, ζ represents the complex attenuation factor which is proportional to the target radar cross section (RCS), and $w(t)$ denotes the measurement and thermal noise process modeled as complex zero mean AWGN.

3.1.1 LFM Radar System Model

Let the transmitted LFM pulse be denoted as,

$$s_{\text{LFM}}(t) = a \exp\left(j\pi\gamma t^2\right), \quad \text{for} \;\; 0 \leq t \leq T_o, \tag{3.4}$$

where a and γ are the amplitude and frequency sweep rate respectively. T_o is the duration of the transmitted baseband LFM pulse.

The instantaneous frequency of $s_{\text{LFM}}(t)$ is

$$f_i(t) = \gamma t, \tag{3.5}$$

where $\gamma = \frac{L\Delta f}{T_o}$ as $L\Delta f$ is the bandwidth of $s_{\text{LFM}}(t)$.

Substituting (3.4) in (3.3) yields the LFM radar return for the m^{th} transmitted pulse as

$$r^m_{\text{LFM}}(t) = \zeta\{s_{\text{LFM}}(t - mT_{\text{PRI}} - \tau_m)\} \exp(j2\pi f_c(t - \tau_m)) + w(t). \tag{3.6}$$

The matched filter output is given by

$$r^m_{\text{LFM}}(t) = \zeta \int_{\tau_m}^{\tau_m + T_o} s_{\text{LFM}}(t - mT_{\text{PRI}} - \tau_m) s^*_{\text{LFM}}(t - mT_{\text{PRI}} - \tau) \exp(-j2\pi f_c \tau_m) dt + w(t).$$

Next taking the Fourier transform, yield

$$r^m_{\text{LFM}}(f) = \zeta \exp(-j2\pi f_c \tau_m) \int \int_{\tau_m}^{\tau_m + T_o} s_{\text{LFM}}(t - mT_{\text{PRI}} - \tau_m) s^*_{\text{LFM}}(t - mT_{\text{PRI}} - \tau) \times \exp(-j2\pi f \tau) dt d\tau + w(f).$$

The above step is basically done to account for significant range migrations from pulse to pulse. Moreover, this avoids the need to interpolate to account for sub-pixel motion and allows to factor out the magnitude square of the Fourier transform of the pulse [2].

Simplification, yield

$$r^m_{\text{LFM}}(f) = \zeta \exp(-j2\pi f_c \tau_m) \int \int_{\tau_m}^{\tau_m + T_o} s_{\text{LFM}}(t - mT_{\text{PRI}} - \tau_m) s^*_{\text{LFM}}(t - mT_{\text{PRI}} - \tau) \times \exp(-j2\pi f(mT_{\text{PRI}} + \tau - t)) \exp(-j2\pi f(t - mT_{\text{PRI}})) dt d\tau + w(f).$$

Further simplification yield

$$r^m_{\text{LFM}}(f) = \zeta \exp(-j2\pi f_c \tau_m) \int_{\tau_m}^{\tau_m + T_o} s_{\text{LFM}}(t - mT_{\text{PRI}} - \tau_m) \exp(-j2\pi f(t - mT_{\text{PRI}} - \tau_m) dt \times \exp(-j2\pi f \tau_m) \int s^*_{\text{LFM}}(t - mT_{\text{PRI}} - \tau) \exp(-j2\pi f(mT_{\text{PRI}} + \tau - t)) d\tau + w(f).$$

The simplified form of $r_m(f)$ is given by

$$r^m_{\text{LFM}}(f) = \mid S_{\text{LFM}}(f) \mid^2 \exp(-j2\pi f_c \tau_m) \exp(-j2\pi f \tau_m) + w(f),$$

where $S_{\text{LFM}}(f)$ is the Fourier transform of $s_{\text{LFM}}(t)$.

Sampling in frequency domain at $l = [0, 1, \ldots, L-1]$ with an interval of Δf, and dividing by $\mid S_{\text{LFM}}(l\Delta f) \mid^2$, yield

$$r_{\text{LFM}}(m, l) = \exp(-j2\pi f_c \tau_m) \exp(-j2\pi l \Delta f \tau_m) + w(m, l).$$

The constant power of the sample of white noise $w(m, l)$ is maintained by assuming that the power spectra of the receiver noise $w(t)$ and transmitted signal $s_{\text{LFM}}(t)$ do not vary much over the processed frequency band [2].

Substituting τ_m from (3.2), we get

$$r_{\text{LFM}}(m,l) = \exp\left(j2\pi m f_d T_{\text{PRI}}\right)\exp\left(-j2\pi l\Delta f\tau_o\right)\exp(j2\pi f_d ml(\frac{T_{\text{PRI}}\Delta f}{f_c})) + w(m,l),$$

where $f_d = \frac{2vf_c}{c}$ is the unknown Doppler shift owing to the target velocity.

Arranging $r_{\text{LFM}}(m,l)$ in a matrix, the radar return matrix $\mathbf{R}_{\text{LFM}}$ from a single scatterer is given by [2].

$$\mathbf{R}_{\text{LFM}} = \zeta\mathbf{S}_{\text{LFM}} + \mathbf{W}, \tag{3.7}$$

where

$$\mathbf{S}_{\text{LFM}} = \begin{bmatrix} 1 & \cdots & \exp\left(-j2\pi(L-1)\Delta f\tau_o\right) \\ \exp\left(j2\pi f_d T_{\text{PRI}}\right) & \cdots & \exp\left(j2\pi f_d T_{\text{PRI}}\right)\exp\left(-j2\pi(L-1)\Delta f\tau_o\right)\exp(j2\pi f_d(L-1)(\frac{T_{\text{PRI}}\Delta f}{f_c})) \\ \vdots & \vdots & \vdots \\ \exp\left(j2\pi(M-1)f_d T_{\text{PRI}}\right) & \cdots & \exp\left(j2\pi(M-1)f_d T_{\text{PRI}}\right)\exp\left(-j2\pi(L-1)\Delta f\tau_o\right)\exp(j2\pi f_d(M-1)(L-1)(\frac{T_{\text{PRI}}\Delta f}{f_c})) \end{bmatrix}. \tag{3.8}$$

is the matrix of signal part for LFM radar, and $\mathbf{W}$ is the matrix of the sampled complex AWGN process.

An individual element of $\mathbf{R}_{\text{LFM}}$ is given by

$$\mathbf{R}_{\text{LFM}}(m,l) = \zeta\exp\left(j2\pi m f_d T_{\text{PRI}}\right)\exp\left(-j2\pi l\Delta f\tau_o\right)\exp(j2\pi f_d ml(\frac{T_{\text{PRI}}\Delta f}{f_c})) + \mathbf{W}(m,l). \tag{3.9}$$

3.1.2 OFDM Radar System Model

Let the transmitted baseband OFDM pulse $s_{\text{OFDM}}(t)$ comprise of L-sub-carriers with a frequency separation of Δf. Then to maintain orthogonality between sub-carriers, T_o

satisfies, $T_o = \frac{1}{\Delta f}$. Hence, the OFDM pulse is given by

$$s_{\text{OFDM}}(t) = \sum_{l=0}^{L-1} a_l \exp\left(j2\pi l \Delta f t\right), \quad \text{for } 0 \leq t \leq T_o, \tag{3.10}$$

where, a_l are the modulation symbol which takes values from the set of constant modulus phase shift key (PSK) constellation set such that $|a_l|^2 = 1$.

The corresponding OFDM radar return is obtained by substituting (3.10) in (3.3) and given as

$$r^m_{\text{OFDM}}(t) = \zeta \sum_{l=0}^{L-1} a_l \exp\left(j2\pi l \Delta f (t - mT_{\text{PRI}} - \tau_m)\right) \exp(j2\pi f_c (t - \tau_m)) + w(t). \tag{3.11}$$

Removing carrier frequency yields

$$r^m_{\text{OFDM}}(t) = \zeta \sum_{l=0}^{L-1} a_l \exp\left(j2\pi l \Delta f (t - mT_{\text{PRI}} - \tau_m)\right) \exp(-j2\pi f_c \tau_m) + w(t). \tag{3.12}$$

After sampling at $t_s = mT_{\text{PRI}} + \frac{n}{L\Delta f}$, in discrete form [1]

$$\begin{aligned} r^m_{\text{OFDM}}(n) =& \zeta \sum_{l=0}^{L-1} a_l \exp\left(j2\pi l \frac{n}{L}\right) \exp\left(-j2\pi l \Delta f \tau_o\right) \exp\left(j2\pi (f_c + l\Delta f)\{\frac{2vmT_{\text{PRI}}}{c}\}\right) \\ & \times \exp(-j2\pi f_c \tau_o) + w(n), \end{aligned} \tag{3.13}$$

where $w(n)$ is AWGN random variable. Assuming $f_c + l\Delta f \simeq f_c$, (3.13) yields

$$r^m_{\text{OFDM}}(n) = \alpha \overbrace{\{\frac{1}{L} \sum_{l=0}^{L-1} a_l \exp\left(-j2\pi l \Delta f \tau_o\right) \exp\left(\frac{j2\pi l n}{L}\right)\}}^{IDFT} \exp\left(j2\pi m f_d T_{\text{PRI}}\right) + w(n), \tag{3.14}$$

where, $\alpha = L\zeta \exp(-j2\pi f_c \tau_o)$. Stacking radar return $r^m_{\text{OFDM}}(n)$ from (3.14) in vector form, the final radar return vector for any arbitrary m^{th} OFDM pulse is given as:

$$\mathbf{r}^m_{\text{OFDM}} \in \mathbb{C}^{L\times 1} = \alpha \exp\left(j2\pi m f_d T_{\text{PRI}}\right)\mathbf{F}^{-1}\mathbf{A}_l \mathbf{d}_l + \mathbf{w}, \tag{3.15}$$

where, $\mathbf{F}^{-1}$ is the inverse discrete Fourier transform (IDFT) matrix

$$\mathbf{F}^{-1} \in \mathbb{C}^{L\times L} = \frac{1}{L}\begin{bmatrix} 1 & 1 & \dots & 1 \\ 1 & \exp\left(\frac{j2\pi}{L}\right) & \dots & \exp\left(\frac{j2\pi(L-1)}{L}\right) \\ \vdots & \vdots & \vdots & \vdots \\ 1 & \exp\left(\frac{j2\pi(L-1)}{L}\right) & \dots & \exp\left(\frac{j2\pi(L-1)(L-1)}{L}\right) \end{bmatrix},$$

$\mathbf{A}_l$ is the diagonal matrix of dimension $L \times L$ whose diagonal elements are the set of PSK modulated symbol $\{a_0, a_1, \dots, a_{L-1}\}$

$$\mathbf{A}_l \in \mathbb{C}^{L\times L} = \begin{bmatrix} a_0 & 0 & \dots & 0 \\ 0 & a_1 & \dots & 0 \\ \vdots & \vdots & \vdots & \vdots \\ 0 & 0 & \dots & a_{L-1} \end{bmatrix},$$

$\mathbf{d}_l$ is the $L \times 1$ vector of exponential whose argument is the phase shift introduced by the unknown delay τ_o

$$\mathbf{d}_l \in \mathbb{C}^{L\times 1} = [1, \exp(-j2\pi\Delta f\tau_o), \dots, \exp(-j2\pi(L-1)\Delta f\tau_o)]^T,$$

and $\mathbf{w} \in \mathbb{C}^{L\times 1} = [w(0), w(1), \dots, w(L-1)]^T$, which follows the distribution define in Subsection 2.1.3 of Chapter 2, i.e. $\mathbf{w} \in \mathcal{N}_{\mathbb{C}}(\mathbf{0}, \boldsymbol{\Sigma}_{\mathbf{w}})$, where $\boldsymbol{\Sigma}_{\mathbf{w}} = \Omega_w^2\mathbf{I}$.

At the receiver to recover the phase shifts introduced by delay and Doppler shift, discrete Fourier transform (DFT) over $r^m_{\text{OFDM}}(n)$ is computed as

$$\mathbf{r}_m = \mathbf{F}\mathbf{r}^m_{\text{OFDM}} = \alpha \exp(j2\pi m f_d T_{\text{PRI}})\mathbf{A}_l\mathbf{d}_l + \mathbf{w}_f, \tag{3.16}$$

where, $\mathbf{F}$ is the DFT matrix, and $\mathbf{w}_f$ is the N-point DFT of $\mathbf{w}$. Since DFT is a linear operation, it will not affect the distribution of $\mathbf{w}$.

Since, for a mono-static radar, the transmitted modulation symbols $\{a_l \forall l\}$ are known at the receiver. This assumption will significantly simplify (3.16) as follows

$$\begin{aligned}\mathbf{A}_l^H\mathbf{r}_m &= \alpha \exp{(j2\pi m f_d T_{\text{PRI}})}\mathbf{A}_l^H\mathbf{A}_l\mathbf{d}_l + \mathbf{A}_l^H\mathbf{w}_f.\\ \mathbf{r}_m^a \in \mathbb{C}^{N\times 1} &= \alpha \exp{(j2\pi m f_d T_{\text{PRI}})}\mathbf{d}_l + \mathbf{w}_f^a.\end{aligned} \tag{3.17}$$

Representation of (3.17), follows from the fact that $\mathbf{A}_l^H\mathbf{A}_l = \mathbf{I}$ since $|a_l|^2 = 1\forall l$. This simplification will not change the statistical properties of $\mathbf{w}_f$. Arranging $\mathbf{r}_m^a$ in the vector form $[\{\mathbf{r}_0^a\}^T, \{\mathbf{r}_1^a\}^T, \dots, \{\mathbf{r}_{M-1}^a\}^T]^T$ for values of $m = 0, 1, \dots, M-1$ and substituting the value of $\mathbf{d}_l$ yields the final analytic form of OFDM radar return matrix, which is given as

$$\mathbf{R}_{\text{OFDM}} = [\{\mathbf{r}_0^a\}^T, \{\mathbf{r}_1^a\}^T, \dots, \{\mathbf{r}_{M-1}^a\}^T]^T = \alpha\mathbf{S}_{\text{OFDM}} + \mathbf{W}, \tag{3.18}$$

where

$$\mathbf{S}_{\text{OFDM}} = \begin{bmatrix} 1 & \exp{(-j2\pi\Delta f\tau_o)} & \dots & \exp{(-j2\pi(L-1)\Delta f\tau_o)} \\ \exp(j2\pi f_d T_{\text{PRI}}) & \exp{(j2\pi f_d T_{\text{PRI}})}\exp{(-j2\pi\Delta f\tau_o)} & \dots & \exp{(j2\pi f_d T_{\text{PRI}})}\exp{(-j2\pi(L-1)\Delta f\tau_o)} \\ \vdots & \vdots & \vdots & \vdots \\ \exp{(j2\pi(M-1)f_d T_{\text{PRI}})} & \exp{(j2\pi(M-1)f_d T_{\text{PRI}})}\exp{(-j2\pi\Delta f\tau_o)} & \dots & \exp{(j2\pi(M-1)f_d T_{\text{PRI}})}\exp{(-j2\pi(L-1)\Delta f\tau_o)} \end{bmatrix}. \tag{3.19}$$

is the signal part for OFDM radar. The individual elements of $\mathbf{R}_{\text{OFDM}}$ are

$$\mathbf{R}_{\text{OFDM}}(m,l) = \alpha \exp{(j2\pi m f_d T_{\text{PRI}})}\exp{(-j2\pi l\Delta f\tau_o)} + \mathbf{W}(m,l). \tag{3.20}$$

From (3.9) and (3.20), it is explicit that the radar echo matrix (for both LFM and OFDM waveform) comprises of orthogonal exponentials, in rows and columns corresponding to the unknown delay τ_o and Doppler shift f_d respectively. Moreover, from (3.9) and (3.20), it is explicit that the unknown delay τ_o and Doppler shift f_d can be estimated if the exact inverse relationship $\big(g(\cdot) : \mathbb{C} \longrightarrow \mathbb{R}\big)$ between the radar return ($\mathbf{R}(m,l)$) and the unknown parameter (i.e. $g(\mathbf{R}(m,l)) \in \mathbb{R} = \tau_o$ or $g(\mathbf{R}(m,l)) \in \mathbb{R} = f_d$) is known. However, estimation of $g(\cdot)$ is non-trivial. Hence, in this work, to estimate $g(\cdot)$, an online learning estimators based on adaptive KLMS algorithm is proposed.

3.2 KLMS-based Estimation of Delay and Doppler shift

In the proposed algorithm, estimation of delay and Doppler shift is pursued independently. This also allows delay and Doppler shift's value space to be limited to one-dimension, i.e. $\{\tau_o, f_d\} \in \mathbb{R}$.

For estimation of delay and Doppler shift, $\mathbf{R}_{\text{LFM}}$ and $\mathbf{R}_{\text{OFDM}}$ are given by

$$\mathbf{R}_{\text{LFM}} = \zeta \mathbf{S}_{\text{LFM}} + \mathbf{W}. \tag{3.21}$$

$$\mathbf{R}_{\text{OFDM}} = \alpha \mathbf{S}_{\text{OFDM}} + \mathbf{W}. \tag{3.22}$$

The estimation of τ_o is carried out by treating f_d as a known quantity. The range $\{\tau_{o_{min}}, \tau_{o_{max}}\}$ in which τ_o is expected to take the value is divided into K equal intervals i.e. $[\tau^1_{o_{min}} \dots \tau^K_{o_{max}}]$. Following this, at any instant k, (3.21) and (3.22) can be represented as the collection of M-radar return vector observations

$$\mathbf{r}^k_m = \exp\left(j2\pi m f_d T_{\text{PRI}}\right) \exp(j2\pi f_d m l\left(\frac{T_{\text{PRI}}\Delta f}{f_c}\right))\mathbf{d}_l + \mathbf{w}^a_f \; \forall\, m = [0, 1, \dots, \; M-1]$$

for LFM radar system and as $\mathbf{r}^k_m = \exp\left(j2\pi m f_d T_{\text{PRI}}\right)\mathbf{d}_l + \mathbf{w}^a_f \; \forall\, m = [0, 1, \dots, \; M-1]$ for OFDM radar system. Hence, this yields

$$\mathbf{r}^k_{\tau_o|f_d} \in \mathbb{C}^{ML\times 1} = [\mathbf{r}^k_0, \mathbf{r}^k_1, \dots, \mathbf{r}^k_{M-1}]^T. \tag{3.23}$$

Equivalently, at instant k, the vector for the observations of radar return corresponding to any arbitrary Doppler shift f^k_d from the set $[f^1_{d_{min}} \dots f^K_{d_{max}}]$ of K-Doppler shifts is given as

$$\mathbf{r}^k_{f_d|\tau_o} \in \mathbb{C}^{ML\times 1} = [\mathbf{r}^k_0, \mathbf{r}^k_1, \dots, \mathbf{r}^k_{L-1}]^T, \tag{3.24}$$

where $\mathbf{r}^k_l = \exp\left(-j2\pi l \Delta f \tau_o\right)\mathbf{d}_m + \mathbf{w}^a_f$.

3.2.1 Estimator based on KLMS

The KLMS algorithm provides convexity in RKHS which aids in the universal approximation of the arbitrary unknown function. Thus in this section, a KLMS based estimator is proposed for both LFM and OFDM radar model.

The objective is to estimate the system with a mapping function $g(\cdot)$ which at k^{th} time instant maps the input vector $\mathbf{r}(k) \in \mathbb{C}^{ML}$ (where $\mathbf{r}(k) = \mathbf{r}^k_{\tau_o|f_d}, \mathbf{r}^k_{f_d|\tau_o}$)[1] respectively, into the corresponding output scalar $d(k) \in \mathbb{C}$ (where $d(k) = {\tau_o}^k, {f_d}^k$) as $\{g(\mathbf{r}(k)) = d(k)\}$. The KLMS algorithm proceeds with mapping the input vector $\mathbf{r}(k)\forall k$ into the high dimensional complex Hilbert space $\mathbb{H}$ via complex reproducing Mercer kernel $\kappa : \mathbb{X} \times \mathbb{X} \longrightarrow \mathbb{C}$, where $\mathbb{X} \subseteq \mathbb{C}^{ML}$. The k^{th} input vector is mapped implicitly in $\mathbb{H}$ as $\Phi(\mathbf{r}(k))$,

$$\Phi(\mathbf{r}(k)) = \kappa(\mathbf{r}(k), \cdot), \tag{3.25}$$

where κ is the mapping function used in a kernel-based adaptive algorithm which implicitly map the observations from finite-dimensional Euclidean space to high dimensional complex Hilbert space $\mathbb{H}$.

From Mercer theorem, the reproducing kernel $\kappa(\mathbf{r}(k), \mathbf{r}(k'))$ can be written as

$$\kappa(\mathbf{r}(k), \mathbf{r}(k')) = \langle \Phi(\mathbf{r}(k)), \Phi(\mathbf{r}(k')) \rangle_{\mathbb{H}}, \tag{3.26}$$

where $\langle \cdot \rangle_{\mathbb{H}}$ represents the inner product operation in $\mathbb{H}$ and k' is the index of vector corresponding to k'^{th} instant.

Let $\omega(k-1)$ be a weight vector defined as function in linear space $\mathbb{H}$, then from the least mean square (LMS) algorithm in $\mathbb{H}$ which is equivalently called KLMS in input space gives estimate of the desired output $d(k)$ as $\hat{g}(k) = \langle \omega(k-1), \Phi(\mathbf{r}(k)) \rangle_{\mathbb{H}}$. The learning rule (weight vector updation rule) for this algorithm is obtained by minimizing MSE, as follows:

$$\mathbb{E}[\mathcal{J}_k(\omega)] = \mathbb{E}[|d(k) - \hat{g}(k)|^2]. \tag{3.27}$$

[1]"," is used in the relation ($\mathbf{r}(k) = \mathbf{r}^k_{\tau_o|f_d}, \mathbf{r}^k_{f_d|\tau_o}$) as a notation for "or" which means that $\mathbf{r}(k)$ can be either $\mathbf{r}^k_{\tau_o|f_d}$ or $\mathbf{r}^k_{f_d|\tau_o}$

In (3.27), MSE is estimated by the error of the instantaneous measurement i.e. $\hat{\mathbb{E}}[\mathcal{J}_k(\boldsymbol{\omega})] = \mathcal{J}_k(\boldsymbol{\omega})$, hence

$$\mathcal{J}_k(\boldsymbol{\omega}) = |d(k) - \hat{g}(k)|^2. \tag{3.28}$$

For stochastic gradient update, the gradient with respect to $\boldsymbol{\omega}$ is calculated, i.e. $\nabla_{\boldsymbol{\omega}}\mathcal{J}_k(\boldsymbol{\omega})$ is computed by applying the rule of Wirtinger's calculus given in [55, 56]. Hence, the adaptation factor by which $\boldsymbol{\omega}$ is updated is $\mathcal{J}_k(\boldsymbol{\omega}) = -e(k)\mu\Phi(\mathbf{r}(k))$, where $e(k) = d(k) - \langle\boldsymbol{\omega}(k-1), \Phi(\mathbf{r}(k))\rangle_{\mathbb{H}}$ and μ is the learning rate parameter. Thus, the final weight vector-update equation is $\boldsymbol{\omega}(k) = \boldsymbol{\omega}(k-1) + \mu e(k)\Phi(\mathbf{r}(k))$, for the initial condition $\boldsymbol{\omega}(0) = \mathbf{0}$, repeated application of the weight vector-update yields

$$\boldsymbol{\omega}(k) = \mu\sum_{i=0}^{k} e(i)\Phi(\mathbf{r}(i)). \tag{3.29}$$

Thus, the estimated output at k^{th} time instant is given by

$$\hat{g}(k) = \langle\Phi(\mathbf{r}(k)), \boldsymbol{\omega}(k-1)\rangle_{\mathbb{H}} = \langle\Phi(\mathbf{r}(k)), \mu\sum_{i=0}^{k-1} e(i)\Phi(\mathbf{r}(i))\rangle_{\mathbb{H}} \tag{3.30}$$

From Mercer's theorem as defined in (3.26), the estimated output $\hat{g}(k)$ at k^{th} iteration is

$$\hat{g}(k) = \mu\sum_{i=0}^{k-1} e(i)\kappa(\mathbf{r}(i), \mathbf{r}(k)). \tag{3.31}$$

In this work and other subsequent chapters on kernel based estimation, the most commonly used Gaussian kernel function

$$\kappa(\mathbf{r}(i), \mathbf{r}(k)) = \exp\left(-\frac{\sum_{j=0}^{ML-1}(\mathbf{r}_j(i) - \mathbf{r}_j^*(k))^2}{\sigma^2}\right)$$

is used [55], where σ is the kernel width and $\mathbf{r}_j(\cdot)$ is the j^{th} element of $\mathbf{r}(\cdot)$.

After replacing desired outputs (true parameters) and their corresponding inputs (observations) as $d(k) = {\tau_o}^k, {f_d}^k$ and $\mathbf{r}(k) = \mathbf{r}^k_{\tau_o|f_d}, \mathbf{r}^k_{f_d|\tau_o}$, the pseudo code for KLMS based estimator, is given in Algorithm-1.

Algorithm 1 KLMS algorithm to estimate τ_o and f_d

1: **Inputs:**
$\mathbf{r}(k) = \mathbf{r}^k_{\tau_o|f_d}, \mathbf{r}^k_{f_d|\tau_o} \forall\, k,\;\; d(k) = {\tau_o}^k, {f_d}^k\;\; \forall\, k$
2: **Initialize:**
$e(0) \leftarrow 0,\;\; \hat{g}(0) \leftarrow \kappa(\mathbf{r}(0), \cdot),\;\; \mathcal{D}_k \leftarrow \{\},\;\; \mathbf{a}_k \leftarrow \{\},$ choose μ and σ, $\mathbf{r}(0) \leftarrow \mathbf{r}^0_{\tau_o|f_d}, \mathbf{r}^0_{f_d|\tau_o}$
3: **while** $\{\mathbf{r}(k), d(k)\}$ available **do**
$\hat{g}(k) = \mu \sum_{i=0}^{k-1} e(i)\kappa(\mathbf{r}(i), \mathbf{r}(k))$
$e(k) = d(k) - \hat{g}(k), \mathcal{D}_k \leftarrow \mathbf{r}(k), \mathbf{a}_k \leftarrow e(k)$
4: **end while**

3.2.2 Estimator based on KLMS-NC

At each instant k and for every input-output pair $\{\mathbf{r}(k), d(k)\}$, iteratively learning and updating the estimates, increases the size of dictionary $\mathcal{D}_k$ as given in Algorithm-1. Dictionary is a collection of all the important centers of Gaussian kernel κ which keeps track of all the input samples used for the training of a system. The increasing dictionary size is due to the utilization of every observation $\mathbf{r}(k)$ for estimation. However, not all the observations play a significant role in estimation of the non-linear system. To address the problem of increasing sample size, Platt's NC for sparsification techniques have been introduced in [43].

In dictionary sparsification technique, for curbing the growth of linearly increasing dictionary size, only important input observations are added as the new center. This is accomplished by applying constraints on the Euclidean distance of an input observation. With each newly incoming input $\mathbf{r}(k)$ its Euclidean distance from the previously stored centers are calculated as $\mathbf{dis}(\mathbf{r}(k), \mathbf{r}(j)) = \|\mathbf{r}(k) - \mathbf{r}(j)\|_2\;\; \forall j = 0, 1, \ldots, S$. If minimum of $\mathbf{dis}(\mathbf{r}(k), \mathbf{r}(j))$ is less than or equal to a pre-assigned small number δ_1 i.e. $\underbrace{min}_{0 \le j \le S} \mathbf{dis}(\mathbf{r}(k), \mathbf{r}(j)) \le \delta_1$ then the input observation will be discarded and not be added in the dictionary $\mathcal{D}_{k-1}$ as a new input center. However, if $\underbrace{min}_{0 \le j \le S} \mathbf{dis}(\mathbf{r}(k), \mathbf{r}(j)) > \delta_1$ then absolute of the error $\mid e(k) \mid$ associated with the input observation is compared against another pre-assigned small number δ_2. If $\mid e(k) \mid > \delta_2$, then the input observation is treated as an important observation and gets added in the dictionary as a new center, thereby results in modification of $\mathcal{D}_{k-1}$ as $\mathcal{D}_k = \{\mathcal{D}_{k-1} \cup \mathbf{r}(k)\}$. Else the observation is discarded, while the contents and size of dictionary remain unchanged. By doing this, the sparsification method effectively reduces the required number of training regressors while preserving a desirable performance.

The pseudo code for the proposed online estimator based on KLMS with sparsification is described in Algorithm 2.

Algorithm 2 KLMS algorithm to estimate τ_o and f_d with sparsification

Inputs:
$\mathbf{r}(k) = \mathbf{r}^k_{\tau_o|f_d}, \mathbf{r}^k_{f_d|\tau_o} \forall\, k,\;\; d(k) = {\tau_o}^k, {f_d}^k \;\; \forall\, k$

Initialize:
$e(0) \leftarrow 0,\;\; \hat{g}(0) \leftarrow \kappa(\mathbf{r}(0), \cdot),\;\; \mathcal{D}_k \leftarrow \{\},\;\; \mathbf{a}_k \leftarrow \{\}$, choose μ and σ, $\mathbf{r}(0) \leftarrow \mathbf{r}^0_{\tau_o|f_d}, \mathbf{r}^0_{f_d|\tau_o}$

while $\{\mathbf{r}(k), d(k)\}$ available **do**
  $\hat{g}(k) = \mu \sum_{i=0}^{|\mathcal{D}_{k-1}|} e(i)\kappa(\mathcal{D}^i_{k-1}, \mathbf{r}(k))$
  $e(k) = d(k) - \hat{g}(k)$
  $\mathbf{dis}(j) = \| \mathbf{r}(k) - \mathcal{D}^j_{k-1} \|$ for $0 \le j \le S$
  if $\underbrace{min}_{0\le j\le S}$ $\mathbf{dis}(j) \ge \delta_1$ and $|e(k)| \ge \delta_2$ **then**
    $\mathcal{D}_k = \{\mathcal{D}_{k-1} \cup \mathbf{r}(k)\}, \mathbf{a}_k = \{\mathbf{a}_{k-1} \cup e(k)\}$
  else
    $\mathcal{D}_k = \mathcal{D}_{k-1},\;\; \mathbf{a}_k = \mathbf{a}_{k-1}$
  end if
end while

3.2.3 Estimator based on KLMS-Modified NC

The width σ is an important parameter for Gaussian kernel function. Both the learning rate and estimates are sensitive to the choice of σ. For large values of σ, all the input vectors will look similar in the RKHS (with inner product close to unity). On the contrary, low values of σ results in almost zero inner product which in turn reflects that all the input vectors are different. Hence, choosing an appropriate value of σ is vital in KLMS. There are methods to choose the finite kernel size like cross-validation, penalizing function, plug-in method, and Silverman's rule. The penalizing function and plug-in methods are computationally expensive in the online learning system. Silverman's rule is derived for Gaussian approximation, and it is widely used to select the kernel size in kernel density estimation [44, 57, 58]. However, for online learning algorithms, Silverman's rule provides the sub-optimum value of kernel width [45, 58].

Thus, as KLMS is an online learning algorithm where the weights are updated at each iteration the kernel width σ can also be updated simultaneously by reducing the MSE at each iteration [45]. If σ_k is the kernel width at k^{th} iteration then the update equation for σ_k is given by

$$\sigma_k = \sigma_{k-1} - \eta \frac{\partial}{\partial \sigma_{k-1}} e^2(k). \tag{3.32}$$

Due to system non-linearity, $d(k)$ can be approximated as, $d(k) = \hat{g}(\mathbf{r}(k)) + u(k)$, wherein, $\hat{g}(\cdot)$ is the approximation of non-linear mapping which recovers the delay/Doppler spread from the radar return, and $u(k)$ is the approximation error at the k^{th} time instant.

If $g_{k-1}\{\cdot\}$ is the estimated mapping after learning upto k^{th} instant, then the error $e(k)$ associated with input $\mathbf{r}(k)$ is

$$e(k) = d(k) - g_{k-1}(\mathbf{r}(k)) = \tilde{g}_{k-1}(\mathbf{r}(k)) + u(k), \tag{3.33}$$

where $\tilde{g}_{k-1}(\mathbf{r}(k)) = \hat{g}(\mathbf{r}(k)) - g_{k-1}(\mathbf{r}(k))$.

Substituting (3.33) in (3.32) yields

$$\begin{aligned}
\sigma_k =& \sigma_{k-1} - 2\eta e(k) \frac{\partial}{\partial \sigma_{k-1}} [\tilde{g}_{k-1}(\mathbf{r}(k)) + u(k)] \\
=& \sigma_{k-1} + 2\eta\mu e(k) e(k-1) \frac{\partial}{\partial \sigma_{k-1}} [\kappa_{\sigma_{k-1}}(\mathbf{r}(k-1)), \mathbf{r}(k)] \\
=& \sigma_{k-1} + \rho e(k) e(k-1) \sum_{j=0}^{ML-1} (\mathbf{r}_j(k-1) - \mathbf{r}_j^*(k))^2 \frac{\kappa_{\sigma_{k-1}}(\mathbf{r}(k-1), \mathbf{r}(k))}{\sigma_{k-1}^3},
\end{aligned} \tag{3.34}$$

where $\rho = 4\eta\mu$ is the kernel width learning parameter.

Similar to μ, ρ controls the speed of convergence of kernel width to its steady-state value. Subsequently, for the guaranteed convergence of kernel width, the detailed derivation for bound on ρ is given in Appendix-A. Pseudo code for the proposed online estimator based on KLMS with adaptive kernel width and sparsification is described in Algorithm 3.

Algorithm 3 KLMS algorithm to estimate τ_o and f_d with adaptive kernel width and sparsification

Inputs:
$\mathbf{r}(k) = \mathbf{r}^k_{\tau_o|f_d}, \mathbf{r}^k_{f_d|\tau_o} \forall\, k,\;\; d(k) = {\tau_o}^k, {f_d}^k \;\; \forall\, k$
Initialize:
$e(0) \leftarrow 0,\;\; \hat{g}(0) \leftarrow \kappa(\mathbf{r}(0), \cdot),\;\; \mathcal{D}_k \leftarrow \{\},\;\; \mathbf{a}_k \leftarrow \{\},$ choose $\mu,\;\; \sigma_0,$ and $\rho,\;\; \mathbf{r}(0) \leftarrow \mathbf{r}^0_{\tau_o|f_d}, \mathbf{r}^0_{f_d|\tau_o}$
while $\{\mathbf{r}(k), d(k)\}$ available **do**
    $\hat{g}(k) = \mu \sum_{i=0}^{|\mathcal{D}_{k-1}|} e^*(i)\kappa(\mathcal{D}^i_{k-1}, \mathbf{r}(k))$
    $e(k) = d(k) - \hat{g}(k)$
    $\mathbf{dis}(j) = \| \mathbf{r}(k) - \mathcal{D}^j_{k-1} \|$ for $0 \le j \le S$
    if $\underbrace{min}_{0 \le j \le S}$ $\mathbf{dis}(j) \ge \delta_1$ and $|e(k)| \ge \delta_2$ **then**
        $\mathcal{D}_k = \{\mathcal{D}_{k-1} \cup \mathbf{r}(k)\},\;\; \mathbf{a}_k = \{\mathbf{a}_{k-1} \cup e(k)\}$
        $\sigma_k = \sigma_{k-1} + \rho e(k) e(k-1) \sum_{j=0}^{ML-1} (\mathbf{r}_j(k-1) - \mathbf{r}^*_j(k))^2 \left(\frac{\kappa_{\sigma_{k-1}}(\mathbf{r}(k-1), \mathbf{r}(k))}{\sigma^3_{k-1}} \right)$
    else
        $\mathcal{D}_k = \mathcal{D}_{k-1},\;\; \mathbf{a}_k = \mathbf{a}_{k-1}$
    end if
end while

3.3 CRLB for Delay and Doppler shift in RKHS

In this section, to assess the performance of proposed estimators, CRLB for delay and Doppler shift estimation are derived. Since the system model for LFM radar and OFDM radar differs only in the observations, derivation for the CRLB is performed by considering the system model of a generalized radar system, where signal model is given as

$$\mathbf{r}_v = \mathbf{s}_v + \mathbf{w}_v. \tag{3.35}$$

The above signal model is generalization for LFM and OFDM radar, as $\mathbf{s}_v$ is the signal part of either LFM or OFDM radar system i.e. $\mathbf{s}_v = \mathrm{vec}(\mathbf{S}_{\text{LFM}})$ or $\mathbf{s}_v = \mathrm{vec}(\mathbf{S}_{\text{OFDM}})$. Similarly, $\mathbf{r}_v$ is the received radar return affected by AWGN $\mathbf{w}_v$ of either LFM or OFDM radar system corresponding to $\mathrm{vec}(\mathbf{S}_{\text{LFM}})$ or $\mathrm{vec}(\mathbf{S}_{\text{OFDM}})$ respectively. Mapping (3.35) to RKHS (through the mapping function $\Phi : \mathbb{C}^N \longrightarrow \mathbb{H}$), (3.35) is given by

$$\Phi(\mathbf{r}_v) = \Phi(\mathbf{s}_v + \mathbf{w}_v) \approx \Phi(\mathbf{s}_v) + \nabla\Phi(\mathbf{s}_v)\mathbf{w}_v, \tag{3.36}$$

where $\nabla\Phi(\mathbf{s}_v)$ is the Jacobian matrix. Let θ represent the unknown parameter whose CRLB is evaluated.

The observations in 3.36 are function of unknown parameter θ, hence CRLB of the system model parametrized by the unknown parameter as in [35, Ch. 3.8] is given by

$$CRLB(\theta) = \nabla\Phi(\mathbf{s}_v)^H I^{-1}(\theta)\nabla\Phi(\mathbf{s}_v), \tag{3.37}$$

where $I(\theta)$ is the Fisher information for the system model described in (3.35) and is given as

$$I(\theta) = -\mathbb{E}\left[\frac{\partial^2}{\partial\theta^2}\ln\mathcal{P}(\mathbf{r}_v;\theta)\right], \tag{3.38}$$

where $\mathcal{P}(\mathbf{r}_v;\theta)$ is the probability distribution function of observation $\mathbf{r}_v$ in Euclidean space.

$$\mathcal{P}(\mathbf{r}_v;\theta) = \frac{1}{\pi^N|\mathbf{\Sigma_w}|}\exp\left(-(\mathbf{r}_v - \mathbf{s}_v)^H\mathbf{\Sigma_w}^{-1}(\mathbf{r}_v - \mathbf{s}_v)\right),$$

where N is the cardinality of $\mathbf{r}_v$ i.e. $N = ML$. Hence solving for (3.38) yields

$$\ln\mathcal{P}(\mathbf{r}_v;\theta) = -N\ln(\pi|\mathbf{\Sigma_w}|^{\frac{1}{N}}) - (\mathbf{r}_v - \mathbf{s}_v)^H\mathbf{\Sigma_w}^{-1}(\mathbf{r}_v - \mathbf{s}_v). \tag{3.39}$$

Substituting (3.39) in (3.38) and utilizing $\mathbb{E}[\mathbf{r}_v] = \mathbf{s}_v$, yields

$$I(\theta) = -2\left(\frac{\partial\mathbf{s}_v}{\partial\theta}^H\mathbf{\Sigma_w}^{-1}\frac{\partial\mathbf{s}_v}{\partial\theta}\right). \tag{3.40}$$

Substituting (3.40) in (3.37) and using the trace identity [59]

$$\begin{aligned} CRLB(\theta) &= -\frac{1}{2}\mathrm{tr}(\nabla\Phi(\mathbf{s}_v)^H\left(\frac{\partial\mathbf{s}_v}{\partial\theta}^H\mathbf{\Sigma_w}^{-1}\frac{\partial\mathbf{s}_v}{\partial\theta}\right)^{-1}\nabla\Phi(\mathbf{s}_v)), \\ &= -\frac{1}{2}\mathrm{tr}(\nabla\Phi(\mathbf{s}_v)^H\nabla\Phi(\mathbf{s}_v)\left(\frac{\partial\mathbf{s}_v}{\partial\theta}^H\mathbf{\Sigma_w}^{-1}\frac{\partial\mathbf{s}_v}{\partial\theta}\right)^{-1}). \end{aligned} \tag{3.41}$$

Since from kernel trick $\nabla\Phi(\mathbf{s}_v)^H\nabla\Phi(\mathbf{s}_v) = \langle\nabla\Phi(\mathbf{s}_v), \nabla\Phi(\mathbf{s}_v)\rangle_{\mathbb{H}} = N$. Hence, (3.41) can be written as

$$CRLB(\theta) = -\frac{N}{2}\mathbf{tr}\left(\left(\frac{\partial \mathbf{s}_v}{\partial \theta}^H \frac{\partial \mathbf{s}_v}{\partial \theta}\mathbf{\Sigma_w}^{-1}\right)^{-1}\right). \tag{3.42}$$

3.3.1 CRLB for Delay

Solving (3.42) for $\theta = \tau_o$ for

LFM radar system $(\mathbf{s}_v = \mathbf{vec}(\mathbf{S}_{\text{LFM}}))$

$$CRLB_{\text{LFM}}(\tau_o) = -\frac{N}{2}\text{tr}\left(\left(\frac{\partial \text{vec}(\mathbf{S}_{\text{LFM}})}{\partial \tau_o}^H \frac{\partial \text{vec}(\mathbf{S}_{\text{LFM}})}{\partial \tau_o}\mathbf{\Sigma_w}^{-1}\right)^{-1}\right) = \frac{N}{8\pi^2 \Delta f^2 M \sum_{l=1}^{L-1} l^2}\text{tr}(\mathbf{\Sigma_w}). \tag{3.43}$$

Substituting $\mathbf{\Sigma_w} = \Omega_w^2 \mathbf{I}$, the final expression for $CRLB_{\text{LFM}}(\tau_o)$ is given by

$$CRLB_{\text{LFM}}(\tau_0) = \frac{3\Omega_w^2 N}{4\pi^2 \Delta f^2 (L-1)(2L-1)}. \tag{3.44}$$

OFDM radar system $(\mathbf{s}_v = \mathbf{vec}(\mathbf{S}_{\text{OFDM}}))$

$$CRLB_{\text{OFDM}}(\tau_o) = -\frac{N}{2}\text{tr}\left(\left(\frac{\partial \text{vec}(\mathbf{S}_{\text{OFDM}})}{\partial \tau_o}^H \frac{\partial \text{vec}(\mathbf{S}_{\text{OFDM}})}{\partial \tau_o}\mathbf{\Sigma_w}^{-1}\right)^{-1}\right) = \frac{3\Omega_w^2 N}{4\pi^2 \Delta f^2 (L-1)(2L-1)}. \tag{3.45}$$

3.3.2 CRLB for Doppler shift

Solving (3.42) for $\theta = f_d$, and for

LFM radar system ($\mathbf{s}_v = \mathbf{vec}(\mathbf{S}_{\text{LFM}})$)

$$CRLB_{\text{LFM}}(f_d) = -\frac{N}{2}\text{tr}\left(\frac{\partial \text{vec}(\mathbf{S}_{\text{LFM}})}{\partial f_d}^H \frac{\partial \text{vec}(\mathbf{S}_{\text{LFM}})}{\partial f_d} \mathbf{\Sigma_w}^{-1}\right)^{-1},$$
$$= \frac{N}{8\pi^2 T_{\text{PRI}}^2 L \sum_{m=1}^{M-1} m^2 (L + \frac{L(L-1)\Delta f}{f_c} + \frac{(L-1)L(2L-1)\Delta f}{6f_c})} \text{tr}(\mathbf{\Sigma_w}). \tag{3.46}$$

Similar to delay, substituting $\mathbf{\Sigma_w} = \Omega_w^2 \mathbf{I}$ and using $\sum_{m=1}^{M-1} m^2 = \frac{(M-1)M(2M-1)}{6}$. The $CRLB_{\text{LFM}}(f_d)$ is given by

$$CRLB_{\text{LFM}}(f_d) = \frac{3\Omega_w^2 N}{4\pi^2 T_{\text{PRI}}^2 L(M-1)(2M-1)(1 + \frac{(5+2L)(L-1)\Delta f}{6f_c})}. \tag{3.47}$$

OFDM radar system ($\mathbf{s}_v = \mathbf{vec}(\mathbf{S}_{\text{OFDM}})$)

$$CRLB_{\text{OFDM}}(f_d) = -\frac{N}{2}\text{tr}\left(\frac{\partial \text{vec}(\mathbf{S}_{\text{OFDM}})}{\partial f_d}^H \frac{\partial \text{vec}(\mathbf{S}_{\text{OFDM}})}{\partial f_d} \mathbf{\Sigma_w}^{-1}\right)^{-1}$$
$$= \frac{3\Omega_w^2 N}{4\pi^2 T_{\text{PRI}}^2 (M-1)(2M-1)}. \tag{3.48}$$

3.4 Simulation Results and Discussion

In this section, simulations for the proposed KLMS based delay and Doppler shift are detailed and validated through simulations. The performance of the proposed estimation algorithms are compared with FT and CRLB. Simulation parameters for both LFM and OFDM radar are given in Table-3.2 and Table-3.3 respectively. Parameters of a waveform used in the simulations are described in Table-3.4. The SNR is fixed at 10 dB for estimation of delay and Doppler shift.

3.4.1 Estimation of Delay for LFM and OFDM Radar

Delay estimation is carried out by uniformly splitting the range of delay true values $\{\tau_{o_{min}}, \tau_{o_{max}}\}$ in 5050 equal parts. Samples corresponding to all 5050 delays are formed

Table 3.1: Comparison of computational complexity of estimators based on KLMS, KLMS-NC, and KLMS-Modified NC

Estimation algorithm	Number of multiplications	Complexity order
KLMS	5000	$O(k)$
KLMS-NC	150	$O(\lvert\mathcal{D}_{k-1}^{NC}\rvert)$
KLMS-Modified NC	100	$O(\lvert\mathcal{D}_{k-1}^{MNC}\rvert)$

The following relation $O(|\mathcal{D}_{k-1}^{MNC}|) < O(|\mathcal{D}_{k-1}^{NC}|) < k$ holds in which $O(|\mathcal{D}_{k-1}^{NC}|)$ and $O(|\mathcal{D}_{k-1}^{MNC}|)$ are the cardinality of the dictionary for estimators based on KLMS-NC and KLMS-Modified NC, respectively.

according to (3.23). From [15], out of 5050 samples, first 5000 samples are used for training and remaining 1% for testing. Comparative plot of MSE convergence versus iteration and dictionary size corresponding to LFM radar and OFDM radar are shown in Fig. 3.1a. From Fig. 3.1a, it is observed that the final MSE achieved by KLMS-NC and KLMS-Modified NC is lower than KLMS. Additionally, modification in KLMS as KLMS-NC and KLMS-Modified NC provides low computational complexity and suitable kernel width, respectively. For both LFM and OFDM radar system, regressors used for the training of estimator in two modifications of KLMS are shown in Fig. 3.1a. In LFM radar system out of 5000 regressors, only 160 and 100 regressors are used after incorporating NC and Modified NC in KLMS, respectively. Similarly, the OFDM radar, utilizes 155 for NC, and 135 for Modified NC, out of 5000 regressors. Therefore, sparsification of samples by NC reduces the computational complexity of an algorithm and provides lower MSE than KLMS without NC as depicted in Fig. 3.1a. Comparative analysis of the number of computations required for the convergence of estimator MSE for KLMS, KLMS-NC, and KLMS-Modified NC for the given LFM and OFDM radar system model and corresponding to Fig. 3.1a is shown in Table-3.1.

3.4.2 Estimation of Doppler Shift for LFM and OFDM Radar

Similar to delay estimation, estimation of Doppler shift is carried out by uniformly splitting the true value range of Doppler shift $\{f_{d_{min}}, f_{d_{max}}\}$ in 5050 equal parts. Input samples

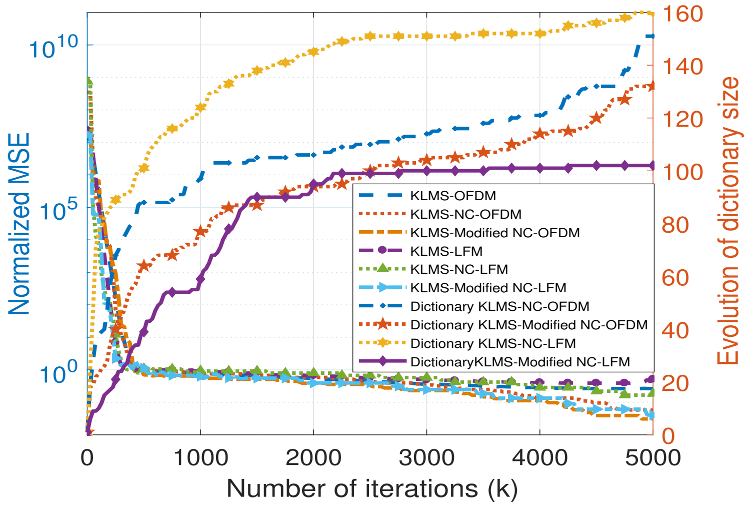

(a)

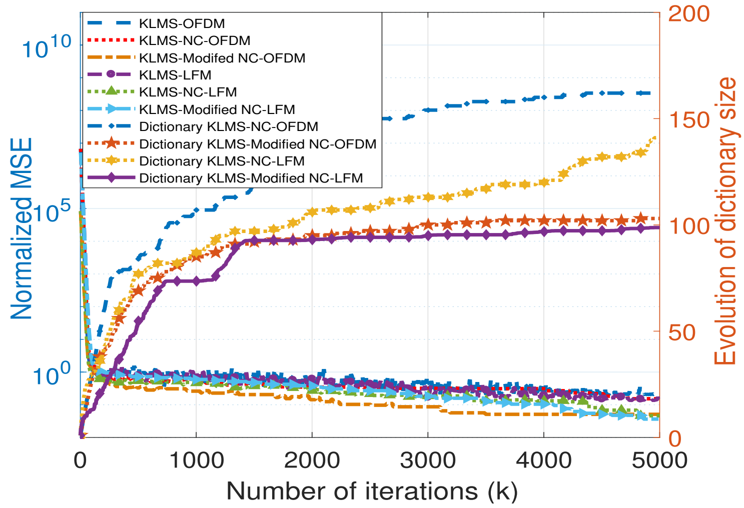

(b)

Figure 3.1: Normalized MSE and Dicitonary size in estimation of (a) delay and (b) Doppler shift for LFM and OFDM radar with estimators based on KLMS, KLMS-NC and KLMS-Modified NC.

of an estimator are formed corresponding to each of 5050 Doppler shifts utilizing (3.24). To illustrate effectiveness of proposed algorithm the input samples are as per [15], where 5000 samples are used for training of an estimator and the last 50 samples are used for testing. At each k^{th} iteration, the value of delay τ_o^k is treated as known and is chosen randomly from its available range $\{\tau_{o_{min}}, \tau_{o_{max}}\}$. Comparative plot for the convergence of MSE in Doppler shift estimation versus iterations and evolution of dictionary size for all three KLMS algorithms for LFM and OFDM radar are shown in Fig. 3.1b. Modification in KLMS by employing NC and Modified NC reduces the final MSE. With Modified

NC, KLMS provides the lowest MSE as compared to KLMS. Moreover, for LFM radar, contrary to NC case where 150 samples are utilized for training of an estimator, KLMS-Modified NC utilizes 100 samples out of 5000 as shown in Fig. 3.1b. Similar to LFM radar, as shown in Fig. 3.1b, in OFDM radar system too the implementation of Modified NC results in the utilization of 100 samples out of 5000. Whereas, KLMS-NC results in the utilization of 160 samples. Improvement in the performance of an estimator for both (LFM radar and OFDM radar) is because of the suitable kernel width which is achieved gradually with successive iteration along with the reduction in estimator MSE.

Table 3.2: Parameters values used for simulations for LFM radar system.

Parameters	KLMS $\{\tau_o, f_d\}$	KLMS-NC $\{\tau_o, f_d\}$	KLMS-Modified NC $\{\tau_o, f_d\}$
μ	$0.15, 0.2$	$0.35, 0.2$	$0.55, 0.1$
σ	$1.25 \times 10^{-6}, 10^{-2}$	$0.4 \times 10^{-6}, 10^{-6}$	Dynamic
ρ	Nil, Nil	Nil, Nil	$10^{4.5}, 10^{6}$
σ_o	Nil, Nil	Nil, Nil	$0.01, 0.01$

Table 3.3: Parameters values used for simulations for OFDM radar system.

Parameters	KLMS $\{\tau_o, f_d\}$	KLMS-NC $\{\tau_o, f_d\}$	KLMS-Modified NC $\{\tau_o, f_d\}$
μ	$0.15, 0.25$	$0.35, 0.25$	$0.25, 0.25$
σ	$10^{-5}, 10^{-2}$	$10^{-5}, 10^{-5}$	Dynamic
ρ	Nil, Nil	Nil, Nil	$10^{6.5}, 10^{6.5}$
σ_o	Nil, Nil	Nil, Nil	$0.01, 0.01$

Table 3.4: Values of radar parameters

Parameters	Values
Number of subcarriers (L)	8
Number of pulses (M)	8
Subcarrier spacing (Δf)	76.25 KHz
Pulse duration ($T_o = \frac{1}{\Delta f}$)	0.013×10^{-3}sec
Pulse repetition interval ($T_{\mathrm{PRI}} = 1.25T_o$)	0.016ms
Bandwidth $\{L\Delta f\}$	610KHz
Set of delay true value $\{\tau_{o_{min}}, \tau_{o_{max}}\}$=$\{\frac{1}{L\Delta f}, T_o\}$	$\{0.0016 \times 10^{-3}, 0.013 \times 10^{-3}\}$sec
Set of Doppler true value $\{f_{d_{min}}, f_{d_{max}}\}$=$\{-\frac{1}{2T_{PRI}}, \frac{1}{2T_{PRI}}\}$	$\{-30.4, 30.4\}$kHz

3.4.3 Performance Comparison of KLMS based Estimators with Fourier transform Method

A performance comparison between KLMS and FT is performed in this section. Since FT method gives approximate ML estimates by minimizing the non-convex cost function, the FT method is prone to produce erroneous estimates for the considered system model. Moreover, as the estimates are obtained by searching location of the peak in the discrete 2D spectrogram, the estimates are susceptible to the resolution of spectrogram peak (finer resolution of peak yields accurate estimates). Hence, for comparison between two estimators (FT and KLMS), the variance of a 2D spectrogram is used as a metric. The metric is chosen to measure the variance in the widening of peak in 2D spectrogram against increase in the noise level.

The performance of FT and KLMS algorithm using NC and Modified NC for the delay and Doppler shift estimation is examined over the SNR ranges from -20 dB to 30 dB. As shown in Fig. 3.2a and Fig. 3.2b, for the whole range of SNR, KLMS-Modified NC performs far better than FT. The improvement in estimation is considerable for LFM radar and OFDMradar, as shown in Fig. 3.2a and Fig. 3.2b, for the range of KLMS typically from 0 dB to 30 dB, KLMS-Modified NC yields estimate of delay with lower variance than KLMS-NC. However, for lower SNR range of -15 dB to -1 dB KLMS-NC and KLMS-Modified NC have similar performance. Similar trend can also be observed for OFDM radar.

From Fig. 3.2a and Fig. 3.2b, it can be observed that KLMS-Modifed NC and KLMS-NC exhibit similar convergence characteristics in certain scenarios when the kernel-width estimates by Silverman's rule are close to the optimal value of the kernel-width. However, from Fig. 3.2b, KLMS-Modified NC performs consistently better than KLMS-NC for OFDM radar in general. Furthermore, KLMS in both extensions (NC and Modified NC), and for both LFM radar and OFDM radar yields estimates (delay and Doppler shift) closest to the CRLBs.

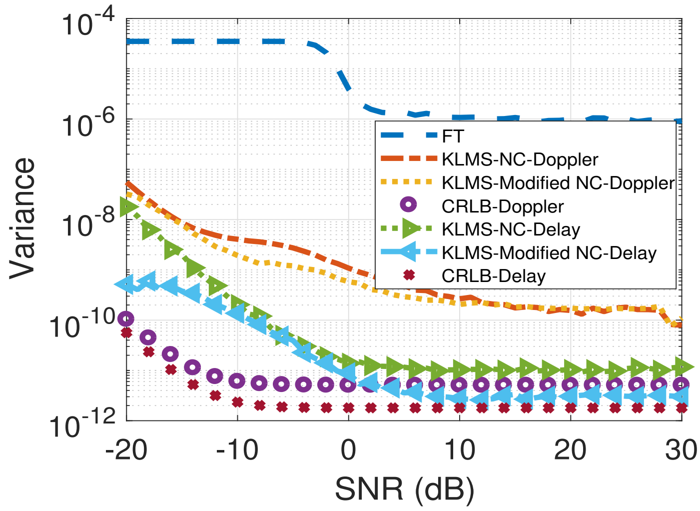

(a)

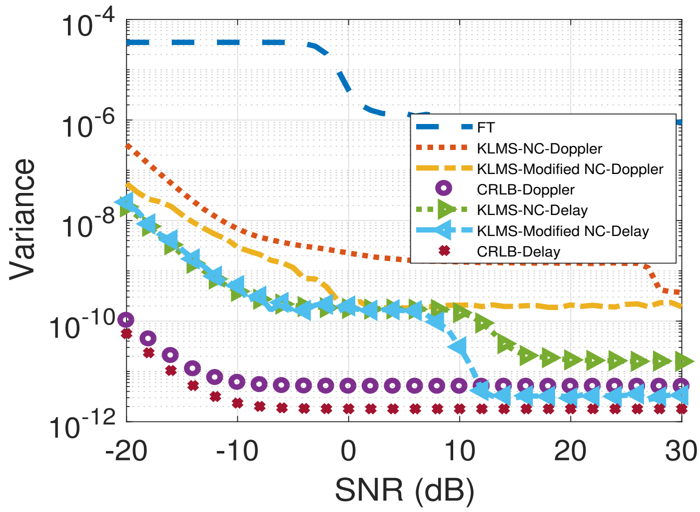

(b)

Figure 3.2: Comparison of FT method with KLMS-NC and KLMS-Modified NC algorithms for delay and Doppler shift estimation in (a) LFM and (b) OFDM radar.

3.5 Summary

In this Chapter, KLMS based estimation algorithms were proposed for LFM and OFDM radar systems. The estimation of the target's unknown parameters is performed via an implicit mapping to RKHS. To facilitate sparse learning without affecting estimator performance, Platt's NC is used to limit the increasing size of training samples. Additionally, a technique is explored for tuning the hyper-parameter σ from observations and is found to be suitable for both LFM and OFDM radar systems in terms of MSE and computational complexity. Moreover, optimization of the convex cost function over an RKHS makes the proposed estimators viable for generalized radar models. Furthermore, an analytical expression is derived for the CRLB of the proposed RKHS based estimators for the given system model. Lastly, from the simulations, it is observed that the variance of the estimates corresponding to the proposed estimators is lower than the existing non-adaptive estimation techniques, and is closer to the achievable CRLB.

In this Chapter, estimation of delay and Doppler shift is pursued by utilizing the radar observations perturbed by Gaussian distributed thermal noise. However, other than the target of interest, practically, the radar surveillance environment is perturbed by reflections from other objects as well called clutter. In practice, the clutter follows the non-Gaussian distribution. The proposed KLMS based estimator uses MSE, which considers second-order statistics of error (between the estimated and true parameter value); consequently, the KLMS based estimators developed in Chapter 3 are suitable only for radar observations perturbed by clutter with Gaussian approximation or Gaussian distributed thermal noise. For extending the use of KAF based estimation techniques for practical radar systems perturbed by non-Gaussian clutter and thermal noise, in the next Chapter, the KMC based estimators are developed. The estimators developed in Chapter 4, instead of using MSE, optimizes correntropy. Correntropy, being information-theoretic learning (ITL) criterion, considers higher-order statistics of the error to incorporate the means of dealing with the effects of non-Gaussian clutter in estimation in a practical scenario.

Chapter 4

Range and Velocity Estimation in non-Gaussian Clutter

In the previous Chapter, for efficient estimation of the target's range and velocity, KLMS based adaptive estimators are developed and tested for LFM and OFDM radar systems perturbed by Gaussian distributed thermal noise. The KLMS based estimators are viable due to the universal approximation of an arbitrary unknown function and convexity of the cost function in RKHS [15, 16, 41, 60]. Convexity and universal representation make estimators based on KLMS better suited in comparison to conventional estimation techniques based on FT. Nevertheless, the radar return is affected by the undesired reflections from objects [4, 61–63], these reflections are collectively called clutter and modeled by non-Gaussian distributions [23, 64–66]. The KLMS based estimator uses MSE for adaptation, which is optimal for additive Gaussian distortion [61, 62]. However, the optimality of KLMS based estimator for additive non-Gaussian distortion is not guaranteed because MSE considers second-order statistics of error.

In this Chapter, the problem of delay and Doppler shift estimation is pursued in the more realistic and practical environment, perturbed by thermal noise and clutter. Subsequently, limitations of the conventional estimators based on FT and KLMS, in the presence of non-Gaussian clutter are overcome by the proposed estimator based on KMC algorithm. The proposed KMC based estimator uses MCC in RKHS and provides improved performance both in terms of computational complexity and estimation accuracy. MCC is an ITL criterion and can be considered as a similarity measure between the two random variables [67, 68]. Moreover, MCC is an online estimate of Renyi-α information criterion for $\alpha = 2$ [69]. Additionally, maximizing the similarity between the desired parameter and estimated parameter, results in a smooth loss function, and rejection of outliers. Furthermore, KMC, unlike other estimators based on KLMS criterion considers higher order statistics for estimation [61, 62, 67, 68, 70, 71]. Hence, maximization of smooth loss function and consideration of higher order statistics makes estimators based on KMC viable in the presence of clutter. However, the practical deployment of KMC based estimator is limited by two aspects: i) KMC based estimator approximates the unknown function using the radar return in RKHS. Consequently, they suffer from linear temporal increase in computational complexity [18, 72], and ii) for smooth function approximation, the KMC based estimator employs a continuous Mercer's kernel; however the accuracy of function approximation by KMC algorithm depends on the choice of appropriate kernel width [15, 16, 45], which makes choice of appropriate kernel-width for MCC based estimation crucial.

To mitigate the above limitations of KMC based estimator for range and velocity estimation in the presence of non-Gaussian clutter, the two variants of KMC based estimator are proposed. Firstly, for curbing increasing computational complexity of KMC based estimation in RKHS, similar to KLMS-NC in Chapter 3, Platt's NC [43] with KMC is used. Secondly, for selection of an appropriate kernel width, an adaptive estimator for stochastic update of the kernel-width using MCC is proposed, namely the KMC-Modified NC.

The Chapter is organized as follows: A brief introduction to the LFM and SF radar return is given first. After that, the proposed estimators based on KMC-NC and KMC-Modified NC are described. Next, analytical expressions are derived for CRLB of the KMC based target-parameter estimation, and overall variance of the estimators is quantified. Followed this, simulation results are presented for validating the proposed KMC based estimators. Finally, conclusion is given.

4.1 System Model

Performance of the proposed estimators is analyzed over both the LFM and SF radar system, which, in a given CPI transmits M radar pulses [5, 31, 54, 73, 74]. The transmitted waveform is a pulse of finite width and repeats after a certain PRI. We consider processing of the waveform on PRI basis. Then, from Section 3.1 of Chapter 3, the transmitted pass-band pulse is given by

$$s_m(t) = \big(s(t - mT_{\text{PRI}})\big)\exp(j2\pi f_c t), \tag{4.1}$$

where $s(t)$ is either the LFM or SF baseband transmitted pulse.

Without loss of generality, let us consider that the target is located at an unknown range R_o and P scatterers are located at range $R_p \forall p = [1, \cdots, P]$ from the radar. The received pass-band radar return for an arbitrary m^{th} pulse is given by

$$r_m(t) = \zeta\big(s_m(t - \tau_m)\big) + \zeta \sum_{p=1}^{P} s_m(t - \tau_m^p) + w(t), \tag{4.2}$$

where τ_m is define in Section 3.1 of Chapter 3, ζ represents the complex attenuation factor proportional to the target RCS and $\tau_m^p = \frac{2R_p}{c}$.

The second term in (4.2) represents the combined effect of all the unwanted reflections from the clutter henceforth, denoted as a random process $c(t)$. Consequently, from (4.1) and (4.2), yield

$$r_m(t) = \zeta\big(s(t - mT_{\text{PRI}} - \tau_m)\big)\exp(j2\pi f_c(t - \tau_m)) + c(t) + w(t). \tag{4.3}$$

4.1.1 Radar return for LFM radar

After substituting (3.4) into (4.3), and following the steps given in [2], the radar return of LFM radar for m^{th} pulse and l^{th} frequency sample is given by

$$r_{\text{LFM}}(m,l) = \zeta x_{\text{LFM}}(m,l) + c(m,l) + w(m,l) \tag{4.4}$$

where $x_{\text{LFM}}(m,l) = \exp(j2\pi m f_d T_{\text{PRI}}) \exp(-j2\pi l \Delta f \tau_o) \exp(j2\pi f_d ml(\frac{T_{\text{PRI}}\Delta f}{f_c}))$, $c(m,l)$ are the sample from clutter follows the K distribution define in Section 1.5 of Chapter 1.

For $m = 0, \cdots, M-1$ and $l = 0, \cdots, L-1$, concatenating (4.4) in a vector yields

$$\mathbf{r}_{\text{LFM}} = \zeta \mathbf{x}_{\text{LFM}} + \mathbf{c} + \mathbf{w}, \tag{4.5}$$

where $\mathbf{r}_{\text{LFM}} = [r_{\text{LFM}}(0,0), r_{\text{LFM}}(0,1), \cdots, r_{\text{LFM}}(M-1, L-1)]^T$, $\mathbf{c} = [c(0,0), c(0,1), \cdots, c(M-1, L-1)]^T$, $\mathbf{w} = [w(0,0), w(0,1), \cdots, w(M-1, L-1)]^T$, and

$$\mathbf{x}_{\text{LFM}} = [x_{\text{LFM}}(0,0), x_{\text{LFM}}(0,1), \cdots, x_{\text{LFM}}(M-1, L-1)]^T$$

4.1.2 Radar return for SF radar

For SF radar, $s(t)$ for m^{th} pulse is given by

$$s(t) = b \exp(j2\pi m \Delta f t), \quad \text{for} \quad 0 \le t \le T_o \tag{4.6}$$

where b is the amplitude, and Δf is the frequency increment of SF waveform.

Substituting (4.6) into (4.3) and sampling at an interval of $lT_o + mT_{\text{PRI}}$, the radar return for SF radar for m^{th} pulse and l^{th} fast time index is given by

$$r_{\text{SF}}(m,l) = \zeta x_{\text{SF}}(m,l) + c(m,l) + w(m,l) \tag{4.7}$$

where $x_{\text{SF}}(m,l) = \exp(j2\pi f_d(mT_{\text{PRI}} + lT_o)) \exp(-j2\pi l \Delta f \tau_o)$

Concatenating (4.7) in a vector yields

$$\mathbf{r}_{\text{SF}} = \zeta \mathbf{x}_{\text{SF}} + \mathbf{c} + \mathbf{w}, \tag{4.8}$$

where $\mathbf{r}_{\text{SF}} = [r_{\text{SF}}(0,0), r_{\text{SF}}(0,1), \cdots, r_{\text{SF}}(M-1, L-1)]^T$, and

$$\mathbf{x}_{\text{SF}} = [x_{\text{SF}}(0,0), x_{\text{SF}}(0,1), \cdots, x_{\text{SF}}(M-1, L-1)]^T$$

For better estimation of delay and Doppler shift, the KLMS based estimator is introduced in Chapter 3. However, since KLMS based estimator works on the principle of minimization of MSE criterion in RKHS, they are prone to yield inaccurate estimates in the presence of non-Gaussian clutter. The estimation of the target's delay and Doppler shift in the presence of non-Gaussian clutter, has not been taken up in literature. To improve estimation of delay and Doppler shift in the presence of non-Gaussian clutter, KMC based sparse estimators are proposed in the next section.

4.2 KMC based Estimators

In the proposed estimators, estimations of delay and Doppler shift are pursued individually, whereby, the true value of delay and Doppler shift is limited to one dimension, i.e. $\tau_o \in \mathbb{R}$, and $f_d \in \mathbb{R}$.

For estimation of delay and Doppler shift, constant attenuation factor, ζ, in (4.5) and (4.8) is considered to be unity, hence

$$\mathbf{r}_{\text{LFM}} = \mathbf{x}_{\text{LFM}} + \mathbf{c} + \mathbf{w}, \tag{4.9}$$

$$\mathbf{r}_{\text{SF}} = \mathbf{x}_{\text{SF}} + \mathbf{c} + \mathbf{w}. \tag{4.10}$$

Subsequently, for given f_d, the range $(\tau_{o_{min}}, \tau_{o_{max}})$ in which τ_o is expected to take the value is divided into K equal intervals i.e. $[\tau^1_{o_{min}} \dots \tau^K_{o_{max}}]$. At any instant k, (4.9) and (4.10) can be written as $\mathbf{r}^k_m = \exp\left(j2\pi m f_d T_{\text{PRI}}\right) \exp(j2\pi f_d m l(\frac{T_{\text{PRI}}\Delta f}{f_c}))\mathbf{d}_l + \mathbf{c} + \mathbf{w}\ \forall\, m =$

$[0,1,\ldots,\ M-1]$ for LFM radar system where $\mathbf{d}_l \in \mathbb{C}^{L\times 1} = [1,\cdots,\exp{(-j2\pi(L-1)\Delta f\tau_o)}]$ and as $\mathbf{r}_m^k = \exp{(j2\pi f_d(mT_{\text{PRI}} + lT_o))}\mathbf{d}_l + \mathbf{c} + \mathbf{w}\ \forall m = [0,1,\ldots,\ M-1]$ for SF radar system where $\mathbf{d}_l \in \mathbb{C}^{L\times 1} = [1,\cdots,\exp{(-j2\pi(L-1)\Delta f\tau_o)}]$. Hence, this yields

$$\mathbf{r}_{\tau_o|f_d}^k \in \mathbb{C}^{ML\times 1} = [\mathbf{r}_0^k, \mathbf{r}_1^k, \ldots, \mathbf{r}_{M-1}^k]^T. \tag{4.11}$$

Equivalently, at k^{th} instant, vector for the observations of radar return for LFM and SF radar system corresponding to any arbitrary Doppler shift f_d^k from the set $[f_{d_{min}}^1 \ldots f_{d_{max}}^K]$ of K-Doppler shifts is given as

$$\mathbf{r}_{f_d|\tau_o}^k \in \mathbb{C}^{ML\times 1} = [\mathbf{r}_0^k, \mathbf{r}_1^k, \ldots, \mathbf{r}_{L-1}^k]^T, \tag{4.12}$$

where $\mathbf{r}_l^k = \exp{(-j2\pi l\Delta f\tau_o)}\mathbf{d}_m + \mathbf{c} + \mathbf{w}$ and

$$\mathbf{d}_m \in \mathbb{C}^{M\times 1} = [1,\ldots,\exp{(j2\pi(M-1)f_d T_{\text{PRI}})}\exp(j2\pi f_d(M-1)l(\frac{T_{\text{PRI}}\Delta f}{f_c}))]^T$$

for LFM radar system and

$$\mathbf{d}_m \in \mathbb{C}^{M\times 1} = [\exp{(j2\pi f_d lT_o)},\cdots,\exp{(j2\pi f_d((M-1)T_{\text{PRI}} + lT_o))}]$$

for SF radar system.

4.2.1 Estimator based on KMC-NC

In this section, the proposed KMC-NC based estimator is described in detail. The KMC algorithm provides convexity in RKHS which aids in robust approximation of the unknown function in RKHS in the presence of clutter. Thus, in this work, KMC-NC based estimator is proposed for parameter estimation from LFM and SF radar model in the presence of non-Gaussian clutter described by (1.8).

The parameters are estimated by using a mapping function $g(\cdot)$, which at k^{th} instant maps the input vector $\mathbf{r}(k) \in \mathbb{C}^{ML}$ (where $\mathbf{r}(k) = \mathbf{r}_{\tau_o|f_d}^k, \mathbf{r}_{f_d|\tau_o}^k$) to corresponding output

$d(k) \in \mathbb{C}$ (where $d(k) = {\tau_o}^k, {f_d}^k$) as $(g(\mathbf{r}(k)) = d(k))$. The KMC algorithm proceeds with mapping the input vector $\mathbf{r}(k)\forall k$ into possibly infinite dimensional RKHS $\mathbb{H}$ by a complex Mercer kernel κ. If the k^{th} input vector is mapped in $\mathbb{H}$ as $\Phi(\mathbf{r}(k))$, then the following relation holds

$$\Phi(\mathbf{r}(k)) = \kappa(\mathbf{r}(k), \cdot). \tag{4.13}$$

From Mercer theorem, the reproducing kernel $\kappa(\mathbf{r}(k), \mathbf{r}(k'))$ [16] can be written as

$$\kappa(\mathbf{r}(k), \mathbf{r}(k')) = \langle \Phi(\mathbf{r}(k)), \Phi(\mathbf{r}(k')) \rangle_{\mathbb{H}}, \tag{4.14}$$

Similar to estimators based on KLMS, described in Chapter 3, if $\boldsymbol{\omega}(k-1)$ ia a weight-vector in linear space $\mathbb{H}$, then from kernel trick, which is equivalently the inner product in $\mathbb{H}$, gives estimate of the desired output $d(k)$ as $\hat{g}(k) = \langle \boldsymbol{\omega}(k-1), \Phi(\mathbf{r}(k)) \rangle_{\mathbb{H}}$. The learning rule given by MCC is

$$\mathcal{J}(\boldsymbol{\omega}) = \mathbb{E}[\kappa_{\sigma_c}(d(k), \hat{g}(k))]. \tag{4.15}$$

where $\kappa_{\sigma_c}(d(k), \hat{g}(k)) = \exp\big(-\frac{(d(k)-\hat{g}(k))^2}{2\sigma_c^2}\big)$ is the correntropy function, and σ_c is correntropy Gaussian kernel function width.

The correntropy in (4.15) is difficult to evaluate without knowing the joint probability density function of $d(k)$ and $\hat{g}(k)$ [61–63]. Therefore, (4.15) is estimated in terms of error of the instantaneous measurement at k^{th} instant as $\hat{\mathcal{J}}(\boldsymbol{\omega}) = \mathcal{J}_k(\boldsymbol{\omega})$ and given by

$$\mathcal{J}_k(\boldsymbol{\omega}) = \kappa_{\sigma_c}(d(k), \hat{g}(k)) = \exp\left(-\frac{(d(k)-\hat{g}(k))^2}{2\sigma_c^2}\right). \tag{4.16}$$

For stochastic gradient update of $\boldsymbol{\omega}$, the gradient of $\mathcal{J}_k(\boldsymbol{\omega})$ with respect to $\boldsymbol{\omega}$ is calculated (i.e. $\nabla_{\boldsymbol{\omega}}\mathcal{J}_k(\boldsymbol{\omega})$). Hence, the weight-vector $\boldsymbol{\omega}$ is updated by the factor $\mu \exp\big(-\frac{e^2(k)}{2\sigma_c^2}\big) e(k)\Phi(\mathbf{r}(k))$, where $e(k) = d(k) - \langle \boldsymbol{\omega}(k-1), \Phi(\mathbf{r}(k)) \rangle_{\mathbb{H}}$ is the instantaneous error in adaptive estimation and μ is the learning rate parameter as $\boldsymbol{\omega}(k) = \boldsymbol{\omega}(k-1) + \mu \exp\big(-\frac{e^2(k)}{2\sigma_c^2}\big) e(k)\Phi(\mathbf{r}(k))$. Subsequently, for the initial condition $\Omega(0) = \mathbf{0}$, repeated application of the weight-vector update yields

$$\boldsymbol{\omega}(k) = \mu \sum_{i=0}^{k} \exp\left(-\frac{e^2(i)}{2\sigma_c^2} \right) e(i) \Phi(\mathbf{r}(i)). \tag{4.17}$$

Thus, the estimated output at k^{th} time instant is given by

$$\begin{aligned} \hat{g}(k) = \langle \Phi(\mathbf{r}(k)), \boldsymbol{\omega}(k-1) \rangle_{\mathbb{H}} &= \langle \Phi(\mathbf{r}(k)), \mu \sum_{i=0}^{k-1} \exp\left(-\frac{e^2(i)}{2\sigma_c^2} \right) e(i) \Phi(\mathbf{r}(i)) \rangle_{\mathbb{H}}, \\ &= \mu \sum_{i=0}^{k-1} \exp\left(-\frac{e^2(i)}{2\sigma_c^2} \right) e(i) \langle \Phi(\mathbf{r}(i)), \Phi(\mathbf{r}(k)) \rangle_{\mathbb{H}}. \end{aligned} \tag{4.18}$$

Using Mercer's theorem, the estimated output $\hat{g}(k)$ at k^{th} iteration is given as

$$\hat{g}(k) = \mu \sum_{i=0}^{k-1} \exp\left(-\frac{e^2(i)}{2\sigma_c^2} \right) e(i) \kappa(\mathbf{r}(i), \mathbf{r}(k)). \tag{4.19}$$

As shown in (4.19), unlike the previously proposed estimator based on KLMS where the estimate $g(k)$ is given by $\hat{g}(k) = \mu \sum_{i=0}^{k-1} e(i)\kappa(\mathbf{r}(i), \mathbf{r}(k))$ (3.31), the estimate of $g(k)$ with the proposed estimator based on KMC have an additional factor $\left(\exp\left(-\frac{e^2(i)}{2\sigma_c^2}\right)\right)$ which depends upon the instantaneous error $e(k)$. With a suitable choice of σ_c, this additional factor, while dealing with non-Gaussian clutter facilitates the estimator based on KMC to suppress the effect of heavy tailed outliers.

Further, similar to estimator based on KLMS, developed in Chapter 3, at each instant k and for every input-output pair $\{\mathbf{r}(k), d(k)\}$, repeated learning and updating the estimates, increases the computational complexity of KMC based estimator as shown in (4.19). The computational complexity increases because each incoming observations $\mathbf{r}(k)$ is used for estimation. However, not all the observations are significant for estimation. Hence, to selectively choose the observations and simultaneously reducing the complexity, the sparsification technique based on NC [43], described in Section 3.2.2 of Chapter 3 is used.

After replacing desired outputs (true parameters) and their corresponding inputs (observations) as $d(k) = {\tau_o}^k, {f_d}^k$ and $\mathbf{r}(k) = \mathbf{r}^k_{\tau_o|f_d}, \mathbf{r}^k_{f_d|\tau_o}$ respectively, the pseudo code for the proposed online estimator based on KMC with sparsification is described in Algorithm

4.

Algorithm 4 KMC algorithm to estimate τ_o and f_d with sparsification

Inputs:
$\mathbf{r}(k) = \mathbf{r}^k_{\tau_o|f_d}, \mathbf{r}^k_{f_d|\tau_o} \forall\, k, \;\; d(k) = {\tau_o}^k, {f_d}^k \;\; \forall\, k$

Initialize:
choose μ and σ, $\mathbf{r}(0) \leftarrow \mathbf{r}^0_{\tau_o|f_d}, \mathbf{r}^0_{f_d|\tau_o}, e(0) \leftarrow 0,$
$\hat{g}(0) \leftarrow \kappa(\mathbf{r}(0), \cdot), \quad \mathcal{D}_k \leftarrow \{\}, \;\; \mathbf{a}_0 \leftarrow e(0)$

while $\{\mathbf{r}(k), d(k)\}$ available **do**
$\hat{g}(k) = \mu \sum_{i=0}^{|\mathcal{D}_{k-1}|} \exp\big(-\frac{e^2(i)}{2\sigma_c^2}\big) e(i) \kappa(\mathcal{D}^i_{k-1}, \mathbf{r}(k))$
$e(k) = d(k) - \hat{g}(k)$
$\mathbf{dis}(j) = \left\|\mathbf{r}(k) - \mathcal{D}^j_{k-1}\right\|$ for $0 \leq j \leq S$
if $\underbrace{\min}_{0 \leq j \leq S} \mathbf{dis}(j) \geq \delta_1 \,\&\, |e(k)| \geq \delta_2$ **then**
$\mathcal{D}_k = \{\mathcal{D}_{k-1} \cup \mathbf{r}(k)\}, \mathbf{a}_k = \{\mathbf{a}_{k-1} \cup e(k)\}$
else
$\mathcal{D}_k = \mathcal{D}_{k-1}, \;\; \mathbf{a}_k = \mathbf{a}_{k-1}$
end if
end while

4.2.2 Estimator based on KMC-Modified NC

As both the learning rate and parameter estimates are sensitive to the choice of σ, a suitable kernel width σ (size of the kernel) is a significant parameter for the proposed estimator based on KMC. Consequently, similar to estimators based on KLMS, selecting a proper value of σ is vital for estimators based on KMC. Therefore, in this section, an iterative update equation to learn σ with radar observation ($\mathbf{r}(k)$) is developed.

Since KMC is an online learning algorithm in which the weights in RKHS are updated at each iteration, the kernel width σ can also be updated simultaneously by applying MCC [45]. If σ_k is the kernel width at k^{th} iteration then the stochastic update equation for σ_k is given by

$$\sigma_k = \sigma_{k-1} - \eta \frac{\partial}{\partial \sigma_{k-1}} \big(\kappa_{\sigma_c}(e(k))\big). \tag{4.20}$$

where $e(k)$ is the instantaneous estimation error s.t. $e(k) = d(k) - \hat{g}(k)$ and $\kappa_{\sigma_c}(\cdot)$ is the correntropy function.

Since $\kappa_{\sigma_c}(e(k)) = \exp\big(-\frac{e^2(k)}{2\sigma_c^2}\big)$, (4.20) can be written as

$$\sigma_k = \sigma_{k-1} + \frac{\eta}{\sigma_c^2}\exp\big(-\frac{e^2(k)}{2\sigma_c^2}\big)e(k)\frac{\partial}{\partial\sigma_{k-1}}(e(k)). \tag{4.21}$$

Subsequently, $d(k)$ can be written as

$$d(k) = \hat{g}(\mathbf{r}(k)) + u(k). \tag{4.22}$$

where $\hat{g}(\cdot)$ is the estimate of mapping which estimate the delay/Doppler spread from the radar return, and $u(k)$ is the approximation error at the k^{th} time instant. If $g_{k-1}(\cdot)$ is the estimated mapping after learning upto k^{th} instant, then error $e(k)$ associated with input $\mathbf{r}(k)$ is given by

$$e(k) = d(k) - g_{k-1}(\mathbf{r}(k)) = \tilde{g}_{k-1}(\mathbf{r}(k)) + u(k), \tag{4.23}$$

where $\tilde{g}_{k-1}(\mathbf{r}(k)) = \hat{g}(\mathbf{r}(k)) - g_{k-1}(\mathbf{r}(k))$.

Substituting (4.23) into (4.21), yield

$$\begin{aligned}\sigma_k =&\sigma_{k-1} + \frac{\mu\eta}{\sigma_c^2}\exp\big(-\frac{e^2(k)}{2\sigma_c^2}\big)e(k)\frac{\partial}{\partial\sigma_{k-1}}\{\tilde{g}_{k-1}(\mathbf{r}(k)) + u(k)\}\\ =&\sigma_{k-1} - \frac{\mu\eta}{\sigma_c^2}\exp\big(-\frac{e^2(k)}{2\sigma_c^2}\big)\exp\big(-\frac{e^2(k-1)}{2\sigma_c^2}\big)e(k)e(k-1)\frac{\partial}{\partial\sigma_{k-1}}[\kappa_{\sigma_{k-1}}(\mathbf{r}(k-1)),\mathbf{r}(k)]\end{aligned} \tag{4.24}$$

Since, $\kappa_{\sigma_{k-1}}(\mathbf{r}(k-1)),\mathbf{r}(k)) = \exp\Bigg(-\frac{\|\mathbf{r}(k-1)-\mathbf{r}^*(k)\|^2}{\sigma_{k-1}^2}\Bigg)$, (4.24) is simplified as

$$\begin{aligned}\sigma_k =&\sigma_{k-1} - \rho\exp\big(-\frac{e^2(k)}{2\sigma_c^2}\big)\exp\big(-\frac{e^2(k-1)}{2\sigma_c^2}\big)e(k)e(k-1)\exp\Bigg(-\frac{\|\mathbf{r}(k-1)-\mathbf{r}^*(k)\|^2}{\sigma_{k-1}^2}\Bigg)\\ &\times\frac{\|\mathbf{r}(k-1)-\mathbf{r}^*(k)\|^2}{\sigma_{k-1}^3}\end{aligned} \tag{4.25}$$

where $\rho = \frac{\mu\eta}{2\sigma_c^2}$ is the kernel width learning parameter.

As shown in (4.25), the kernel width at each iteration k is adaptively updated by the derived expression for learning σ_k, and converges to an optimal kernel width. Moreover, as compared to the estimator based on KLMS-Modified NC (3.34), the additional factor $(\exp\big(-\frac{e^2(k)}{2\sigma_c^2}\big))$ in (4.25), similar to (4.19), compensates for the effect of non-Gaussian clutter, and provides better adaptation of kernel width for the proposed KMC based estimator.

Pseudo-code for the proposed online estimator based on KMC with adpative kernel width and sparsification is described in Algorithm 5.

Algorithm 5 KMC algorithm to estimate τ_o and f_d with adaptive kernel width and sparsification

Inputs:
$\mathbf{r}(k) = \mathbf{r}^k_{\tau_o|f_d}, \mathbf{r}^k_{f_d|\tau_o} \forall\, k,\ \ d(k) = {\tau_o}^k, {f_d}^k\ \ \forall\, k$

Initialize:
$e(0) \leftarrow 0,\ \ \hat{g}(0) \leftarrow \kappa(\mathbf{r}(0), \cdot),\ \ \mathcal{D}_k \leftarrow \{\},\ \ \mathbf{a}_k \leftarrow \{\},$
choose $\mu,\ \sigma_0,$ and $\rho,\ \ \mathbf{r}(0) \leftarrow \mathbf{r}^0_{\tau_o|f_d}, \mathbf{r}^0_{f_d|\tau_o}$

while $\{\mathbf{r}(k), d(k)\}$ available **do**

$\hat{g}(k) = \mu \sum_{i=0}^{|\mathcal{D}_{k-1}|} \exp\big(-\frac{e^2(i)}{2\sigma_c^2}\big) e^*(i)\kappa(\mathcal{D}^i_{k-1}, \mathbf{r}(k))$

$e(k) = d(k) - \hat{g}(k)$

$\mathbf{dis}(j) = \left\|\mathbf{r}(k) - \mathcal{D}^j_{k-1}\right\|$ for $0 \leq j \leq S$

if $\underbrace{min}_{0\leq j\leq S}\ \mathbf{dis}(j) \geq \delta_1\ \&\ |e(k)| \geq \delta_2$ **then**

$\mathcal{D}_k = \{\mathcal{D}_{k-1} \cup \mathbf{r}(k)\},\ \ \mathbf{a}_k = \{\mathbf{a}_{k-1} \cup e(k)\}$

$$\sigma_k = \sigma_{k-1} - \rho \exp\big(-\frac{e^2(k)}{2\sigma_c^2}\big) \exp\big(-\frac{e^2(k-1)}{2\sigma_c^2}\big) e(k)e(k-1) \exp\left(-\frac{\|\mathbf{r}(k-1) - \mathbf{r}^*(k)\|^2}{\sigma^2}\right) \times \frac{\|\mathbf{r}(k-1) - \mathbf{r}^*(k)\|^2}{\sigma_k^3}$$

else

$\mathcal{D}_k = \mathcal{D}_{k-1},\ \ \mathbf{a}_k = \mathbf{a}_{k-1}$

end if

end while

4.3 CRLB for Delay and Doppler shift in RKHS

To assess performance of the proposed estimators, in this section, CRLB for the variance of the estimated delay and Doppler shift for the considered estimation problem in the presence of non-Gaussian clutter and thermal noise is derived. The generalized system model for LFM and SF radar return is given by

$$\mathbf{r} = \mathbf{x} + \mathbf{c} + \mathbf{w}. \tag{4.26}$$

where from 4.9 and 4.10, $\mathbf{x}$ is the signal part of either LFM radar or SF radar (i.e $\mathbf{x} = \mathbf{x}_{\text{LFM}}$ or $\mathbf{x} = \mathbf{x}_{\text{SF}}$ corresponding to $\mathbf{r}_{\text{LFM}}$ or $\mathbf{r}_{\text{SF}}$, respectively).

After mapping (4.26) to RKHS, (4.26) is given by

$$\Phi(\mathbf{r}) = \Phi(\mathbf{x} + \mathbf{c} + \mathbf{w}). \tag{4.27}$$

The first order Taylor series approximation of (4.27) yields

$$\Phi(\mathbf{r}) = \Phi(\mathbf{x}) + \triangledown\Phi(\mathbf{x})(\mathbf{c} + \mathbf{w}). \tag{4.28}$$

where $\triangledown\Phi(\mathbf{x})$ is the Jacobian matrix.

Let θ represent the unknown parameter whose CRLB is evaluated. From (4.28), the observations are a function of unknown parameter θ, hence CRLB of the system model parametrized by the unknown parameter as in [75–77] and [35, Ch. 3.8] is given by

$$CRLB(\theta) = \triangledown\Phi(\mathbf{x})^H I^{-1}(\theta)\triangledown\Phi(\mathbf{x}). \tag{4.29}$$

where $I^{-1}(\theta)$ is given by

$$I^{-1}(\theta) = \mathbb{E}_\alpha\left[I^{-1}(\alpha;\theta)\right] \tag{4.30}$$

In (4.30), $I(\alpha;\theta) = -\mathbb{E}_{\mathbf{r}|\alpha}\left[\frac{\partial^2}{\partial\theta^2}\ln\mathcal{P}(\mathbf{r}|\alpha;\theta)\right]$, where $\mathcal{P}(\mathbf{r}|\alpha;\theta)$ is the PDF of observation $\mathbf{r}$ given α, and parametrized by θ in Euclidean space.

$$\mathcal{P}(\mathbf{r}|\alpha;\theta) = \frac{1}{\pi^N|\mathbf{\Sigma}|}\exp\Bigg(-(\mathbf{r}-\mathbf{x})^H\mathbf{\Sigma}^{-1}(\mathbf{r}-\mathbf{x})\Bigg).$$

Since the marginal PDF of $\mathbf{r}$ is difficult to obtain, modified form of Fisher information, formulated in (4.30) is used.

As $\mathbf{c}$ and $\mathbf{w}$ are independent, for given α, $\mathbf{\Sigma} = \alpha\mathbf{\Sigma_z} + \mathbf{\Sigma_w}$ is the covariance matrix of total equivalent disturbance i.e. $\mathbf{c}+\mathbf{w}$ and $N = ML$.Hence solving for (4.30), yields

$$I^{-1}(\theta) = \frac{1}{2}\Bigg(-\mathbb{E}_\alpha\Bigg[\Bigg(\frac{\partial\mathbf{x}}{\partial\theta}^H\mathbf{\Sigma}^{-1}\frac{\partial\mathbf{x}}{\partial\theta}\Bigg)^{-1}\Bigg]\Bigg). \tag{4.31}$$

4.3.1 LFM Radar System

For LFM radar system $\mathbf{x} = \mathbf{x}_{\text{LFM}}$ and for delay $\theta = \tau_o$, hence CRLB for delay is given by

$$I^{-1}(\tau_o) = \frac{1}{2}\Bigg(\mathbb{E}_\alpha\Bigg[\Bigg(\frac{\partial\mathbf{x}_{\text{LFM}}}{\partial\tau_o}^H\mathbf{\Sigma}^{-1}\frac{\partial\mathbf{x}_{\text{LFM}}}{\partial\tau_o}\Bigg)^{-1}\Bigg]\Bigg), \tag{4.32}$$

From trace identity, (4.32) is given by

$$I^{-1}(\tau_o) = \frac{1}{2}\Bigg(\mathbb{E}_\alpha\Bigg[\mathbf{tr}\Bigg(\Bigg(\frac{\partial\mathbf{x}_{\text{LFM}}}{\partial\tau_o}^H\mathbf{\Sigma}^{-1}\frac{\partial\mathbf{x}_{\text{LFM}}}{\partial\tau_o}\Bigg)^{-1}\Bigg)\Bigg]\Bigg)$$

$$I^{-1}(\tau_o) = \frac{1}{8\pi^2\Delta f^2 M\sum_{l=1}^{L-1} l^2}\mathbb{E}_\alpha[\mathbf{tr}(\mathbf{\Sigma})] \tag{4.33}$$

Solving (4.33), utilizing $\mathbf{\Sigma_z} = \rho^{|i-j|}\ \forall i,j \in [1,\cdots,N]$ and $\mathbf{\Sigma_w} = \Omega_w^2\mathbf{I}$, yield

$$I^{-1}(\tau_o) = \frac{N}{8\pi^2\Delta f^2 M\sum_{l=1}^{L-1} l^2}\Bigg(\mathbb{E}_\alpha[\alpha] + \Omega_w^2\Bigg) \tag{4.34}$$

As defined in Section 1.5 of Chapter 2, α is gamma distributed, hence, $\mathbb{E}_\alpha[\alpha] = \mu_c$ is the mean of α, subsequently (4.34) is given by

$$I^{-1}(\tau_o) = \frac{3(\mu_c + \Omega_w^2)}{4\pi^2 \Delta f^2 (L-1)(2L-1)} \tag{4.35}$$

Substituting (4.35) into (4.29) and using $\nabla\mathbf{\Phi}(\mathbf{x}_{\text{LFM}})^H \nabla\mathbf{\Phi}(\mathbf{x}_{\text{LFM}}) = \langle \nabla\mathbf{\Phi}(\mathbf{x}_{\text{LFM}}), \nabla\mathbf{\Phi}(\mathbf{x}_{\text{LFM}}) \rangle_{\mathbb{H}} = N$, yield

$$CRLB_{\text{LFM}}(\tau_o) = \frac{3N(\mu_c + \Omega_w^2)}{4\pi^2 \Delta f^2 (L-1)(2L-1)}. \tag{4.36}$$

For Doppler shift $\theta = f_d$, hence CRLB for Doppler shift is given by

$$I^{-1}(f_d) = \frac{1}{2}\left(\mathbb{E}_\alpha\left[\left(\frac{\partial \mathbf{x}_{\text{LFM}}}{\partial f_d}^H \mathbf{\Sigma}^{-1} \frac{\partial \mathbf{x}_{\text{LFM}}}{\partial f_d}\right)^{-1}\right]\right), \tag{4.37}$$

From trace identity, (4.37) is given by

$$I^{-1}(f_d) = \frac{1}{2}\left(\mathbb{E}_\alpha\left[\mathbf{tr}\left(\left(\frac{\partial \mathbf{x}_{\text{LFM}}}{\partial f_d}^H \frac{\partial \mathbf{x}_{\text{LFM}}}{\partial f_d} \mathbf{\Sigma}^{-1}\right)^{-1}\right)\right]\right), \tag{4.38}$$

Solving (4.38), yield

$$I^{-1}(f_d) = \frac{N(\mu_c + \Omega_w^2)}{8\pi^2 T_{\text{PRI}}^2 L \sum_{m=1}^{M-1} m^2 (\sum_{l=0}^{L-1}(1) + 2\frac{\Delta f}{f_c}\sum_{l=1}^{L-1} l + \frac{\Delta f}{f_c}\sum_{l=1}^{L-1} l^2)}. \tag{4.39}$$

Using $\sum_{m=1}^{M-1} m^2 = \frac{M(M-1)(2M-1)}{6}$, $\sum_{l=1}^{L-1} l^2 = \frac{L(L-1)(2L-1)}{6}$, and $\sum_{l=1}^{L-1} l = \frac{L(L-1)}{2}$

$$I^{-1}(f_d) = \frac{3(\mu_c + \Omega_w^2)}{4\pi^2 T_{\text{PRI}}^2 L (M-1)(2M-1)(1 + \frac{(L-1)\Delta f}{f_c} + \frac{(L-1)(2L-1)\Delta f}{6 f_c})}. \tag{4.40}$$

Substituting (4.40) into (4.29), yields

$$CRLB_{\text{LFM}}(f_d) = \frac{3N(\mu_c + \Omega_w^2)}{4\pi^2 T_{\text{PRI}}^2 L (M-1)(2M-1)(1 + \frac{(5+2L)(L-1)\Delta f}{6 f_c})}. \tag{4.41}$$

As described in (4.36) and (4.41), modified Fisher information generalizes CRLB expressions for LFM radar system. Consequently, if $\mu_c \longrightarrow 0$ (which is the case for no clutter), generalized CRLB expressions give by (4.36) and (4.41) will correspond to CRLB expressions for Gaussian distributed noise given by (3.44) and (3.47), respectively.

4.3.2 SF Radar System

For SF radar system $\mathbf{x} = \mathbf{x}_{\text{SF}}$ and for delay $\theta = \tau_o$, hence CRLB for delay is given by

$$I^{-1}(\tau_o) = \frac{1}{2}\left(\mathbb{E}_\alpha\left[\left(\frac{\partial \mathbf{x}_{\text{SF}}}{\partial \tau_o}^H \mathbf{\Sigma}^{-1} \frac{\partial \mathbf{x}_{\text{SF}}}{\partial \tau_o}\right)^{-1}\right]\right), \tag{4.42}$$

From trace identity, and similar to delay, (4.42) is given by

$$I^{-1}(\tau_o) = \frac{N}{8\pi^2 \Delta f^2 M \sum_{l=1}^{L-1} l^2}\left(\mathbb{E}_\alpha[\alpha] + \Omega_w^2\right) \tag{4.43}$$

Using $\mathbb{E}_\alpha[\alpha] = \mu_c$ and substituting (4.43) into (4.29), yield

$$CRLB_{\text{SF}}(\tau_o) = \frac{3N(\mu_c + \Omega_w^2)}{4\pi^2 \Delta f^2 (L-1)(2L-1)} \tag{4.44}$$

For Doppler shift $\theta = f_d$, hence CRLB for Doppler shift is given by

$$I^{-1}(f_d) = \frac{1}{2}\left(\mathbb{E}_\alpha\left[\left(\frac{\partial \mathbf{x}_{\text{SF}}}{\partial f_d}^H \mathbf{\Sigma}^{-1} \frac{\partial \mathbf{x}_{\text{SF}}}{\partial f_d}\right)^{-1}\right]\right), \tag{4.45}$$

From trace identity, (4.45) is given by

$$I^{-1}(f_d) = \frac{1}{2}\left(\mathbb{E}_\alpha\left[\mathbf{tr}\left(\left(\frac{\partial \mathbf{x}_{\text{SF}}}{\partial f_d}^H \frac{\partial \mathbf{x}_{\text{SF}}}{\partial f_d} \mathbf{\Sigma}^{-1}\right)^{-1}\right)\right]\right), \tag{4.46}$$

Solving (4.46), yield

$$I^{-1}(f_d) = \frac{3(\mu_c + \Omega_w^2)}{4\pi^2 (T_o^2 (L-1)(2L-1) + T_{\text{PRI}}^2 (M-1)(2M-1) + 3T_o T_{\text{PRI}} (L-1)(M-1))} \tag{4.47}$$

From (4.47) and (4.29), yield

$$CRLB_{\text{SF}}(f_d) = \frac{3N(\mu_c + \Omega_w^2)}{4\pi^2(T_o^2(L-1)(2L-1) + T_{\text{PRI}}^2(M-1)(2M-1) + 3T_oT_{\text{PRI}}(L-1)(M-1))}. \tag{4.48}$$

4.3.3 Analytical Expressions for the Variance in Estimation and Upper-Bound on Estimators' Dictionary-Size

For LFM and SF radar, the overall variance in estimation of delay at steady state for proposed estimator based on KMC and estimator based on KLMS is denoted by $\Omega^2_{\text{KMC}}(\hat{\tau}_o)$, and $\Omega^2_{\text{KLMS}}(\hat{\tau}_o)$ respectively, are given by

$$\Omega^2_{\text{KMC}}(\hat{\tau}_o) = CRLB(\tau_o) + \mathbb{S}_{\text{KMC}} \tag{4.49}$$

$$\Omega^2_{\text{KLMS}}(\hat{\tau}_o) = CRLB(\tau_o) + \mathbb{S}_{\text{KLMS}} \tag{4.50}$$

where $\mathbb{S}_{\text{KMC}} = \frac{\lambda\mu\Omega_w^2}{2-\lambda\mu}$ is the excess mean square error (EMSE) for KMC algorithm, $\mathbb{S}_{\text{KLMS}} = \frac{\mu\Omega_w^2}{2-\mu}$ is the EMSE for KLMS algorithm, and $CRLB(\tau_o)$ is either $CRLB_{\text{LFM}}(\tau_o)$ or $CRLB_{\text{SF}}(\tau_o)$.

Similar to delay, for LFM and SF radar, the overall variance in Doppler shift at steady state for proposed estimator based on KMC and KLMS are denoted by $\Omega^2_{\text{KMC}}(\hat{f}_d)$, and $\Omega^2_{\text{KLMS}}(\hat{f}_d)$ respectively.

$$\Omega^2_{\text{KMC}}(\hat{f}_d) = CRLB(f_d) + \mathbb{S}_{\text{KMC}} \tag{4.51}$$

$$\Omega^2_{\text{KLMS}}(\hat{f}_d) = CRLB(f_d) + \mathbb{S}_{\text{KLMS}} \tag{4.52}$$

where $CRLB(f_d)$ is either $CRLB_{\text{LFM}}(f_d)$ or $CRLB_{\text{SF}}(f_d)$

Subsequently, by Cover's sphere packing theorem in RKHS [16], for both LFM and SF radar, the following upper-bound on dictionary-size of the estimators based on KMC and KLMS [41] is obtained:

$$|\mathcal{D}_\infty|^{\text{KMC}} \leq \left(\frac{1+\Omega^2_{\text{KMC}}}{\zeta}\right)^N \tag{4.53}$$

$$|\mathcal{D}_\infty|^{\text{KLMS}} \leq \left(\frac{1+\Omega^2_{\text{KLMS}}}{\zeta}\right)^N \tag{4.54}$$

where Ω^2_{KMC} and Ω^2_{KLMS} are the overall variance in estimation of delay or Doppler shift, respectively for estimators based on KMC and KLMS, and $\zeta = \sqrt{(2-2\exp(-\frac{\delta_1}{\sigma}))}$.

From (4.49)-(4.52), and for $0 < \lambda = \left(\frac{\sigma_c^2+\Omega_w^2+\mathbb{S}_{\text{KMC}}}{2\mathbb{S}_{\text{KMC}}+2\Omega_w^2+\sigma_c^2}\right) < 1$ [78], it can be inferred that for the proposed estimators based on KMC, the MCC provides robustness against non-Gaussian clutter and results in lower variance as compared to estimators based on KLMS. Additionally, from (4.53) and (4.54), it can be inferred that $|\mathcal{D}_\infty|^{\text{KMC}} < |\mathcal{D}_\infty|^{\text{KLMS}}$, hence, in contrast to estimators based on KLMS, estimators based on KMC results in lower and reasonable dictionary-size/computational complexity. The above arguments made about the variance and computational complexity of the proposed and existing estimators are verified by simulations in Section 4.4.

4.4 Simulation Results and Discussion

In this section, simulation results for delay τ_o and Doppler shift f_d estimation using the proposed estimators is present and discussed. Subsequently, the comparative performance of the proposed KMC based estimators with the previously proposed KLMS based estimators and derived CRLB corresponding to τ_o and f_d is discussed.

The free parameters values of KMC and KLMS algorithm for LFM and SF radar are given in Table-4.1, Table-4.2, Table-4.3and Table-4.4. Parameters of LFM radar and SF radar used in simulations are described in Table-4.5 and Table-4.6, respectively. Without loss of generality, for the estimation of delay and Doppler shift the SCR=$\frac{\mathbf{x}^H\mathbf{x}}{\text{tr}(\mathbb{E}(\mathbf{c}^H\mathbf{c}))}$is fixed at 30 dB, and clutter to noise ratio $\big($clutter to noise ratio (CNR)=$\frac{\text{tr}(\mathbb{E}(\mathbf{c}^H\mathbf{c}))}{N\Omega_w^2}\big)$ is fixed at 10 dB [5].

In this work, for modeling the effect of non-Gaussian clutter, as described in (1.8) of

Table 4.1: Parameters values used for simulations for KMC estimation algorithms for LFM radar.

Parameters	KMC-NC $\{\tau_o, f_d\}$ LFM radar	KMC-Modified NC $\{\tau_o, f_d\}$ LFM radar
μ	$0.55, 0.55$	$0.55, 0.55$
σ	$10^{-5.5}, 10^{-6.4}$	Adaptive
ρ	Nil, Nil	$10^{7.7}, 10^{9.2}$
σ_o	Nil, Nil	$10^{-5.4}, 10^{-6.6}$
σ_c	$0.0025, 0.0017$	$0.0117, 0.012$

Table 4.2: Parameters values used for simulations for KMC estimation algorithms for SF radar.

Parameters	KMC-NC $\{\tau_o, f_d\}$SF radar	KMC- Modified NC $\{\tau_o, f_d\}$SF radar
μ	$0.55, 0.55$	$0.55, 0.55$
σ	$10^{-5.5}, 10^{-6.1}$	Adaptive
ρ	Nil,Nil	$10^{6}, 10^{9.2}$
σ_o	Nil,Nil	$10^{-5.2}, 10^{-6.4}$
σ_c	$0.0025, 0.0036$	$0.01, 0.02$

Section 1.5 of Chapter 1, the clutter is assumed to follow SIRP. Moreover, to consider the effect of impulsive noise and outliers the particular class of heavy tailed SIRP, K-distributed random process is considered. For this, the random variable α in (1.8) is drawn from gamma distribution with shape and size parameter, as ν and μ_c, respectively. As ν decreases, the tail of the resultant distribution function for clutter becomes heavier, which in turn introduces impulsive noises and outliers. Hence, to consider the effect of high tailed clutter, simulations are performed for $\nu = 0.1$ as considered in [65, 66].

4.4.1 Estimation of Delay with KMC-NC and KMC-Modified NC based Estimator

For estimating delay, the set of possible true values of τ_o ($\mathbb{D}$) is formed by partitioning the interval between $\tau_{o_{min}}$ and $\tau_{o_{max}}$ into K parts, i.e $\mathbb{D} \in [\tau^1_{o_{min}} \dots \tau^K_{o_{max}}]$. Thereafter, radar returns (learning and testing samples) corresponding to K different delays are formed as per (4.11). For learning and testing of the estimators based on KMC-NC, KLMS-NC,

Table 4.3: Parameters values used for simulations for KLMS estimation algorithms for LFM radar.

Parameters	KLMS-NC $\{\tau_o, f_d\}$ LFM radar	KLMS-Modified NC $\{\tau_o, f_d\}$ LFM radar
μ	$0.9460, 0.987$	$0.982, 0.983$
σ	$10^{-5.5}, 10^{-6.4}$	Adaptive
ρ	Nil, Nil	$10^{7.7}, 10^{9.2}$
σ_o	Nil, Nil	$10^{-5.4}, 10^{-6.6}$

Table 4.4: Parameters values used for simulations for KLMS estimation algorithms for SF radar.

Parameters	KLMS-NC $\{\tau_o, f_d\}$SF radar	KLMS- Modified NC $\{\tau_o, f_d\}$SF radar
μ	$0.9581, 0.93$	$0.9735, 0.983$
σ	$10^{-5.5}, 10^{-6.1}$	Adaptive
ρ	Nil, Nil	10^{6},
σ_o	Nil, Nil	$10^{-5.2}, 10^{-6.4}$

KMC-Modified NC and KLMS-Modified NC, the K is chosen as 5500. Out of these 5500 radar returns, 5000 are used for the learning of the estimators while the remaining 500 are used to evaluate the estimators' performance.

In Fig. 4.1a, for both LFM and SF radar in the presence of clutter and thermal noise, the MSE performance of the proposed estimators based on KMC-NC is compared with the existing adaptive estimator based on KLMS-NC and two linear estimators based on Kalman filter MCC(MCC-KF) [70], and adaptive MCC(AMCC) [71]. From Fig. 4.1a, it can be observed that the use of MCC in RKHS facilitates mitigation of non-Gaussian clutter. Particularly, with suitable choice of σ_c for the estimator based on KMC-NC

Table 4.5: Values of radar parameters for LFM radar.

LFM radar parameters	Values
Number of frequency index (L)	8
Number of pulses (M)	8
Frequency spacing (Δf)	15.6250 MHz
Pulse duration (T_o)	0.013×10^{-3}sec
Pulse repetition interval (T_{PRI})	0.016ms
Bandwidth ($L\Delta f$)	125 MHz
Set of delay true value ($\tau_{o_{min}}, \tau_{o_{max}}$)	$(0.0016 \times 10^{-3}, 0.013 \times 10^{-3})$sec
Set of Doppler true value ($f_{d_{min}}, f_{d_{max}}$)	$(-30.4, 30.4)$kHz

Table 4.6: Values of radar parameters for SF radar.

SF radar parameters	Values
Number of fast index (L)	20
Number of pulses (M)	25
Frequency spacing (Δf)	5 MHz
Pulse duration (T_o)	0.1μsec
Pulse repetition interval (T_{PRI})	40μs
Bandwidth ($L\Delta f$)	125 MHz
Set of delay true value ($\tau_{o_{min}}, \tau_{o_{max}}$)	$(0.0008 \times 10^{-6}, 40 \times 10^{-6})$sec
Set of Doppler true value ($f_{d_{min}}, f_{d_{max}}$)	$(-12.5, 12.5)$kHz

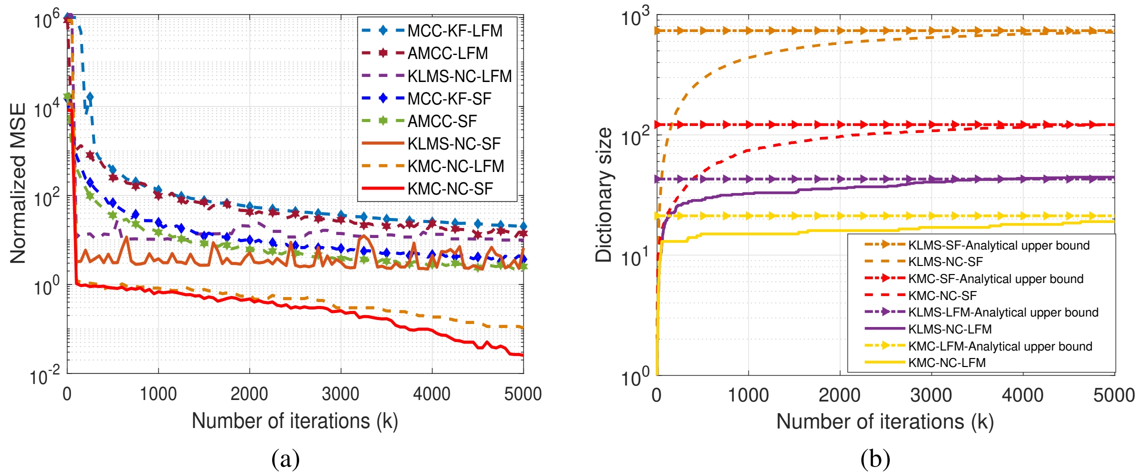

Figure 4.1: (a) Normalized MSE and (b) Dictionary size in estimation of delay for LFM and SF radar with estimators based on KMC-NC, KLMS-NC, AMCC, and MCC-KF in the presence of non-Gaussian clutter.

as given in Table. 4.1, the additional factor $\left(\exp\left(-\frac{e^2(i)}{2\sigma_c^2}\right)\right)$ provides robustness against non-Gaussian clutter, and yields accurate estimates of delay τ_o as compared to estimator based on KLMS-NC, MCC-KF, and AMCC. Also, in Fig. 4.1b, it can be observed that the dictionary-size of the proposed and existing estimator achieve respective upper-bounds and consequently result in lower dictionary-size for KMC-NC based estimator as compared to KLMS-NC based estimator. Furthermore, from Fig. 4.1b, a drastic reduction in the computational complexity is observed for the proposed estimator with KMC-NC, which in turn, makes KMC-NC based estimator practically deployable.

Further, Fig. 4.2a compares MSE corresponding to the estimates of delay for both LFM and SF radar system obtained by the estimators based on KMC-Modified NC and KLMS-Modified NC respectively. As shown in Fig. 4.2a, it is observed that the performance of

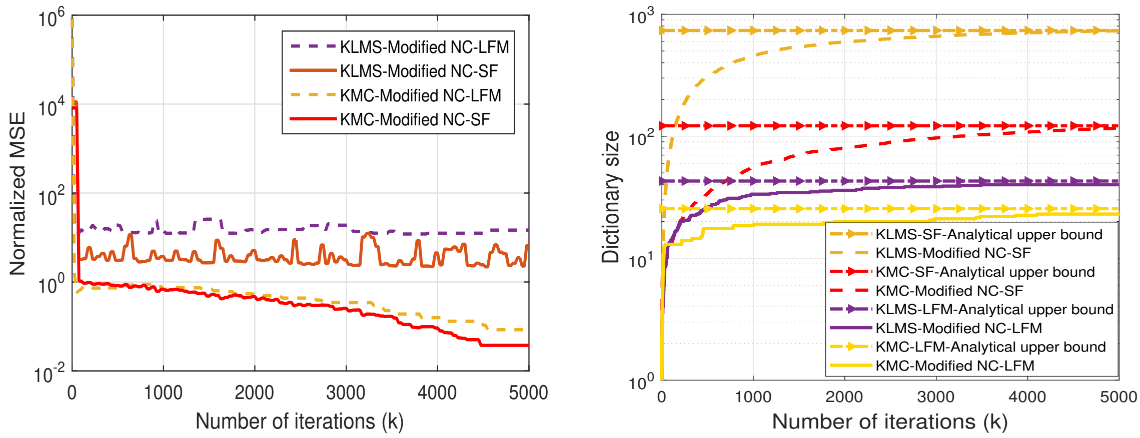

(a) (b)

Figure 4.2: (a) Normalized MSE and (b) Dictionary size in estimation of delay for LFM and SF radar with estimators based on KMC-Modified NC and KLMS-Modified NC in the presence of non-Gaussian clutter.

KLMS-Modified NC based estimator is impaired in presence of clutter. On the contrary, for the estimator based on KMC-Modified NC, using ITL criterion like MCC, and selection of proper kernel width by adaptive-learning at every iteration, provides a better estimate of delay, and hence results in lower MSE floor. Further, in Fig. 4.2b, it is observed that the computational complexity of the proposed estimator based on KMC-Modified NC is reaching analytical upper-bound and significantly reduced in comparison to the estimator based on KLMS-Modified NC. As shown in Fig. 4.2a, due to deleterious effect of clutter on the gradient information (since a stochastic gradient algorithm adapts the kernel-width), the KLMS-Modified NC converges to higher MSE floor. However, for modified kernel MCC, the said effect is less pronounced due to the robustness of the MCC criterion to non-Gaussian clutter.

4.4.2 Estimation of Doppler shift with KMC-NC and KMC-Modified NC based Estimator

For estimating Doppler shift, similar to delay estimation, the interval between $f_{d_{max}}$ and $f_{d_{min}}$ is divided in K parts to form a set of unknown Doppler frequencies as $\mathbb{F} \in [f^1_{d_{min}} \dots f^K_{d_{max}}]$. Thereafter, the radar return (learning and testing samples) are formed

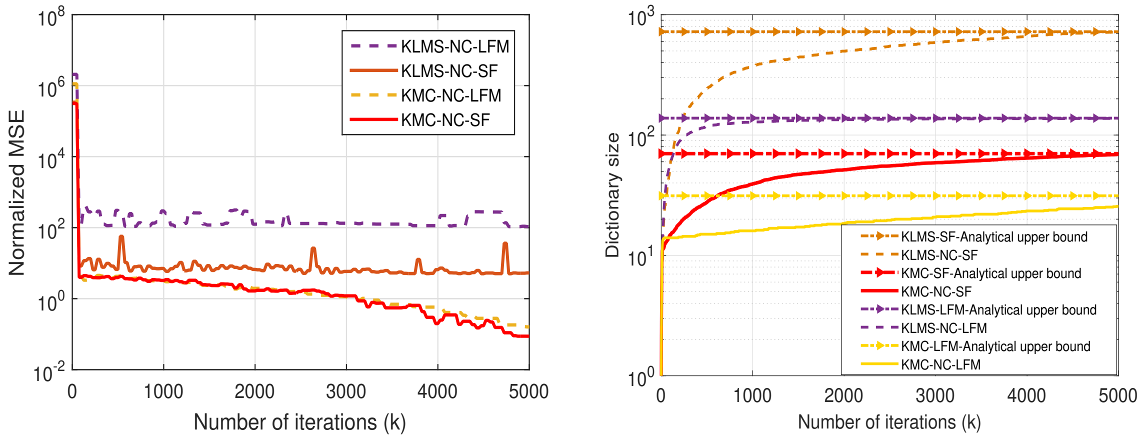

(a) (b)

Figure 4.3: (a) Normalized MSE and (b) Dictionary size in estimation of Doppler shift for LFM and SF radar with estimators based on KMC-NC and KLMS-NC in the presence of non-Gaussian clutter.

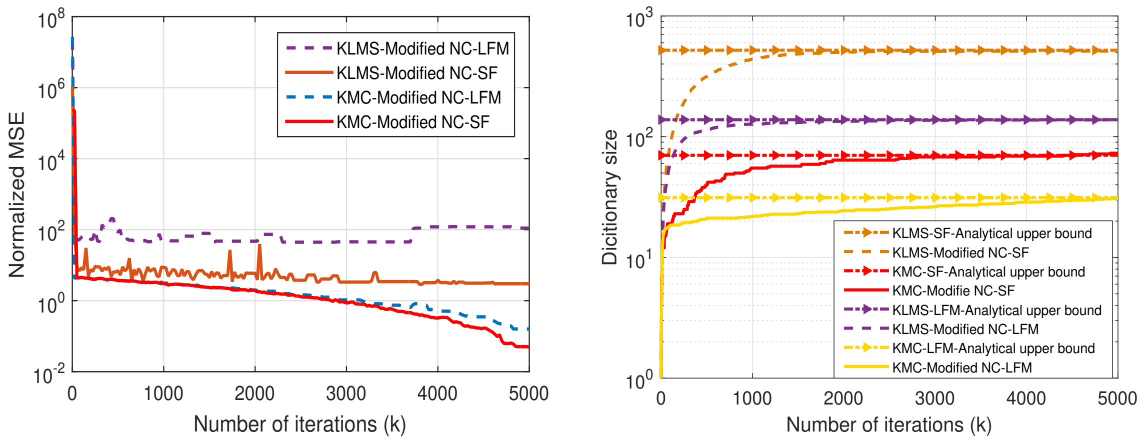

(a) (b)

Figure 4.4: (a) Normalized MSE and (b) Dictionary size in estimation of Doppler shift for LFM and SF radar with estimators based on KMC-Modified NC and KLMS-Modified NC in the presence of non-Gaussian clutter.

corresponding to each Doppler shift utilizing (4.12). The K is chosen as same for the delay estimation, i.e. $K = 5500$, with 5000 samples used for learning and the rest 500 samples used for evaluating the MSE performance. For both the LFM and SF radar system, the improvement in the estimation accuracy and computational complexity of the estimator based on KMC-NC for Doppler shift estimation over estimator based on KLMS-NC is illustrated in Fig. 4.3a and Fig. 4.3b, respectively. Similar to delay estimation, improved estimation of Doppler shift is achieved with lower computational complexity, upon incorporation of ITL criteria like MCC.

Moreover, from Fig. 4.4a-Fig. 4.4b, it can be inferred that adaptive learning of the kernel width for KMC-Modified NC based estimator results in lower MSE with reasonable dictionary-size. Hence, from Fig. 4.4a-Fig. 4.4b, it can be concluded that the proposed estimator based on KMC-Modified NC is viable for Doppler shift estimation as compared to KLMS-Modified NC for deployment in practical radar systems impaired by clutter and thermal noise.

4.4.3 Comparison of Estimators based on KMC and KLMS

For performance-evaluation of the proposed estimators, variance in the estimation of delay and Doppler shift with proposed estimators based on KMC and estimators based on KLMS for both LFM and SF radar is performed at SCR ranges from -20 dB to 30 dB and compared against the derived CRLBs. For simulations, the CNR is fixed at 10 dB.

Next, the performance of estimators based on KMC and KLMS with NC and Modified NC for LFM radar and for delay and Doppler shift estimation are shown in Fig. 4.5. Particularly, as shown in Fig. 4.5a and Fig. 4.5b, the proposed estimator based on KMC-NC for all SCRs outperforms KLMS-NC based estimator and achieves variance closer to CRLB. Further, KMC-Modified NC based estimator converges to a variance lower than KLMS-Modified NC and closer to CRLB.

Further, in Fig. 4.6, for SF radar, the variance of the proposed KMC-NC based estimator is compared with KLMS-NC for estimation of delay and Doppler shift. From Fig. 4.6, it can be observed that the KMC-NC based estimator converges to lower

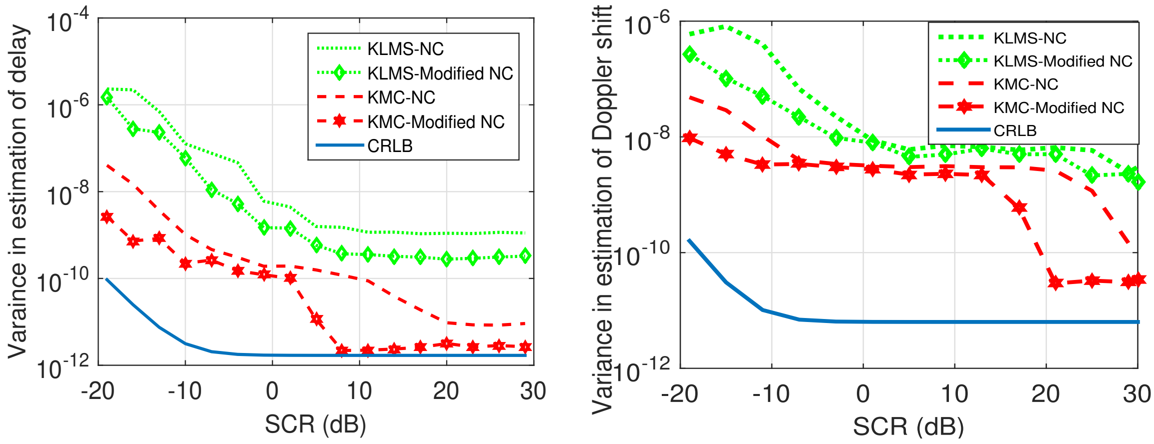

(a) (b)

Figure 4.5: Comparative performance of the estimator based on KMC-NC, KLMS-NC, KMC-Modified NC and KLMS-Modified NC for estimation of (a) delay and (b) Doppler shift for LFM radar system.

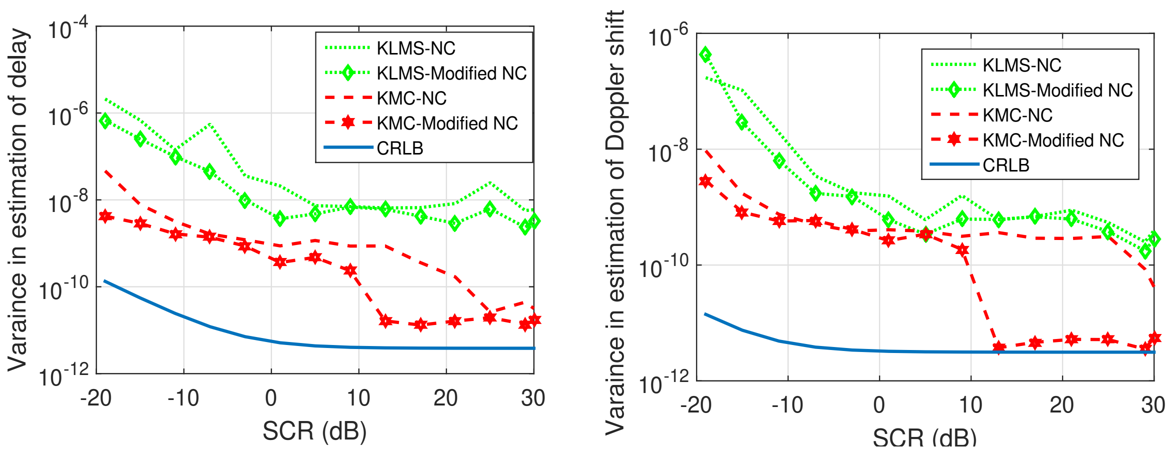

(a) (b)

Figure 4.6: Comparative performance of the estimator based on KMC-NC, KLMS-NC, KMC-Modified NC and KLMS-Modified NC for estimation of (a) delay and (b) Doppler shift for SF radar system.

variance as compared to a corresponding KLMS-NC based estimator. Further, variance in the estimation of delay and Doppler shift using KMC-NC based estimator is closer to the achievable CRLB as compared to KLMS-NC. The same trend of lower estimator-variance, and increased proximity of the estimator variance to the CRLB is observed for KMC-Modified NC based estimator, as compared to KLMS-Modified NC based estimator.

4.5 Summary

In this Chapter, two new KMC based estimation algorithms are proposed for estimation of target's delay and Doppler shift in the presence of non-Gaussian clutter. Estimation of the target's unknown parameters is performed by maximizing a cost function (correntropy) in RKHS, which provides an accurate estimate of delay and Doppler shift in the presence of non-Gaussian clutter. Further, to facilitate sparse learning, and for lowering computational complexity without affecting estimator-performance, Platt's NC is used to limit the increasing size of training samples. Additionally, a technique is explored for tuning the hyper-parameter σ from radar returns, and an adaptive update equation is derived for its convergence to an appropriate value. Subsequently, for the considered radar systems analytical expressions are derived for the CRLBs of the proposed RKHS based estimators. Proofs are provided, which reinforce the viability of KMC as a learning criterion for practical clutter-impaired radar systems. Lastly, simulations performed over realistic LFM and SF radar systems reveal that the proposed KMC based estimators facilitate 40 dB normalized MSE gain over existing KLMS based estimators along with lower computational complexity.

The detection and estimation algorithms proposed in Chapters 2, 3, and 4 are validated over single-antenna radar systems, which includes OFDM radar, LFM radar, and SF radar. The improved performance of communication systems with the advent of MIMO antenna systems motivated the radar engineers and researchers to exploit the MIMO antenna systems for radar purposes also. The initial work in MIMO radar has shown the potential improvement in the estimation of range and velocity over a single-antenna radar system

[79–81]. However, the literature still lacks efficient estimation algorithms for the practical MIMO radar systems in the presence of non-Gaussian clutter. Hence, in the next Chapter, an estimator for the MIMO radar system is developed, which efficiently estimates the targets' DOA, DOD, and velocity in the presence of non-Gaussian clutter and Gaussian distributed thermal noise. The estimator developed in Chapter 5 is based on KMEE, which to mitigate the effects of clutter non-Gaussianity in contrast to estimators based on KLMS and KMC, utilizes another ITL criteria called MEE.

Chapter 5

Estimator for MIMO Radar

MIMO radar was introduced with the intent of improving performance of the radar systems [80, 82]. Diversity in transmitting orthogonal waveforms from transmit antennas and collecting the superposition of echoes at each receiving antenna individually, provides improvement in the performance of MIMO radar over single antenna radar system [83, 84]. For instance, in MIMO radar, if the transmitter has N_{tx} antennas and receiver has N_{rx} antennas, then, contrary to a single antenna radar system, $N_{tx}N_{rx}$ signals are processed at the receiver for detection of targets and estimation of their parameters. Fundamentally, in MIMO radar the parameters which describes the targets' position and velocity are the DOD, DOA, and Doppler shift. Most conventional estimation techniques for MIMO radar assume the absence of clutter [12, 85–87]. However, as mentioned in Chapter 4, practical radar systems are effected by clutter due to the reflections from unwanted objects/scatterers. Hence, estimation techniques introduced in [12, 85–87], when employed in the presence of non-Gaussian clutter, yield inaccurate estimates of parameters with a very high variance.

In MIMO radar, for estimation of the aforementioned targets' parameters in the non-Gaussian clutter environment, various variants of ML estimator are proposed in [88, 89], and [90]. However, the estimation of DOD, DOA, and Doppler shift, in the presence of non-Gaussian clutter, does not have a closed-form solution for optimization of ML cost function [91]. Therefore, in [88], and [89], estimators based on iterative conditional ML, and iterative joint ML are proposed, respectively. The ML based solution, proposed in

[88], and [89] are based on the conditional likelihood, and the joint likelihood of the observations, respectively. Further, in [90], an iterative ML estimator has been proposed that is based on the marginal likelihood of the observations. In [90], it is mentioned and shown that the estimators proposed in [88], and [89] are prone to yield suboptimum estimates of desired parameters. Therefore in [90], an iterative ML estimator has been proposed. The proposed estimator is based on the marginal likelihood of the observations and claimed to perform better than the estimators proposed in [88], and [89]. However, in [90], as the marginal likelihood of the observation is considered, the final estimate depends on the numerical evaluation of integrals, which is computationally demanding. In addition to the need for evaluation of integrals, as mentioned in Section 3, Remark 4 of [90], for say, P targets, the estimate of DOD/DOA, is obtained by performing the $2P$ dimensional grid search algorithm of a highly non-convex function. Implementing a grid search algorithm over the $2P$ dimension is computationally complex.

Thus, in this Chapter, KMEE based estimator is proposed for the estimation of multiple targets' DOD, DOA, and Doppler shift in a MIMO radar setting. Estimation of targets' parameters is pursued in the presence of non-Gaussian clutter and Gaussian distributed thermal noise. The KMEE is the KAF algorithm that uses an iterative stochastic gradient descent algorithm to solve an estimation problem in RKHS. In the previous Chapters, estimation of target's range and velocity has been efficiently handled by the other KAF based estimation algorithms namely KLMS algorithm and KMC algorithm in Chapter 3 and Chapter 4, respectively. However, since KLMS utilizes MSE criterion [18, 41, 92], and is optimum for Gaussian noise, the estimation algorithm developed in Chapter 3 cannot be used for the estimation of parameters in MIMO radar system in the presence of non-Gaussian clutter. In a later attempt, in Chapter 4, to deal with the effects of non-Gaussian clutter, KMC based estimator proves to be better than the estimator based on KLMS. Nevertheless, the performance of KMC based estimator may not be good when faced with a more complicated non-Gaussian clutter scenario. The KMEE based proposed estimator utilizes the MEE criterion, and being an ITL criterion, MEE optimizes the higher-order statistics of error between the desired and the estimated parameter, which makes the estimator based on the KMEE criterion robust against the effects of heavy-tailed non-Gaussian clutter.

The proposed adaptive estimator, unlike conventional non-adaptive estimators, learns the unknown function (relating the MIMO radar return and unknown desired parameters: DOA, DOD, Doppler shift) and iteratively estimate the desired parameters. Therefore, without any sparsification criterion, like estimators based on KLMS and KMC, the computational complexity of the estimators based on KMEE increases linearly and restricts the practical applicability of the proposed estimators [60]. Consequently, similar to Chapter 3 and Chapter 4, for reducing the computational complexity of the proposed estimator based on KMEE, we use a sparsification technique based on Platt's NC [43].

The Chapter is organized as follows: The signal model for MIMO radar return is described first. The proposed KMEE-NC based estimator is described next. Subsequently, the analytical expressions for modified CRLB (MCRLB)[1] using modified Fisher's information matrix for estimation of DOD, DOA and Doppler shift are derived. Next, analytical expression for the variance of the proposed estimator based on KMEE is derived. Simulation results are discussed next. Finally, conclusions are drawn for the Chapter.

5.1 MIMO Radar Signal Model in Non-Gaussian Clutter

In this section, the generalized signal model for MIMO radar is briefly discussed. The considered MIMO radar is assumed to consist of N_{tx} transmit antennas, and N_{rx} receiving antennas. Let the surveillance environment consist of P targets (identified by index p) with unknown DODs and DOAs be

$$\boldsymbol{\theta} = [\theta_1, \theta_2, \cdots, \theta_p, \cdots, \theta_P], \text{and } \boldsymbol{\phi} = [\phi_1, \phi_2, \cdots, \phi_p, \cdots, \phi_P]$$

, respectively. The p^{th} target is assumed to be moving with velocity v_p. Further, if orthogonal waveforms are transmitted, then the $N_{tx} \times N_{rx}$ MIMO radar signal matrix

[1]Because of the non-Gaussian nature of clutter, finding the close form solution of conventional CRLB is difficult. Therefore, in this work, an analytical expression for MCRLB is derived using a modified Fisher information matrix [93].

$\mathbf{R}(m)$ for Q^{th} pulse after matched filtering in one coherent pulse interval at the receiver is given by [94].

$$\mathbf{R}(m) = \sum_{p=1}^{P} \exp(j2\pi f_p m)\mathbf{a}(\theta_p)\mathbf{a}^T(\phi_p) + \mathbf{W}(m) + \mathbf{C}(m) \text{ for } m = [1, 2, \cdots, M], \quad (5.1)$$

where f_p is the Doppler shift for the p^{th} target normalized to the MIMO radar pulse repetition frequency,

$$\mathbf{a}(\theta_p) = \left[\exp\left(j\frac{2\pi \sin(\theta_p)}{\lambda} d_1^t\right),\ \exp\left(j\frac{2\pi \sin(\theta_p)}{\lambda} d_2^t\right),\ \cdots,\ \exp\left(j\frac{2\pi \sin(\theta_p)}{\lambda} d_{N_{tx}}^t\right)\right]^T$$

is the transmit steering vector, and

$$\mathbf{a}(\phi_p) = \left[\exp\left(j\frac{2\pi \sin(\phi_p)}{\lambda} d_1^r\right),\ \exp\left(j\frac{2\pi \sin(\phi_p)}{\lambda} d_2^r\right),\ \cdots,\ \exp\left(j\frac{2\pi \sin(\phi_p)}{\lambda} d_{N_{rx}}^r\right)\right]$$

is the receiving steering vector in which $d_{n_{tx}}^t$, and $d_{n_{rx}}^r$ is distance of n_{tx}^{th} and n_{rx}^{th} antenna from the reference transmit and reference receive antenna, respectively. $\mathbf{W}(m)$ is the $N_{tx} \times N_{rx}$ matrix of samples of thermal noise, and $\mathbf{C}(m)$ is the $N_{tx} \times N_{rx}$ matrix of samples of non-Gaussian clutter follows the characteristics defined in Section 1.5 of Chapter 1.

Concatenating $\mathbf{R}(m)$ from (5.1) into $N_{tx}N_{rx} \times 1$ vector yields

$$\mathbf{r}(m) = \mathbf{A}(\boldsymbol{\theta}, \boldsymbol{\phi})\mathbf{v}(m) + \mathbf{w}(m) + \mathbf{c}(m) \ \text{ for } \ m = [1, 2, \cdots, M]. \quad (5.2)$$

For simplicity, after dropping index m, (5.2) is given by

$$\mathbf{r} = \mathbf{A}(\boldsymbol{\theta}, \boldsymbol{\phi})\mathbf{v} + \mathbf{w} + \mathbf{c}, \quad (5.3)$$

where $\mathbf{A}(\boldsymbol{\theta}, \boldsymbol{\phi}) = [\mathbf{a}(\theta_1, \phi_1), \mathbf{a}(\theta_2, \phi_2), \cdots, \mathbf{a}(\theta_P, \phi_P)]$, $\mathbf{a}(\theta_p, \phi_p) = vec(\mathbf{a}(\theta_p)\mathbf{a}^T(\phi_p))$, $\mathbf{v} = [\exp(j2\pi f_1 m),\ \exp(j2\pi f_2 m),\ \cdots,\ \exp(j2\pi f_p m),\ \cdots,\ \exp(j2\pi f_{P-1} m),\ \exp(j2\pi f_P m)]^T$,

$$\mathbf{w} = [\mathbf{W}(1, 1), \mathbf{W}(1, 2), \cdots, \mathbf{W}(N_{tx}, N_{rx})]^T,$$

and $\mathbf{c} = [\mathbf{C}(1,1), \mathbf{C}(1,2), \cdots, \mathbf{C}(N_{tx}, N_{rx})]^T$.

From (5.1) and (5.3), the unknown parameters of interest θ_p, ϕ_p, and f_p of the p^{th} target are exponentially related to $\mathbf{r}$. Additionally, from (5.1) and (5.3), it is explicit that, the unknown parameters are easily estimated if the unknown inverse relationship between θ_p, ϕ_p, f_p and $\mathbf{r}$ is known. An adaptive estimator which iteratively estimates the unknown inverse relationship for single antenna radar system based on the KLMS and KMC are proposed in Chapter 3 and Chapter 4, respectively. However, since KLMS optimizes MSE, which is optimum for Gaussian noise, and KMC can perform worst, the KLMS based estimator and KMC based estimator cannot be used for MIMO radar signal model perturbed by non-Gaussian clutter. Hence, in this Chapter, estimation of DOD, DOA, and Doppler shift is performed using a KMEE based adaptive estimator. The proposed estimator is based on the optimization of entropy of the error between the true and estimated parameter set. Moreover, as optimization of entropy leads to the minimization of higher-order statistics of error, the proposed estimator provides robustness against the non-Gaussian clutter, which in turn reduces the effect of outliers introduced by the clutter non-Gaussianity.

5.2 Estimator Based on KMEE-NC

This section discusses the proposed estimation technique based on KMEE along-with the sparsification technique incorporated to reduce the computational complexity of the proposed estimator. In this work, estimation of the set of DODs ($\boldsymbol{\theta} = [\theta_1, \theta_2, \cdots, \theta_p, \cdots, \theta_P]$), DOAs ($\boldsymbol{\phi} = [\phi_1, \phi_2, \cdots, \phi_p, \cdots, \phi_P]$), and Doppler shifts $\mathbf{f} = [f_1, f_2, \cdots, f_p, \cdots, f_P]$ for P different targets are done individually and individual parameter set is represented by $\boldsymbol{\Theta}$. Therefore, $\boldsymbol{\Theta}$ can be either $\boldsymbol{\theta}$, $\boldsymbol{\phi}$ or $\mathbf{f}$ depending upon which set of parameter have to be estimated. This makes the considered estimation problem P dimensional i.e $\boldsymbol{\Theta} \in \mathbb{R}^P$. As the proposed estimation algorithm is adaptive and works in two phases: training and testing, the training and testing data is obtained by measuring MIMO radar return given in (5.3) for K different values of $\boldsymbol{\theta}$, $\boldsymbol{\phi}$, and $\mathbf{f}$. For this, the range in which unknown

$\theta_p \in (\frac{-\pi}{2}, \frac{\pi}{2})$, $\phi_p \in (\frac{-\pi}{2}, \frac{\pi}{2})$, and $f_p \in (-0.5, 0.5)$ [90] are expected to take the value, are uniformly divided into K different values. Consequently, the MIMO radar measurements for any k^{th} value of unknown parameter set given the value of other two parameter set are given by

$$\mathbf{r}_{\theta_k|\boldsymbol{\phi},\mathbf{f}} = \mathbf{A}(\boldsymbol{\theta}_k, \boldsymbol{\phi})\mathbf{v} + \mathbf{w}_k + \mathbf{c}_k, \tag{5.4}$$

$$\mathbf{r}_{\boldsymbol{\phi}_k|\boldsymbol{\theta},\mathbf{f}} = \mathbf{A}(\boldsymbol{\theta}, \boldsymbol{\phi}_k)\mathbf{v} + \mathbf{w}_k + \mathbf{c}_k, \tag{5.5}$$

$$\mathbf{r}_{\mathbf{f}_k|\boldsymbol{\theta},\boldsymbol{\phi}} = \mathbf{A}(\boldsymbol{\theta}, \boldsymbol{\phi})\mathbf{v}_k + \mathbf{w}_k + \mathbf{c}_k. \tag{5.6}$$

After measuring the MIMO radar return, the MIMO radar return $\mathbf{r}_k$ (which can be either $\mathbf{r}_{\theta_k|\boldsymbol{\phi},\mathbf{f}}$, $\mathbf{r}_{\boldsymbol{\phi}_k|\boldsymbol{\theta},\mathbf{f}}$ or $\mathbf{r}_{\mathbf{f}_k|\boldsymbol{\theta},\boldsymbol{\phi}}$ at k^{th} instant, corresponding to the estimation of $\boldsymbol{\theta}_k$, $\boldsymbol{\phi}_k$ or $\mathbf{f}_k$, respectively) is mapped into a high dimensional RKHS ($\mathbb{H}$), via an implicit mapping function $\Phi(\cdot) : \mathbb{C}^N \longrightarrow \mathbb{H}$, such that $\mathbf{r}_k$ is mapped in $\mathbb{H}$ as $\Phi(\mathbf{r}_k)$. If $\boldsymbol{\Omega}_{k-1}$ is an unknown explicit weight matrix in $\mathbb{H}$, then the unbiased estimate of the unknown parameter set $\mathbf{g}_k = \hat{\boldsymbol{\Theta}}_k$ is given by

$$\mathbf{g}_k = \langle \boldsymbol{\Omega}_{k-1}, \Phi(\mathbf{r}_k)\rangle_{\mathbb{H}} = \Phi^H(\mathbf{r}_k)\boldsymbol{\Omega}_{k-1}, \tag{5.7}$$

Main objective of an estimator based on MEE is to find the optimum $\boldsymbol{\Omega}_o$ such that the cost function (ξ-entropy [2]) of the error minimizes [95, 96] i.e

$$\boldsymbol{\Omega}_o = \arg\min_{\boldsymbol{\Omega}} H_\xi(\mathbf{e}_k)$$

where $H_\xi(\mathbf{e}_k)$ is the ξ-entropy cost function, $\mathbf{e}_k = \mathbf{d}_k - \mathbf{g}_k$, $\mathbf{d}_k$ is the desired or true value of parameter set i.e. $\mathbf{d}_k = \boldsymbol{\Theta}_k$. Since, minimizing $H_\xi(\mathbf{e}_k)$ analytically is difficult, $H_\xi(\mathbf{e}_k)$ can be minimized iteratively using the weight update equation as

$$\boldsymbol{\Omega}_k = \boldsymbol{\Omega}_{k-1} - \mu \frac{\partial}{\partial \boldsymbol{\Omega}_{k-1}}\Big(\hat{H}_\xi(\mathbf{e}_k)\Big), \tag{5.8}$$

[2] In this work the most commonly used Shannon entropy ($-y \log y$) is used, the other types of entropy is described in [95].

where μ is the learning parameter,

$$\hat{H}_\xi(\mathbf{e}_k) = \frac{1}{L} \sum_{u=k-L+1}^{k} \xi\Big[\hat{\mathcal{P}}_{\mathbf{e}}(\mathbf{e}(k,u))\Big]$$

is the sample estimate of $H_\xi(\mathbf{e}_k)$. The $\hat{\mathcal{P}}_{\mathbf{e}}(\mathbf{e}(k,u))$ is the estimated PDF [97] of $\mathbf{e}_k$ using L most recent errors.

Theoretically, iterative minimization of $\hat{H}_\xi(\mathbf{e}_k)$ guarantees convergence of the estimate $\mathbf{g}_k$ to the true value of parameters. Hence, the ensemble average of the estimated parameters equates to the true value of the parameters, and this makes the proposed estimator unbiased [15, 95]. Substituting $\hat{H}_\xi(\mathbf{e}_k)$ into (5.8), and using $\hat{\mathcal{P}}_{\mathbf{e}}(\mathbf{e}(k,u)) = \frac{1}{L}\sum_{i=k-L+1}^{k} \kappa_d(\mathbf{e}(k,u) - \mathbf{e}(k,i))$, where $\kappa_d(\mathbf{x},\mathbf{y}) = \exp\left(-\frac{\|\mathbf{x}-\mathbf{y}\|^2}{\sigma_d^2}\right)$ and σ_d is the width of the kernel function used for PDF approximation, yields

$$\mathbf{\Omega}_k = \mathbf{\Omega}_{k-1} - \eta \frac{\partial}{\partial \mathbf{\Omega}_{k-1}} \left(\frac{1}{L} \sum_{u=k-L+1}^{k} \xi\left[\frac{1}{L} \sum_{i=k-L+1}^{k} \kappa_d(\mathbf{e}(k,u) - \mathbf{e}(k,i))\right]\right). \tag{5.9}$$

Because of the outer summation, evaluating (5.9) is computationally inefficient. For an on-line adaptation of $\mathbf{\Omega}$, the instantaneous ξ-entropy could be used by dropping the outer summation in (5.9), this, yields the weight update equation as

$$\begin{aligned}
\mathbf{\Omega}_k =& \mathbf{\Omega}_{k-1} - \eta \frac{\partial}{\partial \mathbf{\Omega}_{k-1}} \left(\xi\left[\frac{1}{L} \sum_{i=k-L+1}^{k} \kappa_d(\mathbf{e}(k,k) - \mathbf{e}(k,i))\right]\right), \\
=& \mathbf{\Omega}_{k-1} - \frac{\eta}{L} \xi' \left[\frac{1}{L} \sum_{i=k-L+1}^{k} \kappa_d(\mathbf{e}(k,k) - \mathbf{e}(k,i))\right] \sum_{i=k-L+1}^{k} \kappa'_d(\mathbf{e}(k,k) - \mathbf{e}(k,i)) \left(\frac{\partial \mathbf{e}(k,k)}{\partial \mathbf{\Omega}_{k-1}} - \frac{\partial \mathbf{e}(k,i)}{\partial \mathbf{\Omega}_{k-1}}\right), \\
=& \mathbf{\Omega}_{k-1} + \frac{\eta}{L} \xi' \left[\frac{1}{L} \sum_{i=k-L+1}^{k} \kappa_d(\mathbf{e}(k,k) - \mathbf{e}(k,i))\right] \sum_{i=k-L+1}^{k} \kappa'_d(\mathbf{e}(k,k) - \mathbf{e}(k,i))(\Phi(\mathbf{r}_k) - \Phi(\mathbf{r}_i)).
\end{aligned} \tag{5.10}$$

From (5.7) and (5.2), utilizing Mercer's theorem $\left(\kappa_\sigma(\mathbf{r}_j, \mathbf{r}_k) = \langle \Phi(\mathbf{r}_j), \Phi(\mathbf{r}_k)\rangle_{\mathcal{H}}\right)$ [15], estimate of $\mathbf{\Theta}$ at k^{th} instant is given by

$$\mathbf{g}_k = \sum_{j=1}^{k-1} \boldsymbol{\gamma}_j(k) \kappa_\sigma(\mathbf{r}_j, \mathbf{r}_k), \tag{5.11}$$

where $\kappa_\sigma(\mathbf{r}_j, \mathbf{r}_k) = \exp\left(-\frac{\|\mathbf{r}_j - \mathbf{r}_k^*\|^2}{\sigma^2}\right)$, $\boldsymbol{\gamma}_j(k) = \boldsymbol{\gamma}_j(k-1) + \sum\limits_{l} \zeta_l(k)$, and

$$\zeta_l(k) = \begin{cases} \frac{\eta}{L}\xi'\left[\frac{1}{L}\sum_{i=k-L+1}^{k} \kappa_d(\mathbf{e}(k,k) - \mathbf{e}(k,i))\right] & \\ \times \sum_{i=k-L+1}^{k} \kappa'_d(\mathbf{e}(k,k) - \mathbf{e}(k,i)), & \text{if } l = k \\ -\frac{\eta}{L}\xi'\left[\frac{1}{L}\sum_{i=k-L+1}^{k} \kappa_d(\mathbf{e}(k,k) - \mathbf{e}(k,i))\right] & \\ \times \kappa'_d(\mathbf{e}(k,k) - \mathbf{e}(k,l)), & \text{for} \quad k - L < l < k. \end{cases} \tag{5.12}$$

As shown in (5.11), in evaluating $\mathbf{g}_k$, there is a temporal increase in MIMO radar observation. Consequently, as k (index for number of radar observation) increases, computational complexity of the estimator increases linearly. This, in turn, restricts the practical viability of the estimator. To circumvent this, similar to estimators based on KLMS and KMC, NC [43] is used. According to the criterion the newly arrived MIMO radar observation $\mathbf{r}_k$ [15] will only be used for learning if it satisfies following conditions

$$||\mathbf{e}_k||_2 \geq \delta_1,$$

$$\underbrace{\min}_{0 \leq i \leq S} ||\mathcal{D}_k^i - \mathbf{r}_k||_2 \geq \delta_2,$$

Algorithm-6, describes the pseudo-code of the proposed estimator based on KMEE-NC.

Algorithm 6 Estimation of DOD, DOA, and Doppler shift using sparse estimator based on KMEE-NC

```
Inputs: r_k = r_{θ_k|φ,f}, r_{φ_k|θ,f}, r_{f_k|θ,φ} ∀ k,  d_k = θ_k|{φ_k, f_k}, φ_k|{θ_k, f_k}, f_k|{θ_k, φ_k}  ∀ k
Initialize constants δ_e, δ_d, D_1 = {r_1}, η, γ_1(0), K, L.
while k ≤ K do
    g_k = Σ_{j=1}^{|D_k^j|} γ_j(k) κ_σ(D_k^j, r_k)
    e_k = g_k − d_k
    for l = 1 : L do
        Compute ζ_l(k) according to (5.12)
    end for
    γ_j(k) = γ_j(k − 1) + Σ_{∀l} ζ_l(k)
    if min_i ||D_k^(i) − r_k||_2 ≥ δ_1 and ||e_k||_2 ≥ δ_2 then
        D_{k+1} = D_k ∪ (r_k)
    end if
end while
```

5.3 Modified Cramer-Rao Lower Bound for DOD, DOA, and Doppler shift in the presence of Non-Gaussian Clutter

In this section, an analytical expression is derived for MCRLBs over the variance of the unbiased estimate of DOD, DOA, and Doppler shift. In this work, since the estimation of $\mathbf{\Theta}$ is performed in a high-dimensional space $\mathbb{H}$, therefore, the analytical expression for MCRLB on the variance of the estimate of $\mathbf{\Theta}$ is also derived in $\mathbb{H}$. Thereby, mapping the MIMO radar signal model given in (5.3) into $\mathbb{H}$ via $\Phi(\cdot)$, yields

$$\Phi(\mathbf{r}) = \Phi(\mathbf{s} + \mathbf{w} + \mathbf{c}), \tag{5.13}$$

where $\mathbf{s} = \mathbf{A}(\boldsymbol{\theta}, \boldsymbol{\phi})\mathbf{v}$.

The first order Taylor series approximation of (5.13) yields

$$\Phi(\mathbf{r}) = \Phi(\mathbf{s}) + \triangledown\Phi(\mathbf{s})(\mathbf{w} + \mathbf{c}), \tag{5.14}$$

where $\triangledown\Phi(\mathbf{s})$ is the Jacobian matrix.

From the set of unknown parameter ($\mathbf{\Theta} = [\Theta_1, \Theta_2, \cdots, \Theta_p, \cdots, \Theta_P]$), which is either the set of DODs, DOAs, or Doppler shifts (i.e. $\mathbf{\Theta} = [\theta_1, \theta_2, \cdots, \theta_p, \cdots, \theta_P]$, $\mathbf{\Theta} = [\phi_1, \phi_2, \cdots, \phi_p, \cdots, \phi_P]$ or $\mathbf{\Theta} = [f_1, f_2, \cdots, f_p, \cdots, f_P]$), the MCRLB for Θ_p is given by

$$MCRLB(\Theta_p) = \triangledown\Phi(\mathbf{s})^H[\mathbf{I}^{-1}(\mathbf{\Theta})]_{pp}\triangledown\Phi(\mathbf{s}) \; \forall \; p = [1, 2, \cdots, P] \tag{5.15}$$

where $\mathbf{I}(\mathbf{\Theta})$ is the modified Fisher information matrix for the MIMO radar signal model described in (5.3), subsequently, $\mathbf{I}(\mathbf{\Theta})$ is given by

$$\mathbf{I}(\mathbf{\Theta}) = \mathbb{E}_\alpha\Big[\mathbf{I}(\alpha; \mathbf{\Theta})\Big]. \tag{5.16}$$

In (5.16), elements of $\mathbf{I}(\alpha;\mathbf{\Theta})$ is given by

$$[\mathbf{I}(\alpha;\mathbf{\Theta})]_{pq} = -\mathbb{E}_{\mathbf{r}|\alpha}\left[\frac{\partial^2 \ln \mathcal{P}(\mathbf{r}|\alpha;\mathbf{\Theta})}{\partial\Theta_p\partial\Theta_q}\right], \forall\, p,q = [1,2,\cdots,P] \tag{5.17}$$

where

$$\mathcal{P}(\mathbf{r}|\alpha;\mathbf{\Theta}) = \frac{1}{\pi^{NM}|\mathbf{\Sigma}|}\exp\Big(-(\mathbf{r}-\mathbf{s})^H\mathbf{\Sigma}^{-1}(\mathbf{r}-\mathbf{s})\Big)$$

is the PDF of $\mathbf{r}$ given α, and parametrized by $\mathbf{\Theta}$ in the Euclidean space.

As $\mathbf{w}$ and $\mathbf{c}$ are independent, therefore, for given α, $\mathbf{\Sigma} = \alpha\mathbf{\Sigma}_{\mathbf{z}} + \Omega_w^2\mathbf{I}$ is the covariance matrix of total equivalent additive distortion i.e. $\mathbf{c}+\mathbf{w}$. Solving (5.17) for $\mathbf{s} = \mathbf{A}(\boldsymbol{\theta},\boldsymbol{\phi})\mathbf{v}$, yields

$$[\mathbf{I}(\alpha;\mathbf{\Theta})]_{pq} = 2\left[\frac{\partial(\mathbf{A}(\boldsymbol{\theta},\boldsymbol{\phi})\mathbf{v})^H}{\partial\Theta_p}\mathbf{\Sigma}^{-1}\frac{\partial(\mathbf{A}(\boldsymbol{\theta},\boldsymbol{\phi})\mathbf{v})}{\partial\Theta_q}\right]. \tag{5.18}$$

With the composite form of $\mathbf{\Sigma}$ ($\mathbf{\Sigma} = \alpha\mathbf{\Sigma}_{\mathbf{z}}+\Omega_w^2\mathbf{I}$), solving (5.18) is hard, as $\mathbf{\Sigma}^{-1}$ is difficult to obtain. Therefore, in this work to derive the MCRLB, as per [93], the hypothesis that the clutter power is much greater than the thermal noise i.e. ($\mathbb{E}[\alpha] >>> \Omega_w^2$) is considered. The aforementioned assumption simplifies $\mathbf{\Sigma}$ as $\mathbf{\Sigma} = \alpha\mathbf{\Sigma}_{\mathbf{z}}$. Hence, (5.18) is given by

$$[\mathbf{I}(\alpha;\mathbf{\Theta})]_{pq} = \frac{2}{\alpha}\left[\frac{\partial(\mathbf{A}(\boldsymbol{\theta},\boldsymbol{\phi})\mathbf{v})^H}{\partial\Theta_p}\mathbf{\Sigma}_{\mathbf{z}}^{-1}\frac{\partial(\mathbf{A}(\boldsymbol{\theta},\boldsymbol{\phi})\mathbf{v})}{\partial\Theta_q}\right]. \tag{5.19}$$

Invoking the trace identity, (5.19) is expressed as

$$[\mathbf{I}(\alpha;\mathbf{\Theta})]_{pq} = \frac{2}{\alpha}\mathbf{tr}\left[\frac{\partial(\mathbf{A}(\boldsymbol{\theta},\boldsymbol{\phi})\mathbf{v})}{\partial\Theta_q}\frac{\partial(\mathbf{A}(\boldsymbol{\theta},\boldsymbol{\phi})\mathbf{v})^H}{\partial\Theta_p}\mathbf{\Sigma}_{\mathbf{z}}^{-1}\right]. \tag{5.20}$$

For $\mathbf{\Sigma}_{\mathbf{z}} = \rho^{|k-l|}$, using

$$\mathbf{\Sigma}_{\mathbf{z}}^{-1} = \left\{\begin{array}{lr} 0, & \text{if } |k-l| > 1 \\ 1/(1-\rho^2), & \text{if } k=l=1 \text{ or } k=l=N_{tx}N_{rx} \\ (1+\rho^2)/(1-\rho^2), & \text{if } k=l \text{ and } 2 \le k \le N_{tx}N_{rx}-1 \\ -\rho/(1-\rho^2), & \text{if } |k-l| = 1 \end{array}\right\}$$

the elements of $\mathbf{I}(\alpha;\mathbf{\Theta})$ after using $\mathbf{tr}[\mathbf{BC}] = \sum_{k=1}^{N_{tx}N_{rx}}\sum_{l=1}^{N_{tx}N_{rx}}[\mathbf{B}]_{k,l}[\mathbf{C}]_{l,k}$, are given by

$$[\mathbf{I}(\alpha;\mathbf{\Theta})]_{pq} = \frac{2}{\alpha}\sum_{k=1}^{N_{tx}N_{rx}}\sum_{l=1}^{N_{tx}N_{rx}}[\mathbf{D}]_{k,l}[\mathbf{\Sigma}_{\mathbf{z}}^{-1}]_{l,k}, \tag{5.21}$$

where $\mathbf{D} = \frac{\partial(\mathbf{A}(\boldsymbol{\theta},\boldsymbol{\phi})\mathbf{v})}{\partial\Theta_q}\frac{\partial(\mathbf{A}(\boldsymbol{\theta},\boldsymbol{\phi})\mathbf{v})^H}{\partial\Theta_p}$.

Substituting (5.21) in (5.16), yields

$$[\mathbf{I}(\mathbf{\Theta})]_{pq} = \mathbb{E}_\alpha\left[\frac{2}{\alpha}\right]\sum_{k=1}^{N_{tx}N_{rx}}\sum_{l=1}^{N_{tx}N_{rx}}[\mathbf{D}]_{k,l}[\mathbf{\Sigma}_{\mathbf{z}}^{-1}]_{l,k}. \tag{5.22}$$

In (5.22), since α is Gamma distributed, $\mathbb{E}_\alpha\left[\frac{2}{\alpha}\right] = \frac{2\nu}{\mu_c(\nu-1)}$. Therefore, (5.22) is given by

$$[\mathbf{I}(\mathbf{\Theta})]_{pq} = \frac{2\nu}{\mu_c(\nu-1)}\sum_{k=1}^{N_{tx}N_{rx}}\sum_{l=1}^{N_{tx}N_{rx}}[\mathbf{D}]_{k,l}[\mathbf{\Sigma}_{\mathbf{z}}^{-1}]_{l,k}. \tag{5.23}$$

5.3.1 For DOD estimation

$\mathbf{\Theta} = \boldsymbol{\theta}$, therefore $\forall p, q = [1, \cdots, P]$

$$\frac{\partial(\mathbf{A}(\boldsymbol{\theta},\boldsymbol{\phi})\mathbf{v})}{\partial\theta_p} =$$
$$j\exp(\beta)\frac{2\pi}{\lambda}\left[\cos(\theta_p)d_1^t, \cdots, \cos(\theta_p)d_{N_{tx}}^t, \cdots, \cos(\theta_p)d_1^t, \cdots, \cos(\theta_p)d_{N_{tx}}^t\right]^T_{N_{tx}N_{rx}\times 1}, \tag{5.24}$$

where $\beta = j\frac{2\pi}{\lambda}\Bigg(\sin(\theta_p)d_{n_{tx}}^t + \sin(\phi_p)d_{n_{rx}}^r + \lambda f_p\Bigg)$.

Using (5.24), $\mathbf{D}$ will be a block matrix of dimension $N_{tx} \times N_{rx}$, in which each block $[\mathbf{D}]_{rs} = \mathbf{E}$ is a matrix of dimension $N_{tx} \times N_{tx}$. The elements of $\mathbf{E}$, $\forall r, s = [1, \cdots, N_{rx}]$ are given by

$$\mathbf{E}_{xy} = \begin{Bmatrix} \frac{4\pi^2}{\lambda^2}\cos(\theta_q)\cos(\theta_p)(d_{n_{tx}}^t)^2, & \text{for } x = y = n_{tx} = [1, \cdots, N_{tx}] \\ \frac{4\pi^2}{\lambda^2}\cos(\theta_q)\cos(\theta_p)d_x^t d_y^t, & \text{for } x \neq y \end{Bmatrix}$$

5.3.2 For DOA estimation

$\boldsymbol{\Theta} = \boldsymbol{\phi}$, therefore $\forall p, q = [1, \cdots, P]$

$$\frac{\partial(\mathbf{A}(\boldsymbol{\theta}, \boldsymbol{\phi})\mathbf{v})}{\partial \phi_q} =$$
$$j\exp(\beta)\frac{2\pi}{\lambda}\Bigg[\cos(\phi_q)d_1^t, \cdots, \cos(\phi_q)d_{N_{rx}}^t, \cdots, \cos(\phi_q)d_1^t, \cdots, \cos(\phi_q)d_{N_{rx}}^t\Bigg]^T_{N_{tx}N_{rx}\times 1}, \tag{5.25}$$

where $\beta = j\frac{2\pi}{\lambda}\Bigg(\sin(\theta_p)d_{n_{tx}}^t + \sin(\phi_p)d_{n_{rx}}^r + \lambda f_p\Bigg)$.

Using (5.25), similar to DOD, $\mathbf{D}$ will be a block matrix of dimension $N_{tx} \times N_{rx}$, in which each block $[\mathbf{D}]_{rs} = \mathbf{F}$ is a matrix of dimension $N_{rx} \times N_{rx}$. The elements of $\mathbf{F}$, $\forall r, s = [1, \cdots, N_{tx}]$ are given by

$$\mathbf{F}_{xy} = \begin{Bmatrix} \frac{4\pi^2}{\lambda^2}\cos(\phi_q)\cos(\phi_p)(d_{n_{rx}}^r)^2, & \text{for } x = y = n_{rx} = [1, \cdots, N_{rx}] \\ \frac{4\pi^2}{\lambda^2}\cos(\phi_q)\cos(\phi_p)d_x^r d_y^r, & \text{for } x \neq y \end{Bmatrix}$$

5.3.3 For Doppler shift estimation

$\boldsymbol{\Theta} = \mathbf{f}$, therefore $\forall p, q = [1, \cdots, P]$

$$\frac{\partial(\mathbf{A}(\boldsymbol{\theta}, \boldsymbol{\phi})\mathbf{v})}{\partial f_j} = j\exp(\beta)\frac{2\pi}{\lambda}\Bigg[1, \cdots, 1, \cdots, 1\Bigg]^T_{N_{tx}N_{rx}\times 1}, \tag{5.26}$$

where $\beta = j\frac{2\pi}{\lambda}\Bigg(\sin(\theta_p)d_{n_{tx}}^t + \sin(\phi_p)d_{n_{rx}}^r + \lambda f_p\Bigg)$.

Using (5.26),

$$\mathbf{D} = \frac{4\pi^2}{\lambda^2}\mathbf{I}_{N_{tx}\times N_{rx}}.$$

Substituting $\mathbf{D}$ in (5.23), respectively , for $\boldsymbol{\Theta} = [\theta_1, \theta_2, \cdots, \theta_p, \cdots, \theta_P]$,

$\boldsymbol{\Theta} = [\phi_1, \phi_2, \cdots, \phi_p, \cdots, \phi_P]$ or $\boldsymbol{\Theta} = [f_1, f_2, \cdots, f_p, \cdots, f_P]$, yields the element of $\mathbf{I}(\boldsymbol{\Theta})$ for DOD, DOA, or Doppler shift, respectively. Subsequently, $\mathbf{I}^{-1}(\boldsymbol{\Theta})$ is obtain, and from 5.15, using $\boldsymbol{\Phi}(\mathbf{s})^H\boldsymbol{\Phi}(\mathbf{s}) = \langle\boldsymbol{\Phi}(\mathbf{s}), \boldsymbol{\Phi}(\mathbf{s})\rangle_{\mathcal{H}} = N_{tx}N_{rx}$, the MCRLB for p^{th} target on the variance of DOD, DOA, or Doppler shift is given by

$$MCRLB(\Theta_p) = N_{tx}N_{rx}\frac{\mu_c(\nu-1)}{2\nu}\left[\mathbf{I}^{-1}(\mathbf{\Theta})\right]_{pp}. \tag{5.27}$$

5.4 Analytical Expression for Overall Variance of Estimator based on KMEE

In this section, the generalized analytical expressions for the variance in the estimation of DOD, DOA, and Doppler shift of multiple targets are derived. The variance in the estimation of Θ_p (where Θ_p is either θ_p, ϕ_p, or f_p) of p^{th} target with estimator based on KMEE is given by

$$\Omega^2_{\Theta_p} = MCRLB(\Theta_p) + S_{EMSE}, \tag{5.28}$$

where S_{EMSE} is the steady state EMSE of estimator based on KMEE

The S_{EMSE} is given by

$$S_{EMSE} = \lim_{k\to\infty}\mathbb{E}\left[\ \|\mathbf{e}_a(k)\|^2_{\mathbf{G}(k)}\ \right], \tag{5.29}$$

where $\mathbf{e}_a(k) = \mathbf{\Phi}^H(\mathbf{r}_k)\tilde{\mathbf{\Omega}}_{k-1}$ is the a-priori error vector, i.e. $\tilde{\mathbf{\Omega}}_{k-1} = \mathbf{\Omega}_o - \mathbf{\Omega}_{k-1}$ is the weight error matrix in $\mathbb{H}$ at k^{th} iteration and $\mathbf{G}(k) = \Phi^H(\mathbf{r}_k)\Phi(\mathbf{r}_k)$ is a $L\times L$ Gram matrix.

Using the energy conservation relation as per [95], we get

$$\mathbb{E}[\|\tilde{\mathbf{\Omega}}_k\|^2_{\mathbf{G}(k)}] = \mathbb{E}[\|\tilde{\mathbf{\Omega}}_{k-1}\|^2_{\mathbf{G}(k)}] - 2\eta\mathbb{E}[\mathbf{e}_a^H(k)\mathbf{h}_\phi(\mathbf{e}(k))]\eta^2\mathbb{E}[\mathbf{h}_\phi(\mathbf{e}^H(k))\mathbf{G}(k)\mathbf{h}_\phi(\mathbf{e}(k))],$$

where, from (5.2), $\mathbf{h}_\phi(\mathbf{e}(k)) = \frac{1}{L}\phi'\left[\frac{1}{L}\sum_{i=k-L+1}^{k}\kappa_d(\mathbf{e}(k,k)-\mathbf{e}(k,i))\right]\sum_{i=k-L+1}^{k}\kappa'_d(\mathbf{e}(k,k)-\mathbf{e}(k,i))(\Phi(\mathbf{r}_k)-\Phi(\mathbf{r}_i))$

Solving for $\mathbb{E}[\mathbf{e}_a^H(k)\mathbf{h}_\phi(\mathbf{e}(k))]$ and $\mathbb{E}[\mathbf{h}_\phi^H(\mathbf{e}(k))\mathbf{G}(k)\mathbf{h}_\phi(\mathbf{e}(k))]$ as per [69], yields

$$\mathbb{E}[\mathbf{e}_a^H(k)\mathbf{h}_\phi(\mathbf{e}(k))] = \gamma_k^2 h_G(\gamma_k^2), \tag{5.30}$$

$$\mathbb{E}[\mathbf{h}_\phi(\mathbf{e}^H(k))\mathbf{G}(k)\mathbf{h}_\phi(\mathbf{e}(k))] = h_I(\gamma_k^2)\mathbb{E}[\|\Phi(\mathbf{r}_k)\|^2_{\mathbf{G}(k)}], \tag{5.31}$$

where $h_G(\cdot)$, $h_I(\cdot)$ are defined in [69], and $\gamma_k^2 = \mathbb{E}[\|\mathbf{e}_a(k)\|^2_{\mathbf{G}(k)}]$

The γ_k^2 can be further simplified as

$$\begin{aligned}\gamma_k^2 =& \mathbb{E}[\|\mathbf{e}_a(k)\|^2_{\mathbf{G}(k)}] = \mathbb{E}[\mathbf{e}_a^H(k)\mathbf{G}(k)\mathbf{e}_a(k)] = \mathbb{E}[\tilde{\mathbf{\Omega}}_{k-1}^H \mathbf{\Phi}(\mathbf{r}_k)\mathbf{G}(k)\mathbf{\Phi}^H(\mathbf{r}_k)\tilde{\mathbf{\Omega}}_{k-1}] \\ =& \mathbb{E}[\tilde{\mathbf{\Omega}}_{k-1}^H \|\mathbf{\Phi}(\mathbf{r}_k)\|^2_{\mathbf{G}(k)}\tilde{\mathbf{\Omega}}_{k-1}] = N_{tx}N_{rx}L(\mu_c + \Omega_w^2)\mathbb{E}\big[\,\big\|\tilde{\mathbf{\Omega}}_{k-1}\big\|^2_{\mathbf{G}(k)}\,\big],\end{aligned} \tag{5.32}$$

where $\mathbb{E}[\|\mathbf{\Phi}(\mathbf{r}_k)\|^2_{\mathbf{G}(k)}] = N_{tx}N_{rx}L(\mu_c + \Omega_w^2)$

Substituting (5.31) into (5.30) and using (5.32), yields

$$\begin{aligned}\mathbb{E}[\big\|\tilde{\mathbf{\Omega}}_k\big\|^2_{\mathbf{G}(k)}] =& \mathbb{E}[\big\|\tilde{\mathbf{\Omega}}_{k-1}\big\|^2_{\mathbf{G}(k)}] - 2\eta N_{tx}N_{rx}L(\mu_c + \Omega_w^2)\mathbb{E}\big[\,\big\|\tilde{\mathbf{\Omega}}_{k-1}\big\|^2_{\mathbf{G}(k)}\,\big] h_G\big(N_{tx}N_{rx}L(\mu_c + \Omega_w^2) \\ &\times \mathbb{E}\big[\,\big\|\tilde{\mathbf{\Omega}}_{k-1}\big\|^2_{\mathbf{G}(k)}\,\big]\big) + N_{tx}N_{rx}L\eta^2 h_I\big(N_{tx}N_{rx}L(\mu_c + \Omega_w^2)\mathbb{E}\big[\,\big\|\tilde{\mathbf{\Omega}}_{k-1}\big\|^2_{\mathbf{G}(k)}\,\big]\big) \\ &\times(\mu_c + \Omega_w^2)\end{aligned} \tag{5.33}$$

For steady state analysis taking $\lim\limits_{k\to\infty}$ to both sides of (5.33), yields

$$\begin{aligned}\lim_{k\to\infty}\mathbb{E}[\big\|\tilde{\mathbf{\Omega}}_k\big\|^2_{\mathbf{G}(k)}] =& \lim_{k\to\infty}\mathbb{E}[\big\|\tilde{\mathbf{\Omega}}_{k-1}\big\|^2_{\mathbf{G}(k)}] - 2\eta N_{tx}N_{rx}L(\mu_c + \Omega_w^2)\lim_{k\to\infty}\mathbb{E}\big[\,\big\|\tilde{\mathbf{\Omega}}_{k-1}\big\|^2_{\mathbf{G}(k)}\,\big] \\ &\times h_G\big(N_{tx}N_{rx}L(\mu_c + \Omega_w^2)\lim_{k\to\infty}\mathbb{E}\big[\,\big\|\tilde{\mathbf{\Omega}}_{k-1}\big\|^2_{\mathbf{G}(k)}\,\big]\big) + N_{tx}N_{rx}L\eta^2 \\ &\times h_I\big(N_{tx}N_{rx}L(\mu_c + \Omega_w^2)\lim_{k\to\infty}\mathbb{E}\big[\,\big\|\tilde{\mathbf{\Omega}}_{k-1}\big\|^2_{\mathbf{G}(k)}\,\big]\big)(\mu_c + \Omega_w^2).\end{aligned} \tag{5.34}$$

Since $\lim\limits_{k\to\infty}\mathbb{E}[\big\|\tilde{\mathbf{\Omega}}_k\big\|^2_{\mathbf{G}(k)}] = \lim\limits_{k\to\infty}\mathbb{E}[\big\|\tilde{\mathbf{\Omega}}_{k-1}\big\|^2_{\mathbf{G}(k)}]$, (5.34) is given by

$$\lim_{k\to\infty}\mathbb{E}\big[\,\big\|\tilde{\mathbf{\Omega}}_{k-1}\big\|^2_{\mathbf{G}(k)}\,\big] = \frac{\eta}{2}\frac{h_I\big(N_{tx}N_{rx}L(\mu_c + \Omega_w^2)\lim\limits_{k\to\infty}\mathbb{E}\big[\,\big\|\tilde{\mathbf{\Omega}}_{k-1}\big\|^2_{\mathbf{G}(k)}\,\big]\big)}{h_G\big(N_{tx}N_{rx}L(\mu_c + \Omega_w^2)\lim\limits_{k\to\infty}\mathbb{E}\big[\,\big\|\tilde{\mathbf{\Omega}}_{k-1}\big\|^2_{\mathbf{G}(k)}\,\big]\big)}. \tag{5.35}$$

Representing $S_{WEP} = \lim\limits_{k\to\infty}\mathbb{E}\big[\,\big\|\tilde{\mathbf{\Omega}}_{k-1}\big\|^2_{\mathbf{G}(k)}\,\big]$ as the steady state weight error power, (5.35) is given by

$$S_{WEP} = \frac{\eta}{2}\frac{h_I\big(N_{tx}N_{rx}L(\mu_c + \Omega_w^2)S_{WEP}\big)}{h_G\big(N_{tx}N_{rx}L(\mu_c + \Omega_w^2)S_{WEP}\big)}. \tag{5.36}$$

Using (6.31) and (5.32), S_{EMSE} is given by

Table 5.1: Parameters values used for estimation algorithms based on KMEE-NC, KMC-NC, and KLMS-NC for estimating DOD via simulations.

Parameters	KMEE-NC	KMC-NC	KLMS-NC
μ	0.57	0.57	0.57
σ	10^{-6}	10^{-6}	10^{-6}
σ_c	2×10^{-5}	0.02	Nil
δ_e	$10^{-8.5}$	$10^{-8.5}$	$10^{-8.5}$
δ_d	1.9	1.9	1.9
L	25	Nil	Nil

$$S_{EMSE} = N_{tx}N_{rx}L(\mu_c + \Omega_w^2)S_{WEP}. \tag{5.37}$$

5.5 Simulation Results and Discussion

In this section, we present and discuss simulation results performed to validate performance of the proposed estimator based on KMEE-NC. For evaluating the average NMSE $\left(\text{NMSE}=\frac{1}{K_{te}}\sum_{k=1}^{K_{te}}\frac{\|\boldsymbol{\Theta}_k-\hat{\boldsymbol{\Theta}}_k\|^2}{\|\boldsymbol{\Theta}_k\|^2}\right.$, where K_{te} is the number of MIMO radar observations used for testing$\Big)$ performance of the proposed estimator, the SCR=$\frac{\mathbf{v}^H\mathbf{A}^H(\boldsymbol{\theta},\boldsymbol{\phi})\mathbf{A}(\boldsymbol{\theta},\boldsymbol{\phi})\mathbf{v}}{\mu_c\mathbf{tr}(\boldsymbol{\Sigma}_\mathbf{z})}$, and CNR=$\frac{\mu_c\mathbf{tr}(\boldsymbol{\Sigma}_\mathbf{z})}{N_{tx}N_{rx}\Omega_\mathbf{w}^2}$ are both fixed at 30 dB [5]. The simulations are performed to estimate the DOD, DOA, and Doppler shift of four different targets (i.e $P = 4$) illuminated by the MIMO radar with $N_{tx} = 4$, and $N_{rx} = 3$ [90]. In (5.3), the clutter vector $\mathbf{c}$ is realized from the non-Gaussian distribution described in Section 1.5 of Chapter 1. To compare performance of the proposed estimator with other sparsified version of kernel based estimators (KLMS-NC and KMC-NC) and existing estimators proposed in [88], [89], [90], and [91], variance in estimation of parameters of first target is evaluated in the SCR range from -30 dB to 30 dB with an increment of 2 dB. The reported simulation results are obtained by ensemble of 100 Monte Carlo runs. The free parameter values of KMEE-NC, KMC-NC, and KLMS-NC for the estimation of DOD, DOD, and Doppler shift are summarized in Table 5.1, Table 5.2, and Table 5.3, respectively. The value of free parameters mentioned in Table 5.1, Table 5.2, and Table 5.3 are obtained by cross-validation [15, 16], to achieve a desirable average NMSE convergence speed with minimum average NMSE value.

Table 5.2: Parameters values used for estimation algorithms based on KMEE-NC, KMC-NC, and KLMS-NC for estimating DOA via simulations.

Parameters	KMEE-NC	KMC-NC	KLMS-NC
μ	0.57	0.57	0.57
σ	10^{-6}	10^{-6}	10^{-6}
σ_c	2×10^{-5}	0.02	Nil
δ_e	$10^{-8.5}$	$10^{-8.5}$	$10^{-8.5}$
δ_d	2	2	2
L	20	Nil	Nil

Table 5.3: Parameters values used for estimation algorithms based on KMEE-NC, KMC-NC, and KLMS-NC for estimating Doppler shift via simulations.

Parameters	KMEE-NC	KMC-NC	KLMS-NC
μ	0.55	0.55	0.55
σ	$10^{-7.4}$	$10^{-7.4}$	$10^{-7.4}$
σ_c	2×10^{-5}	0.02	Nil
δ_e	$10^{-8.5}$	$10^{-8.5}$	$10^{-8.5}$
δ_d	6.4	6.4	6.4
L	20	Nil	Nil

5.5.1 Estimation of DOD and DOA

Simulations using estimators based on KMEE-NC, KMC-NC, and KLMS-NC to estimate DOD and DOA of four different targets are performed by dividing the interval of true values of DOD and DOA, i.e., $(\frac{-\pi}{2}, \frac{\pi}{2})$ into $K = 5550$ parts. Subsequently, the MIMO radar observations corresponding to $K = 5550$ true values of DOD and DOA are obtained by using (5.4) and (5.5), respectively. The starting $K_{tr} = 5000$ pair of DOD and DOA true values and respective MIMO radar observations i.e. $(\mathbf{d}_k, \mathbf{r}_{\theta_k|\boldsymbol{\phi},\mathbf{f}})$ or $(\mathbf{d}_k, \mathbf{r}_{\boldsymbol{\phi}_k|\boldsymbol{\theta},\mathbf{f}})$ are used to train the estimators. The rest $K_{te} = 550$ pairs are used for testing performance of the estimators and evaluating the average NMSE.

As shown in Fig. 5.1a, and Fig. 5.2a, the estimator based on KMEE-NC converges to a lower average NMSE of the order 10^{-2} as compared to the estimator based on KLMS-NC. Further, as reported in Fig. 5.1a, and Fig. 5.2a, the estimator based on KMEE-NC yields estimates with average NMSE equal to the estimator based on KMC-NC. However, as shown in Fig. 5.1b, and Fig. 5.2b, the computational complexity (dictionary size) obtained in the estimation of DOD and DOA, using an estimator based on KMEE-NC is lower than the estimator based on KMC-NC and KLMS-NC. The lower average NMSE and lower dictionary size obtained by the estimator based on KMEE-NC, validate the superiority of the proposed estimator over other kernel based estimation techniques (KMC-NC and KLMS-NC).

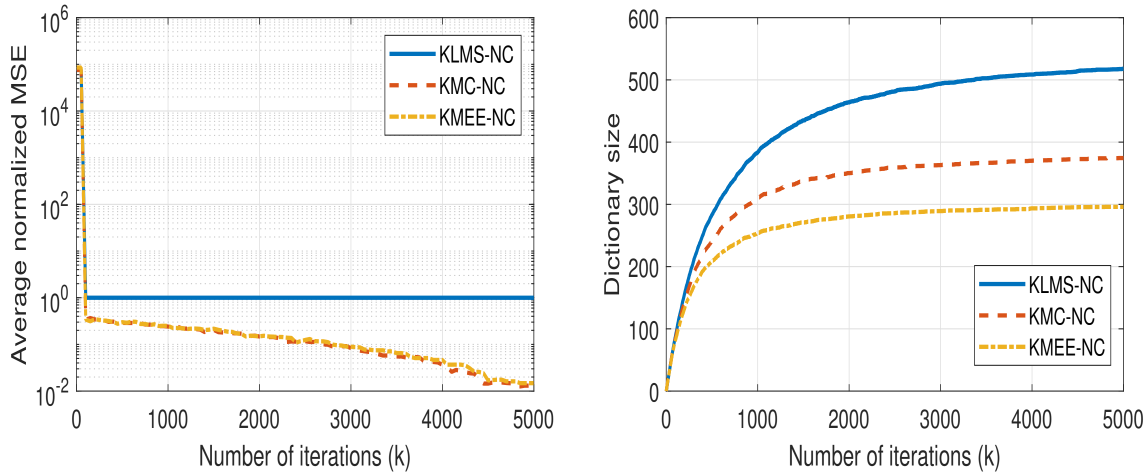

(a) (b)

Figure 5.1: (a) Average normalized MSE, and (b) Dictionary size in the estimation of DOD using estimators based on KMEE-NC, KMC-NC, and KLMS-NC.

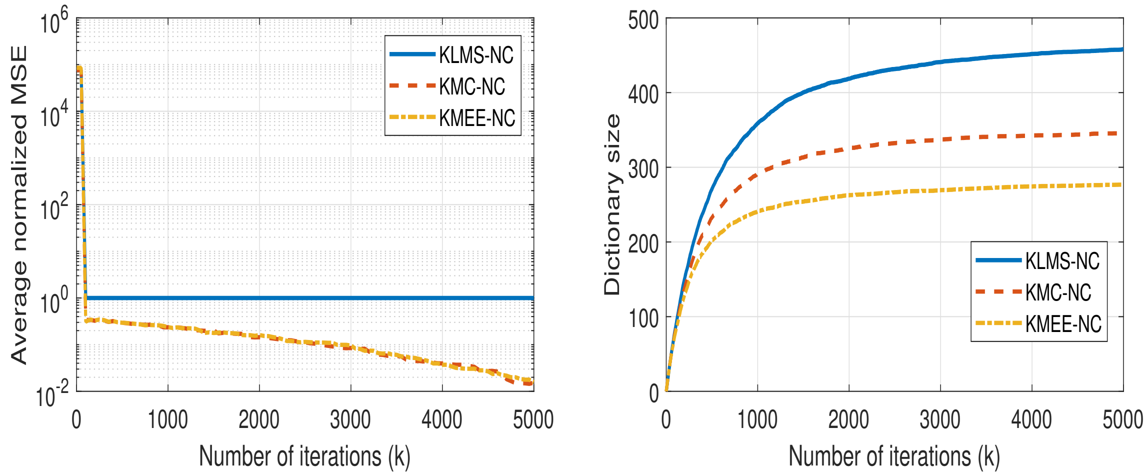

(a) (b)

Figure 5.2: (a) Average normalized MSE, and (b) Dictionary size in the estimation of DOA using estimators based on KMEE-NC, KMC-NC, and KLMS-NC.

5.5.2 Estimation of Doppler shift

Similar to DOD and DOA, simulations to estimate normalized Doppler shift for $P = 4$ using estimators based on KMEE-NC, KMC-NC, and KLMS-NC are performed by dividing the interval of true values of normalized Doppler shift i.e $(-0.5, 0.5)$ into $K = 5550$ parts. The MIMO radar observations corresponding to $K = 5550$ true values of Doppler shift are obtained by using (5.6). Out of the 5550 pair of Doppler shift and MIMO radar observations i.e. $(\mathbf{d}_k, \mathbf{r}_{\mathbf{f}_k|\boldsymbol{\theta},\boldsymbol{\phi}})$, 5000 are used to train the estimators. Subsequently, the average NMSE in estimating normalized Doppler shift are evaluated using the remaining 550 pairs of Doppler shift and MIMO radar observations $(\mathbf{d}_k, \mathbf{r}_{\mathbf{f}_k|\boldsymbol{\theta},\boldsymbol{\phi}})$.

In the estimation of the Doppler shift, as depicted in Fig. 5.3a, average NMSE of the estimator based on KMEE-NC converges to the order of 10^{-2} which is lower than the average NMSE achieved by the estimators based on KLMS-NC. Further, as reported in Fig. 5.3a, performance of the estimator based on KMEE-NC coincides with the performance of estimator based on KMC-NC. However, similar to Doppler shift estimation, estimator based on KMEE-NC offers a gain over KMC-NC and KLMS-NC in terms of computational complexity, as shown in Fig. 5.3b.

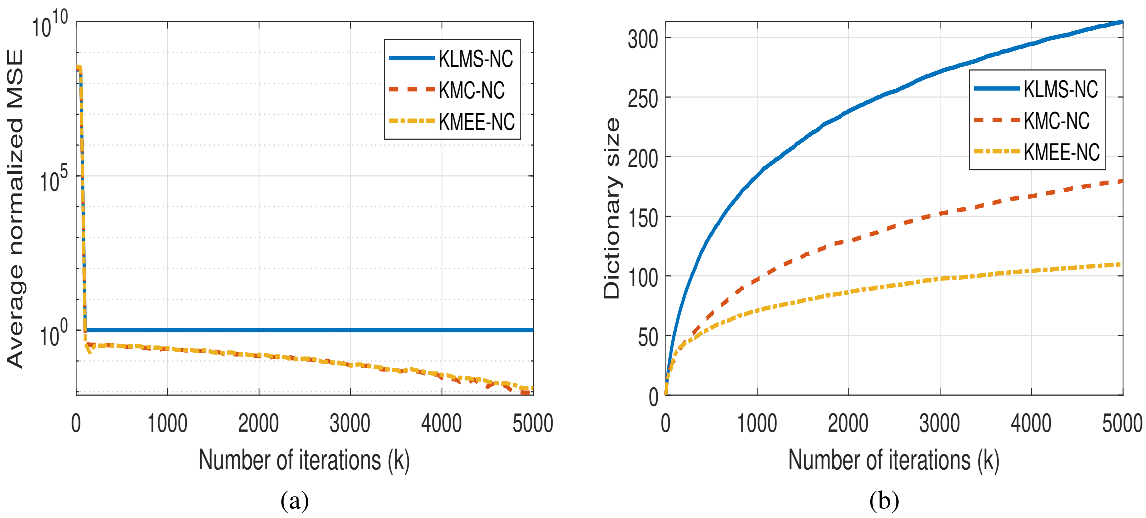

Figure 5.3: (a) Average normalized MSE, and (b) Dictionary size in the estimation of Doppler shift using estimators based on KMEE-NC, KMC-NC, and KLMS-NC.

5.5.3 Comparative Performance of Estimators

For assessing the accuracy of the proposed estimation technique compared to existing kernel based estimators and conventional estimators, the variance of the estimators is compared with the respective MCRLBs. For this, simulations are performed to evaluate variance in the estimation of DOD, DOA, and Doppler shift of the first target, i.e., $p = 1$.

The estimators proposed in [88], [89], [90], and [91] are termed as conditional iterative ML estimator (CIMLE), joint IMLE (JIMLE), marginal IMLE (MIMLE), and approximate ML estimator (AMLE), respectively. As shown in Fig. 5.4a in the estimation of DOD, the variance obtained with KMEE-NC in comparison to KLMS-NC, CIMLE, JIMLE, MIMLE, and AMLE, is closer to the achievable MCRLB. This is because, unlike the CIMLE, JIMLE, MIMLE, and AMLE, the estimator based on KMEE-NC optimizes the convex cost function and result in improved performance as shown in Fig. 5.4a. Furthermore, it is also observed that the variance of the estimator based on KMEE-NC and KMC-NC overlaps. However, as depicted in Fig. 5.1b, Fig. 5.2b, and Fig. 5.3b, KMEE-NC utilizes much lower radar observations than KMC-NC, which results in more moderate computational complexity. Moreover, as shown in Fig. 5.4a, particular to DOD estimation, KMEE-NC has lower variance than KMC-NC in the SCR range of 10 dB to 20 dB. Similar to DOD estimation, in Doppler shift estimation, as shown in Fig. 5.4b, KMEE-NC yields lower variance than KMC-NC in the SCR range of 0 dB to 10 dB.

5.6 Summary

In this Chapter, an estimator for DOD, DOA, and Doppler shift for multiple targets using MIMO radar in the presence of non-Gaussian clutter is proposed. The effect of non-Gaussian clutter is handled by introducing the adaptive estimator based on KMEE. The KMEE optimizes the MEE criterion in RKHS, which yields accurate estimates of parameters by compensating the effect of non-Gaussian clutter. Practical viability of the proposed KMEE based estimator is limited by its high computational complexity/dictionary size. Thus, the computational complexity/dictionary size is reduced by the incorporation of the

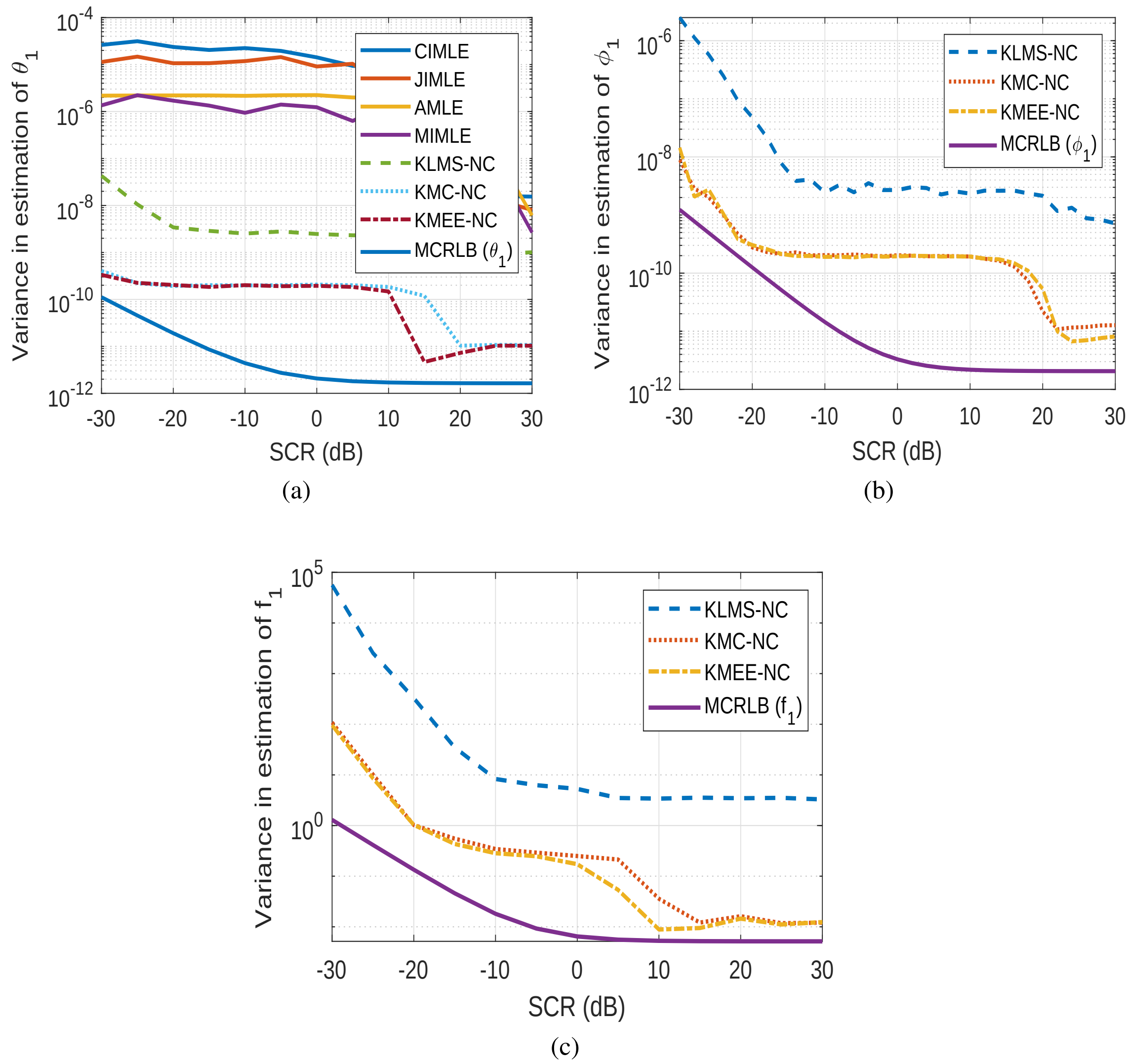

Figure 5.4: Comparative performance of the estimators for estimation of (a) DOD, (b) DOA, and (c) Doppler shift of the first target.

sparsification technique based on NC. Performance of the proposed algorithm is compared with the derived MCRLB for DOD, DOA, and Doppler shift. Further, accuracy of the proposed estimator is validated through computer simulations over realistic MIMO radar systems. The obtained simulation results reveal viability of the proposed KMEE-NC based estimator over other kernel-based adaptive estimators.

In previous Chapters, particularly in Chapter 3, Chapter 4, and Chapter 5, KAF based estimators (estimators based on KLMS, KMC, and KMEE), are developed and found to yields an accurate estimate of vital parameters of targets. Consequently, they proved to be a viable choice over conventional non-adaptive estimators. Nevertheless, for proper working, KAF based estimators require a suitable value of various system parameters like kernel width (σ) and learning rate (μ). The inappropriate value of these parameters adversely affects the estimation accuracy of the KAF based estimator. Moreover, being an adaptive algorithm, more often, KAF based estimators require higher iterations number to converge to an optimum solution corresponding to lower MSE value. Thus, to counter the drawbacks of estimators based on KAF, next, a new class of estimators based on EKF and UKF are developed. Estimation accuracy of the proposed estimators is tested over Gaussian perturbed LFM radar system and compared with their best counterpart; estimator based on KLMS-Modified NC.

Chapter 6

Range and velocity estimation using EKF and UKF based Estimators

As a solution for accurate estimation of delay and Doppler shift in Gaussian distributed thermal noise, in Chapter 3, a KLMS based estimator has been developed and tested over LFM and OFDM radar. The KLMS based estimator uses representer theorem [16] to recursively estimate the unknown inverse function (between the unknown parameters and returning signal) in RKHS [15, 16]. The estimated parameters are adaptively updated using the LMS algorithm [15, 16]. However, as a major drawback of KLMS based estimators, to learn the unknown function ($g(\cdot)$), the KLMS algorithm requires precise knowledge of various system parameters, like the kernel width (σ), step size (μ), and dictionary thresholds (δ_1, δ_2). Suitable values of these parameters are obtained by tuning their values in a fixed range. Moreover, these parameter values are model specific [15, 18, 56], hence a priorly fixed set of parameter values is not appropriate for targets with varying system dynamics (e.g., varying range and radial velocity) which is most common in practical problems. Consequently, the KLMS based estimator is prone to result in poor estimation accuracy. Another drawback is that being a stochastic gradient-based algorithm; the KLMS based estimators require a large number of iterations to converge to a minimum error (between the desired and estimated parameters) solution [16].

The solution of the estimates obtained by KLMS is given in terms of a recursive sum of weighted kernel evaluations, which grows with every new input radar return, which in turn causes calculation of the estimates to be computationally demanding. A general method to constrain the growing network size is to use the sparsification techniques. NC based sparsification technique has been used along with KLMS (KLMS-NC and KLMS-Modified NC) for the radar applications. The sparsified estimator does not use all the arriving radar returns and instead used a selection criterion to determine if the input radar returns will be used for estimation and stored in the dictionary. This enables the estimator to give good performance with a limited dictionary size. While sparsification techniques provides a solution to curb the growing kernel evaluations, they have certain limitations. Firstly, at every time instant, a linear search throughout the existing dictionary is done to establish whether or not the new input radar return is going to be stored in the dictionary. This causes the addition of significant overhead in the estimation process. Secondly, since KLMS-NC and KLMS-Modified NC are a dictionary-based learning approach [17, 18, 60], spurious inputs added to the dictionary at the initial stages of the learning process affect the future inputs which in turn affects the overall performance of the estimator adversely.

This Chapter introduces two novel estimation techniques to counter drawbacks of estimators based on KLMS, and improve the estimation accuracy of delay and Doppler shift. The proposed estimation techniques are based on two popular estimators; the EKF [98], and the UKF [20, 99, 100]. To the best of authors' knowledge, the EKF and UKF have been tested for target tracking using radar-based measurements [19, 21, 22]. The other version of Kalman filter; modified convolution kernel function [101], has been used for parameter estimation of returning signal for the specific application of synthetic aperture radar, modeled as LFM signal. However, EKF and UKF, have not been explored for estimating the delay and Doppler shift for target tracking. The EKF implements the concept of basic Kalman filter [98] and offers a simple and straightforward implementation. However, it approximates the non-linear system models as linear models obtained by first-order linearization. Subsequently, it suffers from poor accuracy and stability, especially in a complex environment such as low SNR and heavy-tailed clutters. A poor accuracy in estimating the target's states causes ambiguity in target identification. Unlike the EKF, the UKF considers the system models in their original form, which is helpful in accurate estimation of a target's parameters in a complex environment. Accuracy of the proposed estimation techniques based on EKF and UKF is compared with the existing best version of KLMS based estimator (KLMS Modified-NC) and estimator based on FT, in terms of NMSE and variance. Simulation results reveal a lower NMSE and variance for the proposed estimators, which concludes an improved accuracy.

The Chapter is organized as follows: Firstly, the signal model for received radar return for the transmitted LFM signal is described. The proposed EKF and UKF based estimators are described next. Further, simulation results along with analytical expressions for CRLB on the variance in estimating the time-delay and Doppler shift are discussed. Finally, the contribution of this work is concluded.

6.1 Signal Model Formulation

In this section, the radar return signal model is derived, which describes relationship between the radar return and the desired unknown parameters viz delay and Doppler shift. The estimation algorithms are implemented to most commonly used radar system called mono-static LFM radar [4, 102].

Following the steps described in Subsection 3.1.1 of Chapter 3. The returning signal for LFM radar is given by

$$r(m,l) = \exp\left(j2\pi m f_d T_{\text{PRI}}\right) \exp\left(-j2\pi l \Delta f \tau_o\right) \exp\left(j2\pi f_d m l \left(\frac{T_{\text{PRI}}\Delta f}{f_c}\right)\right) + w(m,l), \quad (6.1)$$

From (6.1), it is explicit that the returning signal, $r(m,l)$, is exponentially related to the desired delay, τ_o, and Doppler shift, f_d. The adaptive estimators to estimate τ_o and f_d based on KLMS Modified-NC assuming Gaussian distribution for equivalent perturbation is introduced in Chapter 3. However, the performance of the KLMS Modified-NC based estimator is susceptible to inappropriate values of various system parameters. Moreover, being an adaptive algorithm, KLMS Modified-NC requires large number of iterations to reach the theoretical optimum solution, leading to large computational time. In this paper, to mitigate the shortcomings of existing state of the art algorithms, two advanced estimation techniques based on EKF and UKF for estimating τ_o and f_d from the returning signal $r(m,l)$ is introduced.

6.2 EKF and UKF based Estimation of delay and Doppler shift

In this section, the proposed EKF and UKF based estimators for τ_o and f_d are described in details. In noisy environments (as the case of LFM radar system), Bayesian framework based estimators are most accepted for several decades (refer to [98, 103, 104] for detail discussion). The Bayesian framework is based on state space formulation (discussed in Section 6.2.1) [98] of the system model, and it is implemented in two steps: prediction and update. Two popular simplifications of Bayesian framework are Gaussian filtering [98], and particle filtering [105]. The Gaussian filters are preferred over particle filters due to their high estimation accuracy at appreciably low computational cost. The proposed EKF and UKF are two popular Gaussian filters.

In this Chapter, firstly, the state space model for the LFM radar system is formulated, and a brief discussion on Bayesian parameter estimation is provided. After that, elaborate discussion of the proposed EKF and UKF based estimation of τ_o and f_d is given.

6.2.1 State Space Model for LFM Radar System

The state space model consists of state and measurement models, where the state model characterizes the state dynamics while the measurement model represents the mathematical relation between the state and the measurement. Note that, the state is defined with the unknown/desired parameters (τ_o and f_d in our case), while the measurement consists of the observed quantities (the returning signal $r(m,l)$). Subsequently, the state and measurement variables are formulated as $\mathbf{x} = [\tau_o \quad f_d]^T$[1] and $\mathbf{r} = [\mathbf{Re}(r(m,l)) \quad \mathbf{Im}(r(m,l))]^T$, respectively. We formulate the model for targets with constant velocity as special cases of

[1]The i^{th} element of $\mathbf{x}$ is referred as $\mathbf{x}(i)$.

the model for constant acceleration. The change in position is assumed to reflect a constant increase in the time-delay, and any error due to this assumption is compensated with the process noise. Similarly, any error due to the constant velocity is also compensated with the process noise. Subsequently, the state model could be designed as an incremental model, *i.e.*

$$\mathbf{x}_{k+1} = f(\mathbf{x}_k) + \boldsymbol{\eta}_k = \mathbf{x}_k + \Delta\mathbf{x} + \boldsymbol{\eta}_k, \tag{6.2}$$

where $k \in \{1, 2, \cdots, K\}$, $K = ML$ is total number of discretized samples of returning signal and $\Delta\mathbf{x} = [\frac{T_{\text{PRI}}}{K}, 0]^T$ is a constant shift in $\mathbf{x}$ between successive samples of returning signal. $\boldsymbol{\eta}_k$ is additive process noise which models the errors. $\boldsymbol{\eta}_k$ is assumed to be zero mean Gaussian with covariance $\mathbf{Q}_k$ under the Gaussian filtering.

From (6.1), the measurement model can be formulated as

$$\mathbf{r}_{k+1} = h(\mathbf{x}_{k+1}) + \mathbf{v}_{k+1} \tag{6.3}$$

where $\mathbf{v}_k$ represents measurement noise which is added to compensate any error in capturing and/or processing of returning signals, and $h(\mathbf{x}_{k+1})$ is given by

$$h(\mathbf{x}_{k+1}) = \begin{bmatrix} \mathbf{Re}\left(\exp\left(j2\pi m\mathbf{x}_{k+1}(2)T_{\text{PRI}}\right)\exp\left(-j2\pi l\Delta f\mathbf{x}_{k+1}(1)\right)\exp(j2\pi\mathbf{x}_{k+1}(2)ml(\frac{T_{\text{PRI}}\Delta f}{f_c}))\right) \\ \mathbf{Im}\left(\exp\left(j2\pi m\mathbf{x}_{k+1}(2)T_{\text{PRI}}\right)\exp\left(-j2\pi l\Delta f\mathbf{x}_{k+1}(1)\right)\exp(j2\pi\mathbf{x}_{k+1}(2)ml(\frac{T_{\text{PRI}}\Delta f}{f_c}))\right) \end{bmatrix}.$$

Under Gaussian filtering, $\mathbf{v}_k$ is assumed to be zero mean Gaussian with covariance $\mathbf{R}_k$.

6.2.2 Bayesian Framework for Filtering

The Bayesian filtering is performed in two steps:

Prediction

This step constructs the pdf of states one step forward in time (in reference to the available measurements) using Chapman-Kolmogorov equation [98, 103], *i.e.*

$$\mathcal{P}(\mathbf{x}_k|\mathbf{r}_{1:k-1}) = \int \mathcal{P}(\mathbf{x}_k|\mathbf{x}_{k-1})\mathcal{P}(\mathbf{x}_{k-1}|\mathbf{r}_{1:k-1})d\mathbf{x}_{k-1}, \tag{6.4}$$

where $\mathcal{P}(\mathbf{x}_k|\mathbf{r}_{1:k-1})$ is commonly known as prior pdf.

Update

This step reconstructs the pdf $\mathcal{P}(\mathbf{x}_k|\mathbf{r}_{1:k-1})$ on the receipt of a new measurement $\mathbf{y}_k$ using Bayes rule, *i.e.* [98, 103]

$$\mathcal{P}(\mathbf{x}_k|\mathbf{r}_{1:k}) = \mathcal{P}(\mathbf{x}_k|\mathbf{r}_{1:k-1}, \mathbf{r}_k) = \frac{1}{c_k}\mathcal{P}(\mathbf{r}_k|\mathbf{x}_k)\mathcal{P}(\mathbf{x}_k|\mathbf{r}_{1:k-1}), \tag{6.5}$$

where $\mathcal{P}(\mathbf{r}_k|\mathbf{x}_k)$ is measurement likelihood which is obtained from (6.3) and c_k is a normalization constant *i.e.*

$$c_k = \mathcal{P}(\mathbf{r}_k|\mathbf{r}_{1:k-1}) = \int \mathcal{P}(\mathbf{r}_k|\mathbf{x}_k)\mathcal{P}(\mathbf{x}_k|\mathbf{r}_{1:k-1})d\mathbf{x}_k. \tag{6.6}$$

The objective of Bayesian filtering is to construct $\mathcal{P}(\mathbf{x}_k|\mathbf{r}_{1:k})$, which is popularly known as posterior pdf.

Hereafter, denoting $\mathcal{P}(\mathbf{x}_k|\mathbf{r}_{1:k-1}) \sim \mathcal{P}(\mathbf{x}_{k|k-1})$ and $\mathcal{P}(\mathbf{x}_k|\mathbf{r}_{1:k}) \sim \mathcal{P}(\mathbf{x}_{k|k})$, which are standard notations used in estimation and filtering literature [98, 103, 104].

6.2.3 EKF based Estimation of delay and Doppler shift

From the state space model of radar systems ((6.2) and (6.3)), the estimation of τ_o and f_d from returning signal, $r(m, l)$, is simplified as an estimation problem of $\mathbf{x}_k$ from known measurement $\mathbf{r}_k$. A conceptual solution for such problem is introduced as the Bayesian framework. The EKF is an analytical simplification of Bayesian framework. It assumes the conditional pdfs in the Bayesian framework ((6.4) to (6.6)) as Gaussian, *i.e.*

$$\mathcal{P}(\mathbf{x}_{k|k-1}) \sim \mathcal{N}_{\mathbb{R}}(\mathbf{x}_{k|k-1}; \hat{\mathbf{x}}_{k|k-1}, \mathbf{P}_{k|k-1}), \tag{6.7}$$

$$\mathcal{P}(\mathbf{x}_{k|k}) \sim \mathcal{N}_{\mathbb{R}}(\mathbf{x}_{k|k}; \hat{\mathbf{x}}_{k|k}, \mathbf{P}_{k|k}), \tag{6.8}$$

where $\hat{\mathbf{x}}_{k|k}$ and $\mathbf{P}_{k|k}$ are mean and covariance of $\mathbf{x}_{k|k}$. Subsequently, the problem is further simplified to determine $\hat{\mathbf{x}}_{k|k-1}$ and $\mathbf{P}_{k|k-1}$ in prediction step, and $\hat{\mathbf{x}}_{k|k}$ and $\mathbf{P}_{k|k}$ in update step. The computational aspect of the two steps is discussed herewith.

Prediction

$\hat{\mathbf{x}}_{k|k-1}$ and $\mathbf{P}_{k|k-1}$ are obtained from the first and second moments of $\mathbf{x}$, with pdf of $\mathbf{x}$ given in (6.7). A simplified expression for $\hat{\mathbf{x}}_{k|k-1}$ and $\mathbf{P}_{k|k-1}$ are given as [98, 103]

$$\hat{\mathbf{x}}_{k|k-1} = f(\hat{\mathbf{x}}_{k-1|k-1}), \tag{6.9}$$

$$\mathbf{P}_{k|k-1} = \mathbf{F}_k \mathbf{P}_{k-1|k-1} \mathbf{F}_k^T + \mathbf{Q}_k, \tag{6.10}$$

where

$$\mathbf{F}_k = \left.\frac{\partial f(\mathbf{x})}{\partial \mathbf{x}}\right|_{\mathbf{x}=\hat{\mathbf{x}}_{k-1|k-1}} = \begin{bmatrix} 1 & 0 \\ 0 & 1 \end{bmatrix}$$

is Jacobian of $f(\mathbf{x})$ computed at $\hat{\mathbf{x}}_{k-1|k-1}$. The detailed discussion is given in [98, 103, 104].

Update

In the update step, the predicted estimate and covariance, $\hat{\mathbf{x}}_{k|k-1}$ and $\mathbf{P}_{k|k-1}$, are corrected using the information received from new measurement. The correction step requires the statistical information about predicted measurement, which is obtained in the following steps.

- The predicted measurement is obtained as

$$\hat{\mathbf{r}}_{k|k-1} = h(\hat{\mathbf{x}}_{k|k-1}). \tag{6.11}$$

- The error covariance of predicted measurement is obtained as

$$\mathbf{P}^{\mathbf{rr}}_{k|k-1} = \mathbf{H}_k \mathbf{P}_{k-1|k-1} \mathbf{H}_k^T + \mathbf{R}_k, \tag{6.12}$$

where

$$\mathbf{H}_k = \left.\frac{\partial h(\mathbf{x})}{\partial \mathbf{x}}\right|_{\mathbf{x}=\hat{\mathbf{x}}_{k|k-1}} = \begin{bmatrix} \frac{\partial \cos(\theta_1)}{\partial \mathbf{x}_k(1)} & \frac{\partial \cos(\theta_1)}{\partial \mathbf{x}_k(2)} \\ \frac{\partial \sin(\theta_1)}{\partial \mathbf{x}_k(1)} & \frac{\partial \sin(\theta_1)}{\partial \mathbf{x}_k(2)} \end{bmatrix},$$
$$= \begin{bmatrix} -\sin(\theta_1)\frac{\partial \theta_1}{\partial \mathbf{x}_k(1)} & -\sin(\theta_1)\frac{\partial \theta_1}{\partial \mathbf{x}_k(2)} \\ \cos(\theta_1)\frac{\partial \theta_1}{\partial \mathbf{x}_k(1)} & \cos(\theta_1)\frac{\partial \theta_1}{\partial \mathbf{x}_k(2)} \end{bmatrix}. \tag{6.13}$$

is Jacobian of $h(\mathbf{x})$ computed at $\hat{\mathbf{x}}_{k|k-1}$. In (6.13), $\theta_1 = -2\pi l \Delta f \mathbf{x}_k(1) + 2\pi m \mathbf{x}_k(2) T_{\text{PRI}} + 2\pi m l \mathbf{x}_k(2)((T_{\text{PRI}}\Delta f)/f_c)$.

Based on the error covariance of the predicted state and measurement, a Kalman gain is computed as

$$\mathbf{K}_k = \mathbf{P}_{k|k-1}\mathbf{H}_k^T(\mathbf{P}^{\mathbf{rr}}_{k|k-1})^{(-1)}. \tag{6.14}$$

On the receipt of a new measurement $\mathbf{r}_k$, the desired estimate and covariance, $\hat{\mathbf{x}}_{k|k}$ and $\mathbf{P}_{k|k}$, are obtained as

$$\hat{\mathbf{x}}_{k|k} = \hat{\mathbf{x}}_{k|k-1} + \mathbf{K}_k(\mathbf{r}_k - \hat{\mathbf{r}}_{k|k-1}), \tag{6.15}$$

$$\hat{\mathbf{P}}_{k|k} = \hat{\mathbf{P}}_{k|k-1} - \mathbf{K}_k\mathbf{P}^{\mathbf{rr}}_{k|k-1}\mathbf{K}_k^T. \tag{6.16}$$

For a detailed discussion please refer [98, 103, 104].

The posterior estimate $\hat{\mathbf{x}}_{k|k} = [\hat{\tau}_{o_k} \quad \hat{f}_{d_k}]^T$ provides the desired estimate of delay and Doppler shift. The steps involved in EKF based estimation of delay and Doppler shift is summarized in Algorithm 7.

6.2.4 UKF based Estimation of delay and Doppler shift

The UKF [20, 99, 100] uses a derivative-free implementation for estimating $\mathbf{x}_k$ from known measurement $\mathbf{r}_k$, unlike the EKF. Moreover, it propagates the estimate and covariance through true system model instead of propagating them through a derivative-based locally approximated model. Note that, the objective of Gaussian filtering is to obtain the estimate and covariance of states for characterizing the Gaussian pdfs; $\hat{\mathbf{x}}_{k|k-1}$ and $\mathbf{P}_{k|k-1}$ in prediction step and, $\hat{\mathbf{x}}_{k|k}$ and $\mathbf{P}_{k|k}$ in update step. The estimate and covariance are

Algorithm 7 Estimation of delay and Doppler shift using EKF

Input: $f : \mathbf{x}_k \rightarrow \mathbf{x}_{k-1}$, $h : \mathbf{x}_k \rightarrow \mathbf{r}_k$, $\mathbf{Q}_k$, and $\mathbf{R}_k$
Output: $\hat{\mathbf{x}}_{k|k}$
Initialization: $\hat{\mathbf{x}}_{0|0}$, $\mathbf{P_{0|0}}$
while $k \leq K$ **do**
  Derivative computation for state dynamics $\mathbf{F}_k = \left.\frac{\partial f(\mathbf{x})}{\partial \mathbf{x}}\right|_{\mathbf{x}=\hat{\mathbf{x}}_{k-1|k-1}}$
  Prediction
  $\hat{\mathbf{x}}_{k|k-1} = f(\hat{\mathbf{x}}_{k-1|k-1})$
  $\mathbf{P}_{k|k-1} = \mathbf{F}_k \mathbf{P}_{k-1|k-1} \mathbf{F}_k^T + \mathbf{Q}_k$
  Derivative computation for measurement model $\mathbf{H}_k = \left.\frac{\partial h(\mathbf{x})}{\partial \mathbf{x}}\right|_{\mathbf{x}=\hat{\mathbf{x}}_{k|k-1}}$
  Update
  $\hat{\mathbf{r}}_{k|k-1} = h(\hat{\mathbf{x}}_{k|k-1})$
  $\mathbf{P}^{yy}_{k|k-1} = \mathbf{H}_k \mathbf{P}_{k-1|k-1} \mathbf{H}_k^T + \mathbf{R}_k$
  $\mathbf{K}_k = \mathbf{P}_{k|k-1} \mathbf{H}_k^T (\mathbf{P}^{\mathbf{rr}}_{k|k-1})^{(-1)}$
  $\hat{\mathbf{x}}_{k|k} = \hat{\mathbf{x}}_{k|k-1} + \mathbf{K}_k (\mathbf{r}_k - \hat{\mathbf{r}}_{k|k-1})$
  $\hat{\mathbf{P}}_{k|k} = \hat{\mathbf{P}}_{k|k-1} - \mathbf{K}_k \mathbf{P}^{\mathbf{rr}}_{k|k-1} \mathbf{K}_k^T$
  Return $\hat{\mathbf{x}}_{k|k}$
end while

obtained from the first and second moments. For systems with Gaussian assumption on conditional pdfs, the moment computation involves an integral of the form '$\int_{-\infty}^{\infty}$ *arbitrary function* $\times$ *Gaussian pdf*' [106, 107]. The integrals of this form are generally intractable [106, 107], therefore an analytical solution does not exist. The UKF numerically approximates the intractable integrals using unscented transformation [20, 99] based numerical approximation.

The unscented transformation generates a set of $2n+1$ symmetrically distributed sigma points, with n being the system dimension which is two in the considered problem. It also generates a set of $2n + 1$ weights associated with sigma points. Considering $\hat{\mathbf{x}}$ and $\mathbf{P}$ be the estimate and covariance of random variable $\mathbf{x}$ respectively, the set of sigma points, $\boldsymbol{\xi}$, can be obtained as [20, 100]

$$\begin{aligned}
\boldsymbol{\xi}_0 &= \hat{\mathbf{x}}, \\
\boldsymbol{\xi}_i &= \hat{\mathbf{x}} + \left(\sqrt{(n+\kappa)\mathbf{P}}\right)_i, \\
\boldsymbol{\xi}_{n+i} &= \hat{\mathbf{x}} - \left(\sqrt{(n+\kappa)\mathbf{P}}\right)_i,
\end{aligned} \tag{6.17}$$

where $i = 1, 2, \cdots, n$, κ is a constant (practitioner's choice) and $\left(\sqrt{(n+\kappa)\mathbf{P}}\right)_i$ represents i^{th} column of $\left(\sqrt{(n+\kappa)\mathbf{P}}\right)$. A preferred value of κ is $3 - n$ *i.e.* $n + \kappa = 3$. The weights are generated as [20, 100]

$$\begin{aligned} \mathbf{W}_0 &= \kappa/(n+\kappa), \\ \mathbf{W}_i &= \mathbf{W}_{n+i} = 1/(2(n+\kappa))\,. \end{aligned} \tag{6.18}$$

As in (6.17), the sigma points depend on the distribution of random variable (characterized by $\hat{\mathbf{x}}$ and $\mathbf{P}$) which is different for prediction and update steps. Therefore, the UKF generates two different set of sigma points: $\boldsymbol{\xi}_{k-1|k-1}$ in the prediction step and $\boldsymbol{\xi}_{k|k-1}$ in the update step. $\boldsymbol{\xi}_{k-1|k-1}$ is generated with $\hat{\mathbf{x}} = \hat{\mathbf{x}}_{k-1|k-1}$ and $\mathbf{P} = \mathbf{P}_{k-1|k-1}$, while $\boldsymbol{\xi}_{k|k-1}$ is generated with $\hat{\mathbf{x}} = \hat{\mathbf{x}}_{k|k-1}$ and $\mathbf{P} = \mathbf{P}_{k|k-1}$. The weights are independent of distribution of random variable, hence they are same for both the prediction and update steps. The computational aspect of prediction and update steps for the UKF is discussed herewith.

Prediction

The predicted estimate and covariance, $\hat{\mathbf{x}}_{k|k-1}$ and $\mathbf{P}_{k|k-1}$, are obtained as

$$\hat{\mathbf{x}}_{k|k-1} = \sum_{j=1}^{N_s} \mathbf{W}_j \boldsymbol{\xi}^f_{j,k-1|k-1}, \tag{6.19}$$

$$\mathbf{P}_{k|k-1} = \sum_{j=1}^{N_s} \mathbf{W}_j (\boldsymbol{\xi}^f_{j,k-1|k-1} - \hat{\mathbf{x}}_{k|k-1})(\boldsymbol{\xi}^f_{j,k-1|k-1} - \hat{\mathbf{x}}_{k|k-1})^T + \mathbf{Q}_k, \tag{6.20}$$

where

$$\boldsymbol{\xi}^f_{j,k-1|k-1} = f(\boldsymbol{\xi}_{j,k-1|k-1}). \tag{6.21}$$

Update

The computation of updated estimate and covariance, $\hat{\mathbf{x}}_{k|k}$ and $\mathbf{P}_{k|k}$, is based on statistical information on predicted measurement, which is obtained in the following steps:

Algorithm 8 Estimation of time-delay and Doppler shift using UKF

Input: $f : \mathbf{x}_k \rightarrow \mathbf{x}_{k-1}$, $h : \mathbf{x}_k \rightarrow \mathbf{r}_k$, $\mathbf{Q}_k$, and $\mathbf{R}_k$
Output: $\hat{\mathbf{x}}_{k|k}$
Initialization: $\hat{\mathbf{x}}_{0|0}$, $\mathbf{P}_{0|0}$
while $k \leq K$ **do**
    Prediction
    $\boldsymbol{\xi}^{f}_{j,k-1|k-1} = f(\boldsymbol{\xi}_{j,k-1|k-1})$
    $\hat{\mathbf{x}}_{k|k-1} = \sum_{j=1}^{N_s} W_j \boldsymbol{\xi}^{f}_{j,k-1|k-1}$
    Calculate, $\mathbf{P}_{k|k-1}$, using (6.20)
    Update
    $\boldsymbol{\xi}^{h}_{j,k|k-1} = h(\boldsymbol{\xi}_{j,k|k-1})$
    $\hat{\mathbf{r}}_{k|k-1} = \sum_{j=1}^{N_s} W_j \boldsymbol{\xi}^{h}_{j,k|k-1}$
    Calculate, $\mathbf{P}^{rr}_{k|k-1}$ and $\mathbf{P}^{xr}_{k|k-1}$, using (6.22) and (6.23), respectively.
    $\mathbf{K}_k = \mathbf{P}^{xr}_{k|k-1}(\mathbf{P}^{rr}_{k|k-1})^{-1}$
    $\hat{\mathbf{x}}_{k|k} = \hat{\mathbf{x}}_{k|k-1} + \mathbf{K}_k(\mathbf{r}_k - \hat{\mathbf{r}}_{k|k-1})$
    $\mathbf{P}_{k|k} = \mathbf{P}_{k|k-1} - \mathbf{K}_k \mathbf{P}^{rr}_{k|k-1} \mathbf{K}_k^T$
    Return $\hat{\mathbf{x}}_{k|k}$
end while

- The estimate of predicted measurement is obtained as

$$\hat{\mathbf{r}}_{k|k-1} = \sum_{j=1}^{N_s} \mathbf{W}_j \boldsymbol{\xi}^{h}_{j,k|k-1},$$

where

$$\boldsymbol{\xi}^{h}_{j,k|k-1} = h(\boldsymbol{\xi}_{j,k|k-1}).$$

- The error covariance of predicted measurement is obtained as

$$\mathbf{P}^{\mathbf{rr}}_{k|k-1} = \sum_{j=1}^{N_s} \mathbf{W}_j (\boldsymbol{\xi}^{h}_{j,k|k-1} - \hat{\mathbf{r}}_{k|k-1})(\boldsymbol{\xi}^{h}_{j,k|k-1} - \hat{\mathbf{r}}_{k|k-1})^T + \mathbf{R}_k. \tag{6.22}$$

- The cross-covariance between the predicted state and measurement is computed as

$$\mathbf{P}^{\mathbf{xr}}_{k|k-1} = \sum_{j} W_j (\boldsymbol{\xi}_{j,k|k-1} - \hat{\mathbf{x}}_{k|k-1})(\boldsymbol{\xi}^{h}_{j,k|k-1} - \hat{\mathbf{r}}_{k|k-1})^T. \tag{6.23}$$

Based on $\mathbf{P}^{\mathbf{rr}}_{k|k-1}$ and $\mathbf{P}^{\mathbf{xr}}_{k|k-1}$, the Kalman gain is obtained as

$$\mathbf{K}_k = \mathbf{P}^{\mathbf{xr}}_{k|k-1}(\mathbf{P}^{\mathbf{rr}}_{k|k-1})^{-1}. \tag{6.24}$$

The desired parameters, $\hat{\mathbf{x}}_{k|k}$ and $\mathbf{P}_{k|k}$, are obtained by correcting the predicted estimate and covariance on the receipt of new measurement $\mathbf{r}_k$. The correction is based on Kalman gain, and obtained as

$$\hat{\mathbf{x}}_{k|k} = \hat{\mathbf{x}}_{k|k-1} + \mathbf{K}_k(\mathbf{r}_k - \hat{\mathbf{r}}_{k|k-1}),$$

$$\mathbf{P}_{k|k} = \mathbf{P}_{k|k-1} - \mathbf{K}_k\mathbf{P}^{\mathbf{rr}}_{k|k-1}\mathbf{K}_k^T.$$

The estimate $\hat{\mathbf{x}}_{k|k} = [\hat{\tau}_{o_k} \quad \hat{f}_{d_k}]^T$ provides the desired estimate of delay and Doppler shift. The estimation algorithm based on UKF is summarized in Algorithm 8.

Comparison between EKF and UKF

EKF is an early development using filtering under the Bayesian framework. As discussed in Section 6.2.3, its implementation involves derivative-based computation, which causes several limitations, like smoothness requirement for system models and poor stability. Though it outperforms the KLMS Modified-NC based estimator and other estimators used in radar systems, it has certain limitations. For instance, the derivative requires a smooth system model; however, it is not guaranteed in the radar systems. Moreover, the propagation of estimate and covariance through a locally approximated system models leaves scope for further improvement. Despite all the limitations, it attracts practitioners due to fast computation and implementation simplicity, especially in applications where small shift in estimation accuracy does not affect the decisiveness [108–110].

UKF offers a derivative-free implementation, which is based on numerical approximation. Due to derivative-free implementation, it shows better stability in comparison to the EKF. Along with derivative-free implementation, it offers higher order approximation of moments. Thus, it outperforms the EKF in terms of estimation accuracy, especially in complex environments [111–113].

6.3 Simulation Results and Discussion

In this section, performance of the proposed EKF and UKF based estimation techniques are validated over LFM radar system, and a comparative analysis with the existing estimators based on KLMS Modified-NC and FT is discussed. The proposed algorithm is implemented over two mono-static LFM radar systems having different parameter values. The parameter values are shown in Table. 6.1, where Scenario I [2] and Scenario II [3] refer to the two radar systems. As shown in Table. 6.1, the Scenario I represents a practical LFM radar system whose parameter values are different from the other practical LFM radar system refereed as Scenario II. The parameter values for both Scenario I and Scenario II are taken from [2], and [3], respectively. The practicality of the two considered Scenarios are validated from the fact that for the X-band radar the center frequency is in GHz range. The initial values for $\mathbf{x}_{k|k-1}$ and $\mathbf{P}_{k|k-1}$, used in simulations for EKF and UKF are mention in Table. 6.2. In simulations, for both EKF and UKF and for Scenario I, $\mathbf{Q}_k = \begin{bmatrix} 10^{-19.8} & 0 \\ 0 & 0.001 \end{bmatrix}$, and for Scenario II, $\mathbf{Q}_k = \begin{bmatrix} 10^{-16.7} & 0 \\ 0 & 2.5 \times 10^{-6} \end{bmatrix}$.

For both Scenario I and Scenario II and for both estimators based on EKF and UKF, $\mathbf{R}_k = \sigma_v^2 \mathbf{I}$ (where σ_v^2 is obtained according to SNR). The SNR is define as the relative strength of signal with respect to noise, for this work SNR=$\frac{h(\mathbf{x}_{k+1})^T h(\mathbf{x}_{k+1})}{n\sigma_v^2}$. The estimation of time-delay and Doppler shift are obtained for SNR = 20 dB; however, the comparative analysis is provided for various SNRs ranging from −30 dB to 20 dB. In simulations, for UKF and for both Scenario I and Scenario II, $\kappa = 0.5$ and 5 sigma points are considered according to $2n + 1$ (where n is the dimension of the state vector, which is 2 in this work). The estimators based on EKF and UKF are run for 5000 iterations i.e. $K = 5000$.

6.3.1 Estimation of delay and Doppler shift

The EKF and UKF based estimators were implemented with simulated data obtained using (6.2) and (6.3) over 5000 sampling intervals. The true data of states (obtained from (6.2)) are used as reference values for comparison. The NMSE corresponding to the delay and

Table 6.1: LFM radar values of Scenario I [2] and Scenario II [3] used for simulations.

Quantity	Values for Scenario I	Values for Scenario II
Number of pulses (M)	10	20
Number of frequency intervals (L)	500	500
Frequency increment (Δf)	10 MHz	10 MHz
Pulse duration (T_o)	5 μs	200 μs
Pulse repetition interval (T_{PRI})	1 ms	0.4 ms
Center frequency (f_c)	10 GHz	9 GHz

Table 6.2: Initial value of quantities used in simulations for Algorithm 7 and Algorithm 8.

Quantity	EKF for Scenario I	EKF for Scenario II	UKF for Scenario I	UKF for Scenario II
$\hat{\mathbf{x}}_{k\|k-1}$	$[10^{-6.71} \quad 1]$	$[10^{-5.25} \quad 1]$	$[10^{-6.71} \quad 1]$	$[10^{-5.35} \quad 1]$
$\hat{\mathbf{P}}_{k\|k-1}$	$\begin{bmatrix} 10^{-14} & 0 \\ 0 & 1 \end{bmatrix}$	$\begin{bmatrix} 10^{-13.5} & 0 \\ 0 & 0.00025 \end{bmatrix}$	$\begin{bmatrix} 10^{-14} & 0 \\ 0 & 1 \end{bmatrix}$	$\begin{bmatrix} 10^{-14} & 0 \\ 0 & 0.00025 \end{bmatrix}$

Doppler shift are obtained by implementing $M_c = 100$ Monte-Carlo executions, which is given by

$$NMSE_k(i) = \frac{1}{M_c} \sum_{m_c=1}^{M_c} \frac{(\mathbf{x}_k^{m_c}(i) - \hat{\mathbf{x}}_k^{m_c}(i))^2}{(\mathbf{x}_k^{m_c}(i))^2}, \tag{6.25}$$

where i is the index corresponding to delay or Doppler shift. The NMSEs obtained from different estimators are shown in Fig. 6.1, and Fig. 6.2 for Scenario I and Scenario II, respectively. The figures show a reduced NMSE as well as a faster convergence for the proposed EKF and UKF based estimators compared to the KLMS Modified-NC. Specifically, as shown in 6.1a, the EKF and UKF based estimators attain the final NMSE at around 3000^{th} iteration, and KLMS Modified-NC converges at around 4500^{th} iteration. Additionally, the final NMSE attained by EKF and UKF is significantly lower than KLMS-Modified NC. Hence, though the estimators based on EKF, UKF, and KLMS-Modified NC take time to converge, the EKF and UKF based estimators converge fast and attain much lower final MSE as compared to estimator based on KLMS Modified-NC. The reduced NMSE concludes an improved accuracy in estimation of delay and Doppler shift with the proposed estimation techniques. The figures also conclude a relatively better accuracy for the UKF compared to the EKF. Also, as shown in Table. 6.3, the relative computational complexity of EKF and UKF are similar and lower than KLMS Modified-NC and FT as $n^3 << ML$. However, in simulations it is observed that the computational time of UKF is 1.7 times higher as compared to the EKF.

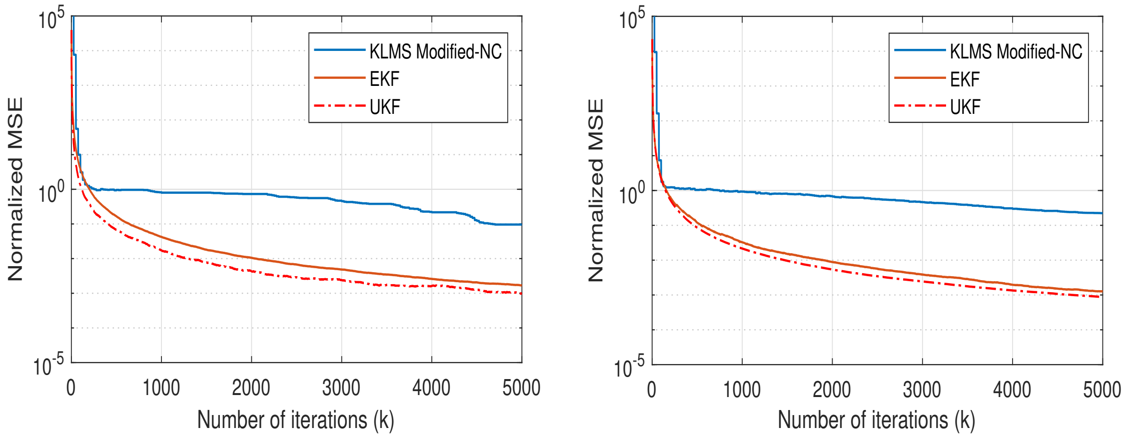

(a) (b)

Figure 6.1: NMSE plots of (a) delay and (b) Doppler shift estimation using estimators based on KLMS Modified-NC, UKF, and EKF for Scenario I.

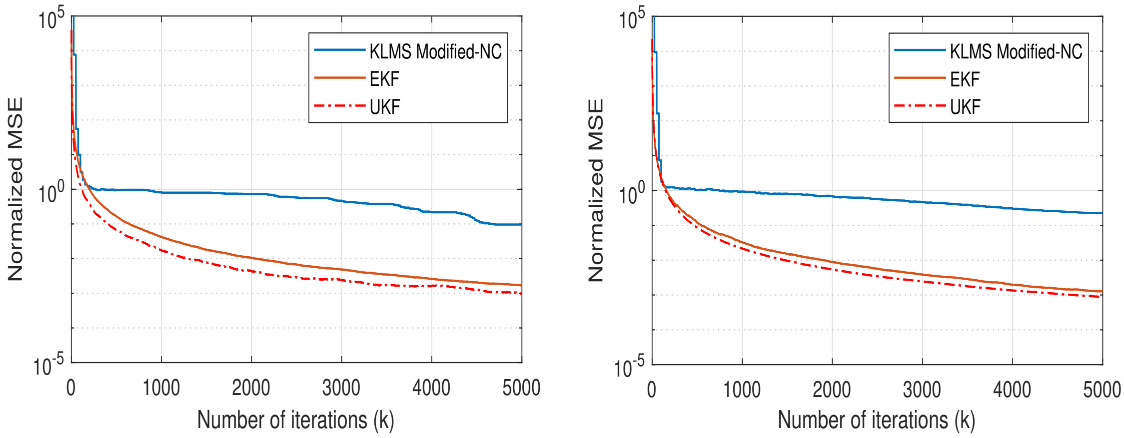

(a) (b)

Figure 6.2: NMSE plots of (a) delay and (b) Doppler shift estimation using estimators based on KLMS Modified-NC, UKF, and EKF for Scenario II.

Table 6.3: Computational complexity of estimators based on FT, KLMS Modified-NC, UKF and EKF.

Estimators	Computational complexity
FT	$O(ML\log_2 ML)$
KLMS Modified-NC	$O(ML)$
UKF	$O(n^3)$
EKF	$O(n^3)$

6.3.2 Analysis with Varying SNR

Accuracy of the proposed estimation techniques for various SNRs is evaluated in terms of error variance. The error variance at k^{th} instant is given as

$$\Omega_k^2(i) = \frac{1}{M_c}\sum_{m_c=1}^{M_c}\big(\mathbf{x}_k^{m_c}(i) - \hat{\mathbf{x}}_k^{m_c}(i)\big)^2. \tag{6.26}$$

The error variance in the estimation of delay and Doppler shift is evaluated at various SNRs ranging from −30 dB to 20 dB. The variances are compared with the achievable analytical CRLBs for each of the delay and Doppler shift. The CRLB analysis provides an efficient tool for performance analysis of the EKF and UKF based unbiased estimators [21, 22, 114], as well as for their comparison with the existing estimators used for time-delay and Doppler shift estimation. In [114], authors derived the approximate expressions for the CRLB on the variance of unbiased estimates of the parameters of a narrow-band radar model in the presence of AWGN as well as interference with known structure. The derived CRLB expression is, however, suitable for the non-Bayesian estimation approach and cannot be applied for Bayesian estimator as considered in this work. Therefore, in this work to derive the CRLB over the Bayesian estimate of τ_o and f_d, following recursive expression of Fisher information matrix ($\mathbf{J}_k$) is used

$$\mathbf{J}_k(i,j) = -\mathbb{E}\left[\frac{\partial^2\big(\ln\mathcal{P}(\mathbf{r}_k,\mathbf{x}_k)\big)}{\partial\mathbf{x}_k(i)\partial\mathbf{x}_k(j)}\right];\ \ i,j = 1,2 \tag{6.27}$$

where $\mathbf{x}_k(i)$ is the i^{th} element of $\mathbf{x}_k$, $\mathbf{J}_k(i,j)$ is the element at i^{th} row and j^{th} column of $\mathbf{J}_k$, and $\mathcal{P}(\cdot)$ is joint probability density function.

From [115], $\mathbf{J}_{k+1}$ can be computed recursively as

$$\mathbf{J}_{k+1} = \mathbf{D}_k^{22} - \mathbf{D}_k^{21}(\mathbf{J}_k + \mathbf{D}_k^{11})^{-1}\mathbf{D}_k^{12}, \tag{6.28}$$

where

$$\begin{aligned}
\mathbf{D}_k^{11} =& \mathbf{F}_k^T \mathbf{Q}_k^{-1} \mathbf{F}_k, \\
\mathbf{D}_k^{12} =& - \mathbf{F}_k^T \mathbf{Q}_k^{-1} = [\mathbf{D}_k^{21}]^T, \\
\mathbf{D}_k^{22} =& \mathbf{Q}_k^{-1} + \mathbf{H}^T \mathbf{R}_{k+1}^{-1} \mathbf{H}.
\end{aligned} \tag{6.29}$$

The analytical expression of CRLB for time-delay and Doppler shift is given by

$$CRLB(\tau_{ok}) = \mathbf{J}_{k+1}^{-1}(1,1), \tag{6.30}$$

$$CRLB(f_{dk}) = \mathbf{J}_{k+1}^{-1}(2,2). \tag{6.31}$$

The variances obtained from the EKF, UKF, KLMS Modified-NC and FT are shown in Fig. 6.3 and Fig. 6.4. As shown in the figures, the variances obtained with the EKF and UKF are closer to the achievable CRLB in comparison to the KLMS Modified-NC and FT. Moreover, the figures validate a marginally better accuracy for the UKF compared to the EKF, though the computational time is increased.

6.4 Summary

Increasing applications of target tracking in space technology, defense systems, and ocean exploration requires highly accurate radar systems. The accuracy of radar is reflected from the accuracy of target localization. The target localization is based on the delay and Doppler shift in the returning signal, which can be estimated stochastically. The recent approaches provide a comparatively accurate estimate than conventional methods. However, they are based on model parameters specific to target dynamics (which vary in practical problems). Also, they ignore the possibility of uncertainties in the modeling of

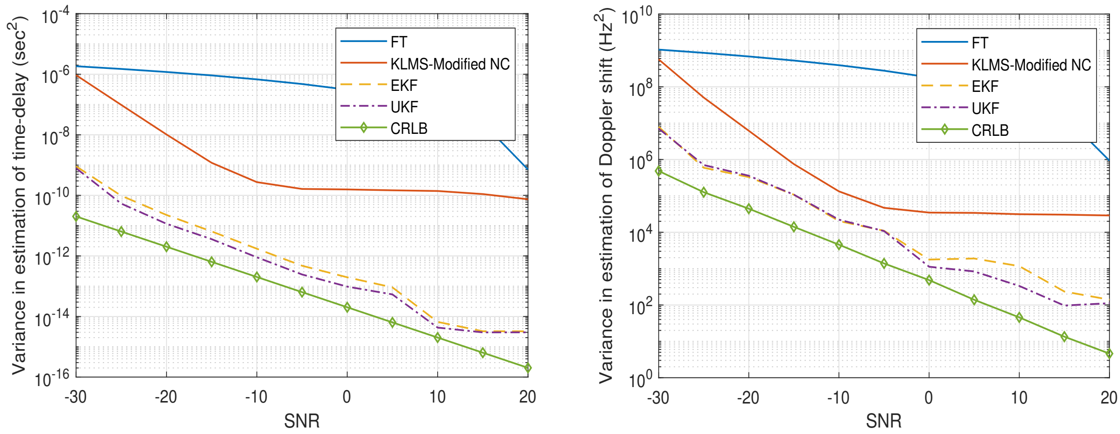

(a) (b)

Figure 6.3: Variance in the estimation of (a) delay, and (b) Doppler shift using estimation techniques based on UKF, EKF, KLMS Modified-NC, and FT for Scenario I.

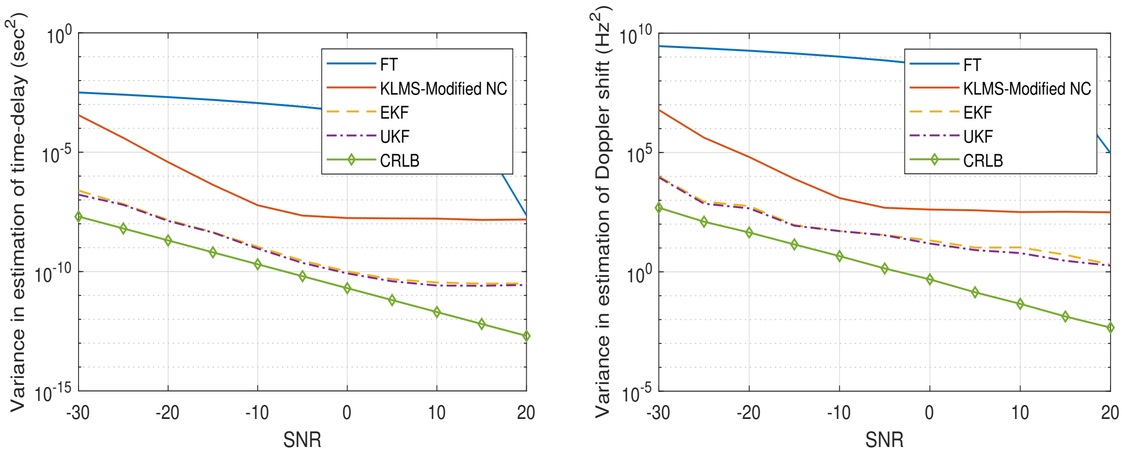

(a) (b)

Figure 6.4: Variance in the estimation of (a) delay, and (b) Doppler shift using estimation techniques based on UKF, EKF, KLMS Modified-NC, and FT for Scenario II.

radar systems. This Chapter introduces two new estimation techniques, based on EKF and UKF, for both delay and Doppler shift estimation in radar systems that outperform the existing estimators in delay and Doppler shift estimation.

Chapter 7

Conclusion, Limitations and Future Work

In this thesis, detection and estimation algorithms in the presence of Gaussian distributed thermal noise, and non-Gaussian clutter is developed and tested for OFDM, LFM, and SF radar systems. The accuracy and utility of the proposed algorithms are validated via detailed theoretical and simulation analysis. In this Chapter, the key contributions of each Chapter along with inferences drawn from the simulation and theoretical analysis are summarized. The Chapter ends discussing the limitations of the presented work and the corresponding scope of the work in the future.

7.1 Conclusion

Initially, novel techniques to measure radar return for OFDM signal from radar return for SF signal in the marine environment perturbed by sea clutter is proposed. For this, the radar channel is modeled as an FIR filter with unknown filter coefficients. Subsequently, the value of filter coefficients is estimated by optimizing the LS cost function, which is further used for measuring the radar return for the OFDM signal. Next, a signal model for modeling the OFDM radar return data is proposed. After that, a modified GLRT based detector is proposed, in which the ML estimate of the unknown scattering matrix is used. Subsequently, an analytical expression for the ROC of the proposed detection test with an assumption of Gaussian distributed clutter is derived. Simulations to estimate radar return for the OFDM signal is performed using real radar return data collected by CSIR for SF signal. The detection test performed using estimated data reveals the advantages of using OFDM radar over conventional SF radar. For estimated OFDM radar return data, a significant gain in detection performance is reported in the simulations of proposed detector ROC. The performance of OFDM radar is further improved by increasing the number of transmitted orthogonal sub-carriers. The detector performance obtained for the estimated OFDM radar return is verified by the detector performance of simulated OFDM radar return data. Finally, an agreement between the theoretical and simulated ROC of the detector under the assumption of Gaussian distributed clutter confirms the advantages of OFDM radar over conventional radar for surveillance in the marine environment.

Next, the problem of estimating a target's delay and Doppler shift is dealt with a perspective of approximating the unknown inverse function. For this, firstly, a popular RKHS based function approximation technique using the KLMS algorithm is developed. Subsequently, the linear increase in computational complexity of the KLMS based estimator is controlled by utilizing the NC based sparsification technique. The resulting KLMS-NC based estimator instead of utilizing every radar observations selectively selects the radar observations for estimation. The estimation accuracy of the proposed estimators is further increased by adaptively learning a suitable kernel width of the kernel function, and the resulting estimator is termed as KLMS-Modified NC. Performance of the proposed estimators: KLMS, KLMS-NC, and KLMS-Modified NC, is tested for LFM and OFDM radar systems. The proposed estimators are found to achieve minimum MSE in the estimation of both delay and Doppler shift with reasonable computational complexity. Moreover, due to the optimization of the convex cost function in RKHS, and contrary to the conventional estimator based on FT, the variance of the proposed estimators are found closer to the achievable CRLB.

Further, estimators based on another class of KAFs utilizing MCC is explored for estimating delay and Doppler shift in the radar environment perturbed by non-Gaussian clutter. The proposed KMC based estimator, contrary to estimators based on KLMS, considers the higher-order statistics of error in optimization. Consequently, optimization of higher-order statistics of error makes the estimator based on KMC capable of dealing with the deleterious effects of clutter. However, similar to estimators based on KLMS, KMC based estimator suffers from a linear increase in the radar observations, thereby resulting in higher computational complexity. Therefore, KMC-NC based sparsified estimator, which utilizes the NC sparsification technique, is developed. Furthermore, to choose an appropriate kernel width, a technique is developed for tuning the kernel width from radar returns, and an adaptive update equation is derived to choose an appropriate value of kernel width. Subsequently, analytical proofs regarding CRLB and estimators dictionary upper bounds are provided, which reinforces viability of KMC based estimators as an efficient estimator for practical clutter-impaired radar systems. Simulations performed over realistic LFM and SF radar systems reveal superiority of the proposed KMC based estimators over existing estimators based on KLMS. Lastly, variance of the proposed estimators is found to be nearer to the CRLB as compared to the KLMS based estimators.

Furthermore, in MIMO radar, for the estimation of DOD, DOA, and Doppler shift of multiple targets in the presence of non-Gaussian clutter, the adaptive estimator based on KMEE is introduced. Estimator based on KMEE optimizes the MEE criterion in RKHS , and yields accurate estimates of parameters by compensating the effect of non-Gaussian clutter. Nevertheless, practical viability of the proposed KMEE based estimator is hindered by its high dictionary size. Therefore, continuously increasing dictionary size is reduced by the incorporation of the sparsification technique based on NC. Simulations performed over MIMOradar reveals capability of compensating the effects of non-Gaussian clutter in comparison to other kernel-based adaptive estimators. Lastly, based on the comparative performance of the proposed estimator and existing estimator with the derived MCRLB, it can be concluded that the KMEE based estimator is preferred for the MIMO radar system.

Finally, two novel estimation techniques, based on EKF and UKF, for both delay and Doppler shift estimation in radar systems in the presence of Gaussian distributed thermal noise are proposed. The KLMS-Modified NC based estimator provides a comparatively accurate estimate than the conventional estimator based on FT. However, to work, estimator based on KLMS-Modified NC requires appropriate values of various hyper-parameter. On the contrary, the proposed estimators based on EKF and UKF are free from such problem of choosing an appropriate values of various hyper-parameter. The better performance of the proposed estimators in comparison to estimator based on KLMS-Modified NC is guaranteed by the proximity of the variance of the proposed estimator to CRLB. Further, the UKF based estimator marginally outperforms the EKF, however, with an increase in computational complexity.

7.2 Limitations and Future work

- In Chapter 2, batch processing estimation technique based on LS is used, which for large data becomes computationally complex. Also, currently, the detection algorithm is developed for known values of a Doppler shift; however, in practice, a Doppler shift is unknown. Moreover, the effect of a target velocity on the orthogonality of OFDM sub-carriers has not been considered in the current work.

  In the future, instead of using an estimation technique based on batch processing, some online estimation techniques can be explored. Furthermore, there is a possibility of developing a detection algorithm for unknown Doppler shift. Also, in the future, the effect of target velocity on the orthogonality of OFDM sub-carriers can be explored.

- In Chapter 3, Chapter 4, and Chapter 5, the estimation of target's range and velocity is done individually. The joint estimation of parameters, however, is required, especially in multiple target scenarios.

  The developed estimators based on KAF can be explored for joint estimation of the target's range and velocity, especially in the multiple target scenario where the exact paring of estimated parameters is challenging.

- The KAF based estimators, proposed in Chapter 3, Chapter 4, and Chapter 5 suffers with an unbounded temporal increase in computational/storage complexity. The temporal increase in computational/storage complexity is mitigated by NC based sparsification technique. However, the NC based sparsified estimator at every time instant utilizes a linear search throughout the existing dictionary, which causes significant computational overhead.

In future, the unknown radar parameters may be estimated through an explicit random Fourier feature based mapping, as opposed to existing implicit dictionary-based RKHS formulations.

- In Chapter 6, the estimator based on EKF and UKF is applied over the radar system perturbed by Gaussian distributed thermal noise. However, as described in Chapter 4, and Chapter 5, the practical radar environment is perturbed by non-Gaussian distributed clutter.

  In the future, variants of Kalman filter based estimator capable of dealing with the effect of non-Gaussian clutter can be explored.

Appendix A

Derivation of bound on kernel width (σ) learning parameter (ρ)

The kernel width update equation for KLMS-Modified NC is given by

$$\sigma_k = \sigma_{k-1} + \rho e(k-1)e(k) \| \mathbf{r}(k-1) - \mathbf{r}(k) \|^2 \frac{\kappa_{\sigma_{k-1}}(\mathbf{r}(k-1), \mathbf{r}(k))}{\sigma_{k-1}^3} \tag{A.1}$$

If $\tilde{\sigma}_{k-1} = \sigma_{k-1} - \sigma^*$, and $\tilde{\sigma}_k = \sigma_k - \sigma^*$, where σ^* is the optimum kernel width, then subtracting σ^* from (A.1) yields.

$$\tilde{\sigma}_k = \tilde{\sigma}_{k-1} - \rho e(k-1)e(k) \| \mathbf{r}(k-1) - \mathbf{r}(k) \|^2 g(\sigma_{k-1}) \tag{A.2}$$

where $g(\sigma_{k-1}) = \frac{\kappa_{\sigma_{k-1}}(\mathbf{r}(k-1), \mathbf{r}(k))}{\sigma_{k-1}^3}$

Squaring both the sides of (A.2) yields

$$\begin{aligned} \tilde{\sigma}_k^2 = \tilde{\sigma}_{k-1}^2 &- 2\tilde{\sigma}_{k-1}\rho e(k-1)e(k) \| \mathbf{r}(k-1) - \mathbf{r}(k) \|^2 g(\sigma_{k-1}) \\ &+ \rho^2 e^2(k-1)e^2(k) \| \mathbf{r}(k-1) - \mathbf{r}(k) \|^2 \times g^2(\sigma_{k-1}) \end{aligned} \tag{A.3}$$

From (A.3), the following relation holds

$$\mathbb{E}[\rho^2 e^2(k-1)e^2(k)\| \mathbf{r}(k-1) - \mathbf{r}(k) \|^2 \times g^2(\sigma_{k-1})] \leq \tag{A.4}$$
$$\mathbb{E}[2\tilde{\sigma}_{k-1}\rho e(k-1)e(k)\| \mathbf{r}(k-1) - \mathbf{r}(k) \|^2 \times g(\sigma_{k-1})]$$

Further, from (A.4)

$$\rho \leq \frac{2\mathbb{E}[\tilde{\sigma}_{k-1}g(\sigma_{k-1})]}{\mathbb{E}[g^2(\sigma_{k-1})]} \tag{A.5}$$

From the above equation, it can be observed that calculation of the upper bound involves finding expression for $\mathbb{E}[\tilde{\sigma}_{k-1}g(\sigma_{k-1})]$ (denoted as $\mathscr{I}_1$), and $\mathbb{E}[g^2(\sigma_{k-1})]$ (denoted as $\mathscr{I}_2$). Therefore, in order to evaluate the upper bound on step-size, we derive analytical expressions for $\mathscr{I}_1$, and $\mathscr{I}_2$ in the forthcoming subsections.

Calculation of $\mathscr{I}_1$:

In this section, we first calculate the value of $\mathscr{I}_1$.

$$\mathbb{E}[\tilde{\sigma}_{k-1}g(\sigma_{k-1})] = \mathbb{E}[\tilde{\sigma}_{k-1}g(\sigma^* + \tilde{\sigma}_{k-1})] \tag{A.6}$$

Under the assumption of Gaussian distribution for $\tilde{\sigma}_{k-1}$, (A.6) can be evaluated as

$$\int_{-\infty}^{\infty} \frac{\tilde{\sigma}_{k-1}}{(\sigma^* + \tilde{\sigma}_{k-1})^3} \exp\left(\frac{-\| \mathbf{r}(k-1) - \mathbf{r}(k) \|^2}{2(\sigma^* + \tilde{\sigma}_{k-1})^2}\right) \exp\left(\frac{-\tilde{\sigma}_{k-1}^2}{2\beta^2}\right) d\tilde{\sigma}_{k-1}$$

where, β^2 is the variance of $\tilde{\sigma}_{k-1}$. Next we rewrite the above integral equivalently as follows

$$\int_{-\infty}^{\infty}\int_{-\infty}^{\infty} \frac{\tilde{\sigma}_{k-1}}{(\sigma^* + \tilde{\sigma}_{k-1})^3} \hat{\mathcal{P}}(\mathbf{r}|\mathbf{r}_k)\hat{\mathcal{P}}(\mathbf{r}|\mathbf{r}_{k-1}) \exp\left(\frac{-\tilde{\sigma}_{k-1}^2}{2\beta^2}\right) d\tilde{\sigma}_{k-1} d\mathbf{r}_k$$

We note that $\mathcal{P}(\mathbf{r}|\mathbf{r}_{k-1}) = \mathcal{P}(\mathbf{r}|\mathbf{r}_k)$, and the fact that the Renyi's-α information potential with $\alpha = 2$ can be expressed as

$$-H_2(\mathbf{r}|\mathbf{r}_k) = \log_2(\int_{-\infty}^{\infty} \mathcal{P}^2(\mathbf{r}|\mathbf{r}_k) d\mathbf{r}_k$$

Next, we define a constant $R_\phi = 2^{-H_2}$, and re-express the integral as follows:

$$= R_\phi \int_{-\infty}^{\infty} \int_{-\infty}^{\infty} \frac{\tilde{\sigma}_{k-1}}{(\sigma^* + \tilde{\sigma}_{k-1})^3} \exp\left(\frac{-\tilde{\sigma}_{k-1}^2}{2\beta^2}\right) d\tilde{\sigma}_{k-1} \tag{A.7}$$

In (A.7), $\exp\left(\frac{-\|\mathbf{r}(k-1)-\mathbf{r}(k)\|^2}{2(\sigma^*+\tilde{\sigma}_{k-1})^2}\right) = R_\phi$ denotes Renyi's information potential. Hence, (A.7) can be expressed as

$$= R_\phi \int_{-\infty}^{\infty} \frac{\tilde{\sigma}_{k-1}}{(\sigma^* + \tilde{\sigma}_{k-1})^3} \exp\left(\frac{-\tilde{\sigma}_{k-1}^2}{2\beta^2}\right) d\tilde{\sigma}_{k-1} \tag{A.8}$$

Replacing $\tilde{\sigma}_{k-1} = \sigma^* \tan^2(\theta)$, $\sin^2(\theta) = \psi$, and solving yields

$$= \frac{R_\phi}{\sigma^*} \int_0^1 \psi \exp\left(-\frac{\sigma^{*2}}{2\beta^2} \frac{\psi^2}{(1-\psi)^2}\right) d\psi \tag{A.9}$$

Further, (A.9) can be simplified as

$$= \frac{R_\phi}{\sigma^*} \sum_{j=0}^{\infty} \frac{(-1)^j}{j!} \frac{\sigma^{*2j}}{2\beta^{2j}} \int_0^1 \frac{\psi^{2j+1}}{(1-\psi)^{2j}} d\psi \tag{A.10}$$

(A.10) is solved by series expansion and invoking properties of Mellin transform [**?** , eq. (6.2.6)]

$$f\left(\frac{\sigma^{*2}}{2\beta^2}\right) = \frac{R_\phi}{\sigma^*} \sum_{j=0}^{\infty} \frac{(-1)^j}{j!} \frac{\sigma^{*2j}}{2\beta^{2j}} j(2j+1)\pi \csc(2\pi j) \tag{A.11}$$

By Ramanujan's master theorem, we can write the Mellin transform of $f(\cdot)$ as

$$M(s) = \Gamma(s)(-s)(1-2s)\pi \csc(-2s\pi) \frac{R_\phi}{\sigma^*} \tag{A.12}$$

By Mellin transform inversion

$$f\left(\frac{\sigma^{*2}}{2\beta^2}\right) = \frac{G^{3,2}_{2,3}\left(\begin{smallmatrix}0,\frac{1}{2}\\0,\frac{1}{2},1\end{smallmatrix}\middle|\frac{\sigma^{*2}}{2\beta^2}\right) - 2G^{3,2}_{2,3}\left(\begin{smallmatrix}0,\frac{1}{2}\\\frac{1}{2},1,1\end{smallmatrix}\middle|\frac{\sigma^{*2}}{2\beta^2}\right)}{2\pi}\frac{R_\phi}{\sigma^*}$$

where $G^{m,n}_{p,q}\left(\begin{smallmatrix}a_1,\ldots,a_p\\b_1,\ldots,b_q\end{smallmatrix}\middle|z\right)$ denotes the Meijer's G function.

Calculation of $\mathscr{I}_2$:

In this section an expression for $\mathscr{I}_2$ is derived for $\mathbb{E}[g^2(\sigma_{k-1})]$ as follows

$$\mathbb{E}[g^2(\sigma_{k-1})] = \mathbb{E}[g^2(\sigma^* + \tilde{\sigma}_{k-1})] \tag{A.13}$$

Under the assumption of Gaussian distribution for $\tilde{\sigma}_{k-1}$, (A.13) can be evaluated as

$$= R_\phi \int_{-\infty}^{\infty} \frac{1}{(\sigma^* + \tilde{\sigma}_{k-1})^6} \exp\left(\frac{-\tilde{\sigma}_{k-1}^2}{2\beta^2}\right) d\tilde{\sigma}_{k-1} \tag{A.14}$$

Replacing $\tilde{\sigma}_{k-1} = \sigma^* \tan^2(\theta)$, $\sin^2(\theta) = p$, and assuming a Gaussian pdf, (A.14) yields

$$= \frac{R_\phi}{\sigma^{*6}} \int_0^1 (1-p)^4 \sum_{j=0}^{\infty} \frac{(-\frac{\sigma^{*2}}{2\beta^2})^j}{j!} \left(\frac{p}{1-p}\right)^{2j} dp \tag{A.15}$$

or

$$g\left(\frac{\sigma^{*2}}{2\beta^2}\right) = \frac{R_\phi}{2\sigma^{*6}} \sum_{j=0}^{\infty} \frac{1}{j!} \left(\frac{-\sigma^{*2}}{2\beta^2}\right)^j \frac{\Gamma(5-2j)\Gamma(1+2j)}{120} \tag{A.16}$$

By Ramanujan's master theorem, the Mellin transform can be written as

$$M(s) = \Gamma(s)\Gamma(5+2s)\Gamma(1-2s)$$

Inverting the Mellin transform gives us the following expression for $g\left(\frac{\sigma^{*2}}{2\beta^2}\right)$

$$g\left(\frac{\sigma^{*2}}{2\beta^2}\right) = \frac{\frac{R_\phi}{7.5\pi} G^{3,2}_{2,3}\left(\begin{smallmatrix}0,\frac{1}{2}\\0,\frac{5}{2},3\end{smallmatrix}\middle|\frac{\sigma^{*2}}{2\beta^2}\right)}{\sigma^{*6}}$$

Also, we note that

$$\tilde{y}_k \approx (1-\mu)\tilde{y}_{k-1}$$
$$\implies \mathbb{E}[e_k e_{k-1}] = \mathbb{E}[\tilde{y}_k \tilde{y}_{k-1}] = (1-\mu)\mathbb{E}[|\tilde{y}_{k-1}|^2]$$

Further, by Jensen's inequality,

$$\mathbb{E}[e_k^2 e_{k-1}^2] = \mathbb{E}[(e_k e_{k-1})^2] \geq \{\mathbb{E}[e_k e_{k-1}]\}^2 = (1-\mu)^2\mathbb{E}[|\tilde{y}_{k-1}|^2]^2$$

This gives the following (tighest) bound for ρ at ${\sigma_n}^2 << \mathbb{E}[|\tilde{y}_k|^2]$:

$$0 < \rho < \frac{3.75\sigma^{*4}\left[G_{2,3}^{3,2}\left(\begin{smallmatrix}0,\frac{1}{2}\\0,\frac{1}{2},1\end{smallmatrix}\middle|\frac{\sigma^{*2}}{2\beta^2}\right) - 2G_{2,3}^{3,2}\left(\begin{smallmatrix}0,\frac{1}{2}\\\frac{1}{2},1,1\end{smallmatrix}\middle|\frac{\sigma^{*2}}{2\beta^2}\right)\right]}{G_{2,3}^{3,2}\left(\begin{smallmatrix}0,\frac{1}{2}\\0,\frac{5}{2},3\end{smallmatrix}\middle|\frac{\sigma^{*2}}{2\beta^2}\right)[3(1-\mu)+\mu^2{\sigma_n}^2]} \tag{A.17}$$

References

[1] M. A. Richards, *Fundamentals of Radar Signal Processing*. Tata McGraw-Hill Education, 2005.

[2] T. J. Abatzoglou and G. O. Gheen, "Range, radial velocity, and acceleration MLE using radar LFM pulse train," *IEEE Trans. Aerosp. and Electron. Sys.*, vol. 34, no. 4, pp. 1070–1083, 1998.

[3] Y. X. Zhang, R. J. Hong, P.-P. Pan, Z. M. Deng, and Q. F. Liu, "Frequency domain range sidelobe correction in stretch processing for wideband LFM radars," *IEEE Trans. Aerosp. Electron. Syst.*, vol. 53, no. 1, pp. 111–121, 2017.

[4] M. A. Richards, J. Scheer, W. A. Holm, and W. L. Melvin, *Principles of Modern Radar*. Citeseer, 2010.

[5] S. Sen and A. Nehorai, "Target detection in clutter using adaptive OFDM radar," *IEEE Trans. Signal Process.*, vol. 16, no. 7, pp. 592–595, 2009.

[6] N. Prasad, V. Shameem, U. Desai, and S. Merchant, "Improvement in target detection performance of pulse coded Doppler radar based on multicarrier modulation with fast Fourier transform," *IET Radar, Sonar Navig.*, vol. 151, no. 1, pp. 11–17, 2004.

[7] S. H. Dokhanchi, M. R. B. Shankar, T. Stifter, and B. Ottersten, "OFDM-based automotive joint radar-communication system," in *IEEE Radar Conf.*, April 2018, pp. 0902–0907.

[8] M. Braun, C. Sturm, and F. K. Jondral, "Maximum likelihood speed and distance estimation for OFDM radar," in *IEEE Radar Conf.*, 2010, pp. 256–261.

[9] A. Turlapaty, Y. Jin, and Y. Xu, "Range and velocity estimation of radar targets by weighted ofdm modulation," in *2014 IEEE Radar Conference*. IEEE, 2014, pp. 1358–1362.

[10] C. Shi, F. Wang, M. Sellathurai, J. Zhou, and S. Salous, "Power minimization-based robust OFDM radar waveform design for radar and communication systems in coexistence," *IEEE Trans. Signal Process.*, vol. 66, no. 5, pp. 1316–1330, 2017.

[11] D. Garmatyuk, P. Giza, N. Condict, and S. Mudaliar, "Randomized OFDM waveforms for simultaneous radar operation and asynchronous covert communications," in *IEEE Radar Conf.*, April 2018, pp. 0975–0980.

[12] L. Xu, J. Li, and P. Stoica, "Target detection and parameter estimation for MIMO radar systems," *IEEE Trans. Aerosp. Electron. Syst.*, vol. 44, no. 3, pp. 927–939, 2008.

[13] R. F. Tigrek, W. J. De Heij, and P. Van Genderen, "Ofdm signals as the radar waveform to solve Doppler ambiguity," *IEEE Trans. Aerosp. Electron. Syst.*, vol. 48, no. 1, pp. 130–143, 2012.

[14] D. Rife and R. Boorstyn, "Single tone parameter estimation from discrete-time observations," *IEEE Transactions on information theory*, vol. 20, no. 5, pp. 591–598, 1974.

[15] W. Liu, P. P. Pokharel, and J. C. Principe, "The kernel least-mean-square algorithm," *IEEE Trans. Signal Process.*, vol. 56, no. 2, pp. 543–554, Jan. 2008.

[16] W. Liu, J. C. Principe, and S. Haykin, *Kernel adaptive filtering: a comprehensive introduction*. John Wiley & Sons, 2011, vol. 57.

[17] R. Mitra and V. Bhatia, "Finite dictionary variants of the diffusion KLMS algorithm," *arXiv:1509.02730*, 2015.

[18] ——, "Finite dictionary techniques for MSER equalization in RKHS," *Signal, Image and Video Processing*, vol. 11, no. 5, pp. 849–856, 2017.

[19] G. Y. Kulikov and M. V. Kulikova, "The accurate continuous-discrete extended Kalman filter for radar tracking," *IEEE Trans. Signal Process*, vol. 64, no. 4, pp. 948–958, 2015.

[20] S. J. Julier and J. K. Uhlmann, "New extension of the Kalman filter to nonlinear systems," in *Signal processing, sensor fusion, and target recognition VI*, vol. 3068. Int. Soc. Optics Photon., 1997, pp. 182–194.

[21] E. Cortina, D. Otero, and C. E. D'Attellis, "Maneuvering target tracking using extended Kalman filter," *IEEE Trans. Aerosp. Electron. Syst.*, vol. 27, no. 1, pp. 155–158, 1991.

[22] A. Farina, B. Ristic, and D. Benvenuti, "Tracking a ballistic target: comparison of several nonlinear filters," *IEEE Trans. Aerosp. Electron. Syst.*, vol. 38, no. 3, pp. 854–867, 2002.

[23] T. Jian, Y. He, F. Su, C. Qu, and D. Ping, "Cascaded detector for range-spread target in non-Gaussian clutter," *IEEE Trans. Aerosp. and Electron. Sys.*, vol. 48, no. 2, pp. 1713–1725, 2012.

[24] G. Trunk and S. George, "Detection of targets in non-Gaussian sea clutter," *IEEE Trans. Aerosp. and Electron. Sys.*, no. 5, pp. 620–628, 1970.

[25] F. Gini and M. Greco, "Suboptimum approach to adaptive coherent radar detection in compound-Gaussian clutter," *IEEE Trans. Aerosp. Electron. Syst.*, vol. 35, no. 3, pp. 1095–1104, 1999.

[26] M. Andric, D. Bujakovic, B. Bondzulic, S. Simic, and B. Zrnic, "Analysis of radar Doppler signature from human data," *Radioengineering*, vol. 23, no. 1, pp. 11–19, 2014.

[27] Z. Raida, Z. Kolka, R. Marsalek, J. Petrzela, A. Prokes, J. Sebesta, T. Gotthans, Z. Hrubos, Z. Kincl, L. Klozar *et al.*, "Communication subsystems for emerging wireless technologies," *Radioengineering*, vol. 21, no. 4, pp. 1036–1049, 2012.

[28] S. K. Chronopoulos, C. Votis, V. Raptis, G. Tatsis, and P. Kostarakis, "In depth analysis of noise effects in orthogonal frequency division multiplexing systems, utilising a large number of subcarriers," in *AIP Conf. Proceedings*, vol. 1203, no. 1, 2010, pp. 967–972.

[29] C. Koliopanos, S. Chronopoulos, A. M. Tzechilidou, and C. T. Angelis, "Simulation, modeling, and performance analysis of IEEE802.16e OFDMA systems for urban and rural environments," in *2nd International Conf. Signals Circuits Syst.*, 2008, pp. 1–4.

[30] S. K. Chronopoulos, V. Christofilakis, G. Tatsis, and P. Kostarakis, "Preliminary BER study of a TC-OFDM system operating under noisy conditions," *Journal of Eng. Sci. Techno. Rev.*, vol. 9, no. 4, pp. 13–16, 2016.

[31] G. Lellouch, A. Mishra, and M. Inggs, "Impact of the Doppler modulation on the range and Doppler processing in OFDM radar," in *IEEE Radar Conf.*, 2014, pp. 0803–0808.

[32] P. Herselman, C. Baker, and H. De Wind, "An analysis of X-band calibrated sea clutter and small boat reflectivity at medium-to-low grazing angles," *Int. J. Navig. Observ.*, vol. 2008, 2008.

[33] C. R. Ilvedson, "Transfer function estimation using time-frequency analysis," Ph.D. dissertation, Massachusetts Institute of Technology, 1998.

[34] N. Petrov, F. Le Chevalier, and A. G. Yarovoy, "Detection of range migrating targets in compound-Gaussian clutter," *IEEE Trans. Aerosp. Electron. Syst.*, vol. 54, no. 1, pp. 37–50, 2018.

[35] S. M. Kay, *Fundamentals of Statistical Signal Processing: Estimation Theory*. Prentice Hall PTR, 1993.

[36] G. Lellouch, A. K. Mishra, and M. Inggs, "Orthogonal frequency division multiplexing phenomenology: radar technique combining genetic algorithm-based pulse design and energy detector for target recognition," *IET Radar, Sonar Navig.*, vol. 10, no. 5, pp. 912–922, 2016.

[37] F. Gini, "Sub-optimum coherent radar detection in a mixture of K-distributed and Gaussian clutter," *IET Radar, Sonar Navig.*, vol. 144, no. 1, pp. 39–48, 1997.

[38] F. Gini and M. Greco, "Covariance matrix estimation for CFAR detection in correlated heavy tailed clutter," *Signal Process.*, vol. 82, no. 12, pp. 1847–1859, 2002.

[39] M. Abramowitz and I. A. Stegun, *Handbook of Mathematical Functions: With Formulas, Graphs, and Mathematical Tables*. Courier Corporation, 1964, vol. 55.

[40] P. Herselman and H. De Wind, "Improved covariance matrix estimation in spectrally inhomogeneous sea clutter with application to adaptive small boat detection." *IEEE Int. Conf. Radar*, 2008.

[41] R. Mitra and V. Bhatia, "Low complexity post-distorter for visible light communications," *IEEE Commun. Letters*, vol. 21, no. 9, pp. 1977–1980, 2017.

[42] B. Chen, S. Zhao, P. Zhu, and J. C. Príncipe, "Quantized kernel least mean square algorithm," *IEEE Trans. Neural Net. Learn. Syst.*, vol. 23, no. 1, pp. 22–32, Dec. 2012.

[43] J. Platt, "A resource-allocating network for function interpolation," *MIT Press Neural comput.*, vol. 3, no. 2, pp. 213–225, 1991.

[44] B. W. Silverman, *Density estimation for statistics and data analysis*. CRC press, Apr. 1986, vol. 26.

[45] B. Chen, J. Liang, N. Zheng, and J. C. Principe, "Kernel least mean square with adaptive kernel size," *Elsevier Neuro comput.*, vol. 191, pp. 95–106, May. 2016.

[46] N. Levanon, "Multifrequency complementary phase-coded radar signal," *IEE Proc. Radar, Sonar and Navig.*, vol. 147, no. 6, pp. 276–284, Dec. 2000.

[47] C. Sturm, E. Pancera, T. Zwick, and W. Wiesbeck, "A novel approach to OFDM radar processing," in *IEEE Radar Conf.*, May. 2009, pp. 1–4.

[48] C. Sturm, T. Zwick, and W. Wiesbeck, "An OFDM system concept for joint radar and communications operations," in *Vehicular Technology Conf.*, 2009, pp. 1–5.

[49] C. Sturm, T. Zwick, W. Wiesbeck, and M. Braun, "Performance verification of symbol-based OFDM radar processing," in *IEEE Radar Conf.*, 2010, pp. 60–63.

[50] G. Lellouch, A. K. Mishra, and M. Inggs, "Design of OFDM radar pulses using genetic algorithm based techniques," *IEEE Trans. Aerosp. and Electron. Sys.*, vol. 52, no. 4, pp. 1953–1966, 2016.

[51] ——, "Stepped OFDM radar technique to resolve range and Doppler simultaneously," *IEEE Trans. Aerosp. and Electron. Sys.*, vol. 51, no. 2, pp. 937–950, Apr. 2015.

[52] G. Lellouch and A. K. Mishra, "Optimization of OFDM radar waveforms using genetic algorithms," *arXiv:1405.4894*, 2014.

[53] G. Lellouch, A. Mishra, and M. Inggs, "Convex optimization for optimal PMEPR and mismatched filter design in OFDM radar," in *Radar Conference, 2015 IEEE*. IEEE, 2015, pp. 37–41.

[54] G. Lellouch and A. K. Mishra, "Multi-carrier based radar signal optimization using genetic algorithm," in *Springer International Conf. Soft Comput. Problem Solving*, Mar. 2014, pp. 525–534.

[55] P. Bouboulis and S. Theodoridis, "Extension of Wirtinger's calculus to reproducing kernel Hilbert spaces and the complex kernel LMS," *IEEE Trans. Signal Process.*, vol. 59, no. 3, pp. 964–978, Dec. 2011.

[56] R. Mitra and V. Bhatia, "The Diffusion-KLMS algorithm," in *Information Technology (ICIT), 2014 International Conference on*. IEEE, 2014, pp. 256–259.

[57] V. Bhatia, B. Mulgrew, and D. D. Falconer, “Non-parametric maximum-likelihood channel estimator and detector for OFDM in presence of interference,” *IET Commun.*, vol. 1, no. 4, pp. 647–654, Aug. 2007.

[58] S. Theodoridis, *Machine learning: a Bayesian and optimization perspective*. Academic Press, Apr. 2015.

[59] G. Strang, *Introduction to linear algebra*. Wellesley-Cambridge Press Wellesley, MA, 1993, vol. 3.

[60] R. Mitra and V. Bhatia, “Adaptive sparse dictionary-based kernel minimum symbol error rate post-distortion for nonlinear LEDs in visible light communications,” *IEEE Photon. J.*, vol. 8, no. 4, pp. 1–13, Jun. 2016.

[61] S. Zhao, B. Chen, and J. C. Principe, “Kernel adaptive filtering with maximum correntropy criterion,” in *International Joint Conference on Neural Networks (IJCNN)*, 2011, pp. 2012–2017.

[62] Y. He, F. Wang, J. Yang, H. Rong, and B. Chen, “Kernel adaptive filtering under generalized maximum correntropy criterion,” in *International Joint Conference on Neural Networks (IJCNN)*, 2016, pp. 1738–1745.

[63] A. Singh and J. C. Principe, “Using correntropy as a cost function in linear adaptive filters,” in *International Joint Conference on Neural Networks (IJCNN)*, 2009, pp. 2950–2955.

[64] M. Rangaswamy, D. Weiner, and A. Ozturk, “Computer generation of correlated non-Gaussian radar clutter,” *IEEE Trans. Aerosp. and Electron. Sys.*, vol. 31, no. 1, pp. 106–116, 1995.

[65] P. l. Shui, M. Liu, and S. w. Xu, “Shape-parameter-dependent coherent radar target detection in K-distributed clutter,” *IEEE Trans. Aerosp. and Electron. Sys.*, vol. 52, no. 1, pp. 451–465, 2016.

[66] M. Sahed, A. Mezache, and T. Laroussi, "A novel [z log (z)]-based closed form approach to parameter estimation of K-distributed clutter plus noise for radar detection," *IEEE Trans. Aerosp. and Electron. Sys.*, vol. 51, no. 1, pp. 492–505, 2015.

[67] L. Shi and Y. Lin, "Convex combination of adaptive filters under the maximum correntropy criterion in impulsive interference," *IEEE Signal Process. Lett.*, vol. 21, no. 11, pp. 1385–1388, 2014.

[68] R. He, W.-S. Zheng, and B.-G. Hu, "Maximum correntropy criterion for robust face recognition," *IEEE Transactions on Pattern Analysis and Machine Intelligence*, vol. 33, no. 8, pp. 1561–1576, 2011.

[69] B. Chen, Y. Zhu, J. Hu, and J. C. Principe, *System parameter identification: information criteria and algorithms*. Newnes, 2013.

[70] B. Hou, Z. He, X. Zhou, H. Zhou, D. Li, and J. Wang, "Maximum correntropy criterion Kalman filter for α-jerk tracking model with non-Gaussian noise," *Entropy*, vol. 19, no. 12, p. 648, 2017.

[71] F. Jin and T. Qiu, "Adaptive time delay estimation based on the maximum correntropy criterion," *Digital Signal Processing*, vol. 88, pp. 23–32, 2019.

[72] B. Chen, S. Zhao, S. Seth, and J. C. Principe, "Online efficient learning with quantized KLMS and L1 regularization," in *International Joint Conference on Neural Networks (IJCNN)*, 2012, pp. 1–6.

[73] S. Sen and A. Nehorai, "Adaptive OFDM radar for target detection in multipath scenarios," *IEEE Trans. Signal Process.*, vol. 59, no. 1, pp. 78–90, Feb. 2011.

[74] ——, "Adaptive design of OFDM radar signal with improved wideband ambiguity function," *IEEE Trans. Signal Process.*, vol. 58, no. 2, pp. 928–933, Feb. 2010.

[75] S. Sen, "Adaptive OFDM radar waveform design for improved micro-Doppler estimation," *IEEE Sensors J.*, vol. 14, no. 10, pp. 3548–3556, 2014.

[76] A. Jung, S. Schmutzhard, and F. Hlawatsch, "The RKHS approach to minimum variance estimation revisited: Variance bounds, sufficient statistics, and exponential families," *IEEE Trans. Inf. Theory*, vol. 60, no. 7, pp. 4050–4065, 2014.

[77] A. Jung, S. Schmutzhard, F. Hlawatsch, Z. Ben-Haim, and Y. C. Eldar, "Minimum variance estimation of a sparse vector within the linear Gaussian model: An RKHS approach," *IEEE Trans. Inf. Theory*, vol. 60, no. 10, pp. 6555–6575, 2014.

[78] B. Chen, L. Xing, J. Liang, N. Zheng, and J. C. Principe, "Steady-state mean-square error analysis for adaptive filtering under the maximum correntropy criterion," *IEEE Signal Process. Lett.*, vol. 21, no. 7, pp. 880–884, 2014.

[79] B. Friedlander, "On the relationship between MIMO and SIMO radars," *IEEE Trans. on Signal Process.*, vol. 57, no. 1, pp. 394–398, 2008.

[80] E. Fishler, A. Haimovich, R. Blum, D. Chizhik, L. Cimini, and R. Valenzuela, "MIMO radar: An idea whose time has come," in *Proceedings of the IEEE radar conf.*, vol. 2004. Newark, NJ, USA, 2004, pp. 71–78.

[81] M. L. Bencheikh and Y. Wang, "Joint DOD-DOA estimation using combined ESPRIT-MUSIC approach in MIMO radar," *Electronics Letters*, vol. 46, no. 15, pp. 1081–1083, 2010.

[82] J. Li and P. Stoica, "MIMO radar with colocated antennas," *IEEE Signal Process. Mag.*, vol. 24, no. 5, pp. 106–114, 2007.

[83] D. R. Fuhrmann and G. San Antonio, "Transmit beamforming for mimo radar systems using signal cross-correlation," *IEEE Trans. Aerosp. Electron. Syst.*, vol. 44, no. 1, pp. 171–186, 2008.

[84] P. Stoica, J. Li, and Y. Xie, "On probing signal design for MIMO radar," *IEEE Trans. Signal Process.*, vol. 55, no. 8, pp. 4151–4161, 2007.

[85] A. Hassanien, S. A. Vorobyov, and A. B. Gershman, "Moving target parameters

estimation in noncoherent MIMO radar systems," *IEEE Trans. Signal Process.*, vol. 60, no. 5, pp. 2354–2361, 2012.

[86] I. Bekkerman and J. Tabrikian, "Target detection and localization using MIMO radars and sonars," *IEEE Trans. Signal Process.*, vol. 54, no. 10, pp. 3873–3883, 2006.

[87] B. Tang, J. Tang, Y. Zhang, and Z. Zheng, "Maximum likelihood estimation of DOD and DOA for bistatic MIMO radar," *Signal Process.*, vol. 93, no. 5, pp. 1349–1357, 2013.

[88] X. Zhang, M. N. El Korso, and M. Pesavento, "Maximum likelihood and maximum a posteriori direction-of-arrival estimation in the presence of SIRP noise," in *Int. Conf. Acoust, Speech, Signal Process. (ICASSP).* IEEE, 2016, pp. 3081–3085.

[89] ——, "MIMO radar target localization and performance evaluation under SIRP clutter," *Signal Process.*, vol. 130, pp. 217–232, 2017.

[90] B. Meriaux, X. Zhang, M. N. El Korso, and M. Pesavento, "Iterative marginal maximum likelihood DOD and DOA estimation for MIMO radar in the presence of SIRP clutter," *Signal Process.*, vol. 155, pp. 384–390, 2019.

[91] O. Besson, Y. Abramovich, and B. Johnson, "Direction-of-arrival estimation in a mixture of k-distributed and gaussian noise," *Signal Process.*, vol. 128, pp. 512–520, 2016.

[92] R. Mitra and V. Bhatia, "Diffusion-KLMS algorithm and its performance analysis for non-linear distributed networks," *arXiv preprint arXiv:1509.01352*, 2015.

[93] F. Gini, "A radar application of a modified Cramer-Rao bound: parameter estimation in non-Gaussian clutter," *IEEE Trans. Signal Process.*, vol. 46, no. 7, pp. 1945–1953, 1998.

[94] A. M. Haimovich, R. S. Blum, and L. J. Cimini, "MIMO radar with widely separated antennas," *IEEE Signal Process. Mag.*, vol. 25, no. 1, pp. 116–129, 2007.

[95] B. Chen, Z. Yuan, N. Zheng, and J. C. Príncipe, "Kernel minimum error entropy algorithm," *Neurocomputing*, vol. 121, pp. 160–169, 2013.

[96] T. Ogunfunmi and C. Safarian, "A quaternion kernel minimum error entropy adaptive filter," in *Int. Conf. Acoustics, Speech and Signal Process.* IEEE, 2018, pp. 4149–4153.

[97] V. A. Epanechnikov, "Non-parametric estimation of a multivariate probability density," *Theory of probability & its applications*, vol. 14, no. 1, pp. 153–158, 1969.

[98] Y. Bar-Shalom, X. R. Li, and T. Kirubarajan, *Estimation with Applications to Tracking and Navigation: Theory Algorithms and Software*. John Wiley & Sons, 2004.

[99] S. Julier, J. Uhlmann, and H. F. Durrant-Whyte, "A new method for the nonlinear transformation of means and covariances in filters and estimators," *IEEE Trans. Autom. Control*, vol. 45, no. 3, pp. 477–482, 2000.

[100] S. J. Julier and J. K. Uhlmann, "Unscented filtering and nonlinear estimation," *Proceedings of the IEEE*, vol. 92, no. 3, pp. 401–422, 2004.

[101] T. Gu, G. Liao, Y. Li, Y. Quan, Y. Guo, and Y. Huang, "An impoved parameter estimation of lfm signal based on MCKF," in *IEEE Int. Geoscience and Remote Sensing Sympo.* IEEE, 2019, pp. 596–599.

[102] N. Levanon and E. Mozeson, *Radar Signals*. John Wiley & Sons, 2004.

[103] B. D. Anderson and J. B. Moore, *Optimal Filtering*. Courier Corporation, 2012.

[104] R. G. Brown, P. Y. Hwang *et al.*, *Introduction to Random Signals and Applied Kalman Filtering*. Wiley New York, 1992, vol. 3.

[105] M. S. Arulampalam, S. Maskell, N. Gordon, and T. Clapp, "A tutorial on particle filters for online nonlinear/non-Gaussian Bayesian tracking," *IEEE Trans. Signal Process.*, vol. 50, no. 2, pp. 174–188, 2002.

[106] I. Arasaratnam and S. Haykin, "Cubature Kalman filters," *IEEE Trans. Autom. Control*, vol. 54, no. 6, pp. 1254–1269, 2009.

[107] A. K. Singh, R. Radhakrishnan, S. Bhaumik, and P. Date, "Adaptive sparse-grid Gauss–hermite filter," *J. Comput. Applied Mathematics*, vol. 342, pp. 305–316, 2018.

[108] M. Athans, R. Wishner, and A. Bertolini, "Suboptimal state estimation for continuous-time nonlinear systems from discrete noisy measurements," *IEEE Trans. Autom. Control*, vol. 13, no. 5, pp. 504–514, 1968.

[109] S. K. Rao, "Modified gain extended Kalman filter with application to bearings-only passive manoeuvring target tracking," *IEE Radar, Sonar Navig.*, vol. 152, no. 4, pp. 239–244, 2005.

[110] T. Song and J. Speyer, "A stochastic analysis of a modified gain extended Kalman filter with applications to estimation with bearings only measurements," *IEEE Trans. Autom. Control*, vol. 30, no. 10, pp. 940–949, 1985.

[111] R. Zhan and J. Wan, "Iterated unscented Kalman filter for passive target tracking," *IEEE Aerosp. Electron. Syst. Mag.*, vol. 43, no. 3, pp. 1155–1163, 2007.

[112] Z. Jiang, Q. Song, Y. He, and J. Han, "A novel adaptive unscented Kalman filter for nonlinear estimation," in *46th Conf. Decision Control*. IEEE, 2007, pp. 4293–4298.

[113] L. Chang, B. Hu, A. Li, and F. Qin, "Transformed unscented Kalman filter," *IEEE Trans. Autom. Control*, vol. 58, no. 1, pp. 252–257, 2013.

[114] M. P. Masarik and N. S. Subotic, "Cramer-Rao lower bounds for radar parameter estimation in noise plus structured interference," in *IEEE Radar Conference*. IEEE, 2016, pp. 1–4.

[115] P. Tichavsky, C. H. Muravchik, and A. Nehorai, "Posterior Cramer-Rao bounds for

discrete-time nonlinear filtering," *IEEE Trans. Signal Process*, vol. 46, no. 5, pp. 1386–1396, 1998.

List of publications

Journals:

1. U. K. Singh, V. Bhatia, and A.K. Mishra, "Small Boat Detection Using OFDM Radar", *Radioengineering*, vol. 28, no. 4, pp. 765-775, 2019. `https://www.radioeng.cz/fulltexts/2019/19_04_0765_0775.pdf`

2. U. K. Singh, R. Mitra, V. Bhatia, and A. K. Mishra, "Kernel LMS-Based Estimation Techniques for Radar Systems", *IEEE Trans. Aerosp. Electron. Syst.*, vol. 55, no. 5, pp. 2501-2515, 2019. `https://ieeexplore.ieee.org/abstract/document/8603824/`

3. U. K. Singh, R. Mitra, V. Bhatia and A. K. Mishra, "Range and Velocity Estimation Using Kernel Maximum Correntropy Based Nonlinear Estimators in Non-Gaussian Clutter", *IEEE Trans. Aerosp. Electron. Syst.*, vol. 56, no. 3, pp. 1992-2004, 2020. `https://ieeexplore.ieee.org/abstract/document/8880529`.

4. U. K. Singh, R. Mitra, V. Bhatia, and A. K. Mishra, "Kernel Minimum Error Entropy based Estimator for MIMO Radar in Non-Gaussian Clutter" (Submitted).

5. U. K. Singh, A. K. Singh, V. Bhatia, and A. K. Mishra, "EKF and UKF based Estimators for Radar System" (Submitted).

Conferences:

1. U. K. Singh, V. Bhatia, and A. K. Mishra, "Multiple Target Detection and Estimation of Range and Doppler for OFDM-RADAR System", *In International Conference on Signal Processing and Integrated Networks IEEE*, pp. 27-32, 2017. `https://ieeexplore.ieee.org/abstract/document/8049910`

2. U. K. Singh, R. Mitra, V. Bhatia, and A. K. Mishra, "Target Range Estimation in OFDM Radar System via Kernel Least Mean Square Technique", *IET*

Digital Library, 2017. https://digital-library.theiet.org/content/conferences/10.1049/cp.2017.0409

3. U. K. Singh, V. Bhatia, and A. K. Mishra, "Delay and Doppler shift Estimation for Non-Constant Envelope Modulation in OFDM radar system", *IET Digital Library*, 2017. https://digital-library.theiet.org/content/conferences/10.1049/cp.2017.0410

4. U. K. Singh, R. Mitra, V. Bhatia, and A. K. Mishra, "Low-Complexity Complex KLMS based Non-linear Estimators for OFDM Radar System", *In International Conference on Advanced Networks and Telecommunications Systems IEEE*, pp. 1-6, 2018. https://ieeexplore.ieee.org/abstract/document/8710142

5. U. K. Singh, R. Mitra, V. Bhatia and A. K. Mishra, "Vector-Valued KLMS based Multiple Target Range and Velocity Estimation using IEEE 802.11p Waveform for Autonomous Vehicle", *International Conference on Advanced Networks and Telecommunications Systems IEEE*, pp. 1-6, 2019. https://ieeexplore.ieee.org/abstract/document/9118030

6. A. Ramesh, U. K. Singh, R. Mitra, V. Bhatia and A. K. Mishra, "Fixed Budget Kernel LMS based Estimator using Random Fourier Features", *IEEE Radar Conference*, pp. 1-6, 2020. https://ieeexplore-ieee-org.proxy.bnl.lu/document/9266618